



# **Model based feasibility evaluation of a novel photobioreactor**

Part of this chapter has been published as:

M. Castrillo, R. Díez, I. Tejero. Design of a novel photobioreactor with enhanced incident solar light utilization. 4th International Congress on Energy and Environment Engineering and Management. Mérida, Spain. May 2011. School of Industrial Engineering of the Extremadura University. ISBN 8499780148, 9788499780146

---



## Abstract

A novel photobioreactor design was conceived with the aim of improving the solar light utilization efficiency of microalgae cultures, optimizing light distribution over the culture surface and thus minimizing photoinhibition and photosaturation phenomena occurrence. A preliminary model based on local light intensities and local growth rates was developed in order to check the viability of the idea. The model was applied to a photobioreactor unit located in Santander and areal productivities of  $15.17 \text{ g m}^{-2} \text{ d}^{-1}$  and  $34.57 \text{ g m}^{-2} \text{ d}^{-1}$  were predicted for the most unfavorable and favorable months respectively, both under monthly average cloud cover. These results are, in average, 2.72 times higher than predicted values for an open pond bioreactor under identical irradiance. A preliminary design optimization revealed that the optimal distribution of the cones when scaling-up this technology in the location of Santander makes a regular rhomboid grid with diagonal of 0.47 m.

## Resumen

Se ha desarrollado un nuevo diseño de fotobiorreactor con el objetivo de mejorar la utilización de la luz solar por parte de los cultivos de microalgas, optimizando la distribución de la luz incidente sobre la superficie del cultivo y por lo tanto minimizando la aparición de los fenómenos de fotoinhibición y fotosaturación. Se desarrolló un modelo basado en intensidades de luz locales y tasas de crecimiento locales para comprobar la viabilidad de la idea. Se obtuvieron predicciones de productividad por unidad de superficie de  $15,17 \text{ g m}^{-2} \text{ d}^{-1}$  y  $34,57 \text{ g m}^{-2} \text{ d}^{-1}$  para el mes más desfavorable y el más favorable respectivamente, ambos bajo condiciones de nubosidad media. Estos resultados son, de media, 2,72 veces mayores que los predichos para un reactor de tipo *open pond* bajo idénticas condiciones de irradiancia. En una optimización preliminar del diseño se observó que la distribución óptima de los conos cuando se escala esta tecnología, para la localización de Santander, conforma una red romboidal regular con diagonal de 0,47 m.





#### 4.1. Introduction

Microalgae are cultivated in production facilities that make use of light to produce biomass and valuable byproducts that are currently being commercialized (Pulz and Gross 2004; Spolaore et al. 2006). However the design of large scale efficient production systems is an issue that remains unsolved, mainly due to the nature of light that is attenuated while passing through the culture (Cuauresma et al. 2011; Janssen et al. 2003).

The illuminated surface to volume ratio is a key parameter in the photobioreactor design field, and with this in mind a wide variety of devices, mainly consisting on narrow channels or panels, has been developed (Ugwu, Aoyagi, and Uchiyama 2008). On the way to find an effective utilization of light energy, systems that include internal light sources have been proposed. Internally illuminated photobioreactors are characterized, as conventional closed photobioreactors, by having a high illuminated surface to volume ratio. They, however, allow for more compact designs compared to the conventional closed photobioreactors (Ogbonna and Tanaka 2000). According to Ogbonna et al. (Ogbonna et al. 1996), internal illumination seems to be the only practical means of constructing efficient, large-scale stirred tank photobioreactors. With the purpose of getting an appropriate distribution of solar energy, light harvesting and distributing methods have been proposed, especially by making use of Fresnel lenses to harvest light and then distribute it by means of optical fiber (Ogbonna, Soejima, and Tanaka 1999; An and Kim 2000). More recently, systems trying to drive the light deep into the reactor by means of vertical plastic light guides or empty chambers have been proposed (Zijffers et al. 2008a; Zijffers et al. 2008b; Hsieh and Wu 2009). The increase of the inner surface by introducing transparent components into the internal reactor volume is seen as an action to improve the performance of photobioreactors (Posten 2009).

However, nowadays solar light is considered the only source of light energy that can make feasible large scale culture and an efficient utilization of the sunlight hitting the photobioreactor surface is the key factor (Wijffels and Barbosa 2010). The use of solar light implies a big challenge in the field of photobioreactor design, since it is a non-scalable parameter which, in addition, varies cyclically but also unpredictably. Furthermore, in nutrient-limited systems, the limiting factor is a component of the medium, so it can be controlled by varying the dilution rate, but in light-limited systems, the limiting factor is not directly dependent of the dilution rate and cannot be assumed to be homogeneously distributed in the photobioreactor volume (Evers 1991). In a culture volume four different zones are usually found as a function of its light intensity: complete dark, light limitation, light saturation and

---

light inhibition (Ogbonna and Tanaka 2000). Ideally, during the design process of a photobioreactor the light inhibition and the complete dark zones should be avoided or at least minimized, keeping the light intensity between the critical and the saturation intensities. Then, nowadays the challenge consists on modulate the irradiance over the culture surface by varying its geometry or orientation in order to achieve a light “dilution effect”, with dilution factors ranging from 5 to 10 (Morweiser et al. 2010). According to Posten, 2009 (Posten 2009) the answer of process engineering is to design vertically mounted photobioreactors with a large surface, where the sunlight falling on a given ground area is spread over a larger reactor surface. As a guidance value, it is said that the surface to ground area ratio should be 10 or higher.

With these ideas as premises, a novel photobioreactor has been conceived to take advantage of the irradiance falling over the photobioreactor surface. The new configuration consists on a tank including a series of conical structures semi-submerged in the culture volume that allow for a light dilution over the upper layers of the culture. To preliminarily evaluate the technical feasibility of a new configuration the photosynthetic activity should be modelled.

Large scale photobioreactor optimization and modelling is governed by two main types of phenomena: on the one hand the growth and chemicals productivity kinetics of the species to be cultured, and on the other hand the photobioreactor physical structure that determines the radiant light transport. At the same time, when designing a solar based photobioreactor, two main types of factors must be taken into account. Firstly, the shape and geometry of the photobioreactor like its exposed surface and the presence of shadowing elements, and secondly geographical factors like the latitude and the relative position of the Sun. In non-sun tracking photobioreactors, direct irradiance over the reactor surface depends on the incident angle, which depends on the solar position. However, sun tracking photobioreactors are usually designed to receive the optimal radiation over the time, thus their geometry and dimensions must be designed and calculated according to the different positions of the Sun from the sunrise to the sunset through the year. Since daily Sun path varies along the year, especially in high latitudes, the optimized design must satisfy the global maximum productivity, thus averaged irradiance values should be avoided.

Knowing the angle of incidence of the direct light beams all over the day becomes essential to calculate light gradients inside the culture and to avoid heterogeneously irradiated surfaces. The study of the tilt angle for optimal year-round energy collection and, when possible, the adjustment of this angle through the year has been recognized to result in an enhancement of the overall annual productivity (Qiang, Faiman, and Richmond 1998; Slegers et al. 2011).

Many approaches can be found in scientific literature to model volumetric or areal productivity of microalgae. As a first classification, two border cases can be distinguished: models that predict the photosynthetic activity according to the local conditions of a cell at a given position inside the photobioreactor and models that use averaged parameters. Secondly, within each group, the light dependence can be calculated in different ways although the most common approach is to consider that light dependence follows Monod-type kinetics. Among the models that use averaged parameters, the most basic approach is to consider the light intensity in the photobioreactor as the average of all the local intensities within the same. The average irradiance can be defined as the irradiance experienced by a single cell randomly moving inside the culture (Rabe and Benoit 1962). However, average irradiance is not a sufficient criterion of culture performance because it considers only the total length of the dark and the light periods, not their frequency and reactors presenting identical averaged irradiances can show different productivity (Fernández et al. 1997; Ogbonna and Tanaka 2000), so more sophisticated models have been developed based on averaged parameters, as it is reported below.

Yun et al. (Yun and Park 2003) compared four different models: two models based on local conditions and two other ones using averaged-parameters. Within each type the light dependence can be expressed as a function of the photon flux density or the photon absorption rate. According to their results, the models based on local conditions could predict the experimental data more accurately.

Bosma et al. (Bosma et al. 2007) compared a no-light integration and a full-light integration model, based on photosynthetic yields, both using local photon fluxes. The first case assumes that microalgae that move through the light gradient are able to adapt immediately to the new conditions, then photosynthetic yields can be calculated with local light intensities. On the contrary, the fully-integrated approach assumes that acclimation processes occur slower than the light/dark cycles in the photobioreactor, which means that the cells are adapted to the average light intensity, thus photosynthetic yields are dependent on the average intensity. According to the work of Bosma et al. 2007, the light integration approach over-predicts the productivity since in this model no photoinhibition can occur. In contrast, the no-light integrated approach under-predicts the productivity because it over-estimates the photoinhibition and photolimitation processes.

In this work, a model based on local growth rates was applied to a unit of volume of the photobioreactor. This model approach is useful to know the sensitivity of the productivity to the geometry of the reactor as well as to the culture conditions. It was assumed that the reactor is fully mixed and that cells experiment a growth rate depen-

---

dent on instant conditions. The scale-up of this photobioreactor would be performed by repeating identical units, but the relative positions of the photobioreactor units must be carefully decided in order to allow for a maximum light harvest. Therefore, a tool to define the cones distribution in order to maximize the light capture when scaling-up this photobioreactor was also developed.

## **4.2. Materials and methods**

In the following pages the design criteria for the novel photobioreactor configuration, a detailed description of the model, and its application to assess the feasibility and scalability of the photobioreactor are shown.

### **4.2.1. Novel photobioreactor design criteria**

The design of this novel photobioreactor was mainly based on a light distribution criterion, with the basic premise of using solar light, although the device is adaptable for artificial light. Furthermore, the need for maintaining the culture properly mixed and the easiness to scale-up are factors that were present during the conception of the idea. A photobioreactor that can be scaled-up as a repetition of units is desirable, being one unit a single light distributing device and the surrounding culture (Ogbonna et al. 1996). At a given light intensity there is an optimum unit size, and this should be theoretically or experimentally determined.

With this in mind, the first outline consisted on a deep tank (between 1 and 2 meters) that contains the microalgae culture, in which a number of transparent conical structures are submerged or semi-submerged with their apex towards the bottom of the reactor, to drive the light all along the depth of the tank. These structures are orientated by means of a solar tracking system to catch the direct solar radiation. Several geometries of the transparent structures were discussed until the geometry of a cone was found to meet the criteria of distributing the light uniformly and modulate the light intensity to provide the desired values to the culture, preventing from photoinhibition and photosaturation. While other geometries like a tube would result in a high irradiance on the bottom and only diffuse irradiance over the lateral walls, the conical shape allows for a homogeneous irradiance which, furthermore, can be modulated during the design process in accordance to the specific needs of the culture and the irradiance of the geographical area where the photobioreactor is going to be installed.

The irradiance over a surface takes its maximum value when this surface is perpendicular to the solar beams. As the tilt angle of the surface is higher, the

irradiance decreases, as it is stated by Lambert's Cosine Law.

For a cone with an aperture angle of  $2\varphi$ , the irradiance over the internal face of the cone is

$$I' = I \cdot \cos(90 - \varphi)$$

thus the irradiance over the culture for a given geographical area can be modulated by determining the aperture of the cone.

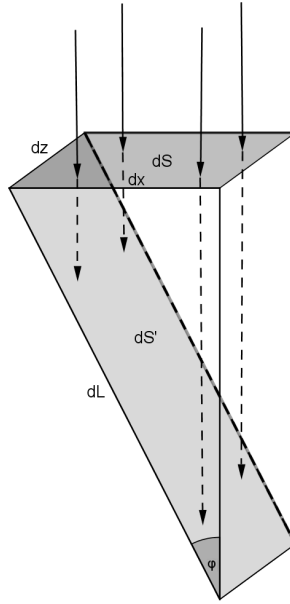


Figure 4.1: Representation of the solar beams incidence over the lateral wall of a cone with aperture angle  $2\varphi$ .

#### 4.2.2. Description of the model

In order to model the productivity in the novel photobioreactor, the solution was approximated by the finite element method. The domain of the problem was defined as a unit of volume of the photobioreactor, which is the minimum unit that would be repeated when scaling-up this technology. This unit consists on a right circular

---

cylinder with a right circular cone inscribed in it and the domain of the problem being the volume that remains between the cylinder and the cone.

The aperture of the cone ( $2\varphi$ ) was used to calculate light falling over the reactor surface from irradiance over the cone's base. According to the reflected irradiance over the inner surface of the cone, several subdomains were defined. The determination of their boundary conditions is described in the following section.

A two dimensional section of the cylinder holding the cone was represented in a two-dimensional Cartesian coordinate system that has its origin situated in a point of the perimeter of the cone's base, the abscissa axis orientated in the direction of the base of the cone and the ordinate axis parallel to the longitudinal axis of the cone. The position of a point  $P$  according to its coordinates  $x$  and  $y$  at a distance  $z$  of the surface of the cone is represented in Figure 4.2.

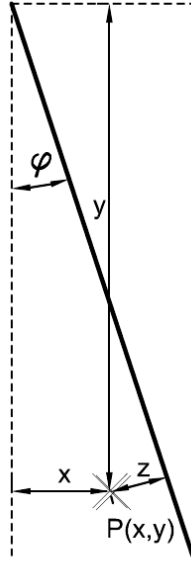


Figure 4.2: Location of a point  $P(x, y)$  in the two-dimensional coordinate system and its distance  $z$  to the irradiated surface.

The whole domain was discretized on a mesh composed by  $1\text{ cm} \times 1\text{ cm}$  squares with their sides parallel to the abscissa and ordinate axis.

A scheme of the model is presented in Figure 4.3. The variables and constants that operate in the model are given in Table 4.1.

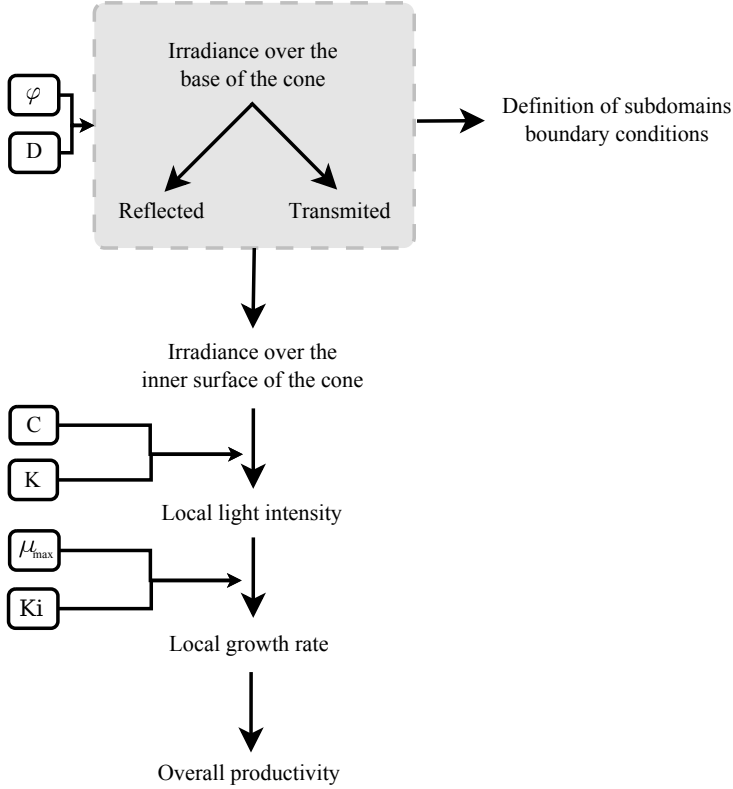


Figure 4.3: Calculation scheme.

In order to compare the obtained results with a conventional well-known technology, the same calculation scheme was applied to an open pond with the same ground surface occupancy. In the case of the open pond the domain is the whole volume of the tank. Variables and constants were identical in both cases.

#### 4.2.2.1. Incident light

The total irradiance received by a surface on the Earth is the addition of the direct radiation, the diffuse radiation and the reflected radiation. Direct radiation arrives to

Variables		
Name	Abbreviation	Unit
Half of the aperture angle	$\varphi$	$^{\circ}$
Cone base diameter	$D$	m
Culture concentration	$C$	$\text{kg m}^{-3}$

Constants		
Light extinction coefficient	$k$	$\text{m}^2 \text{kg}^{-1}$
Maximum growth rate	$\mu$	$\text{d}^{-1}$
Half-saturation constant	$K_i$	$\mu \text{mol m}^{-2} \text{s}^{-1}$
Air refractive index	$n_1$	
Cone's material refractive index	$n_2$	
Culture suspension refractive index	$n_3$	
Transmittance	$Tr$	
Specular factor	$S$	
% PAR within global radiation	% PAR	

Table 4.1: Variables and constants of the model.

the Earth's surface without having varied its direction. In the case of the cone, the direct irradiance received over its inner surface is homogeneous and its value is the irradiance of the geographical place over a two-axis tracking system but applying the Lambert's Cosine Law. In the case of the open pond, the incident irradiance is the irradiance over a horizontal surface. Diffuse radiation arrives to the Earth's surface after having varied its direction during its path through the atmosphere due to scattering. Direct radiation has a definite direction while diffuse radiation may come from any direction. Finally, reflected radiation is defined as that that hits some object and is reflected arriving to the object of interest. Photobioreactors are usually considered to be away from where the reflected light can arrive, so reflected radiation rarely accounts for a significant part of the sunlight striking their surface. However, in the present case, the direct radiation received by the inner surface of the cones is not totally transmitted to the culture; some portion can be reflected and fall over another part of the cone. According to the Fresnel equations the fraction of light that is transmitted ( $T$ ) and the fraction that is reflected ( $R$ ) depend on the angle that the incident rays make to the normal ( $\theta_i$ ) and the refractive index of the object ( $n$ ). Due to the shape of the cones, the reflected radiation is redirected to the bottom of the cones, so losses by reflection are minimized thanks to the shape of the cone and most of the cone's surface receives homogeneous radiation. Furthermore, since reflected radiation is directed towards the bottom of the cone, higher irradiance arrives to the deepest zone of the reactor, where normally the darkest conditions are found. In the



case of the pond, a fraction of light is reflected and lost.

Considering that the incident light is unpolarised,  $R$  can be calculated as follows:

$$R = \frac{R_S + R_P}{2}$$

where  $R_S$  is the reflectance of an incident light ray that is polarized with its electric field perpendicular to the plane containing the incident, reflected, and refracted rays and  $R_P$  is the reflectance of an incident light ray that is polarized with its electric field parallel to the plane described above, then  $T$ :

$$T = 1 - R$$

The Fresnel equations are given below:

$$\begin{aligned} R_S &= \left( \frac{n_1 \cdot \cos \theta_i - n_2 \cos \theta_t}{n_1 \cdot \cos \theta_i + n_2 \cos \theta_t} \right)^2 \\ R_P &= \left( \frac{n_1 \cdot \cos \theta_t - n_2 \cos \theta_i}{n_1 \cdot \cos \theta_t + n_2 \cos \theta_i} \right)^2 \end{aligned} \quad (4.1)$$

where  $n_1$  and  $n_2$  are the refractive indexes of media 1 and media 2 respectively,  $\theta_i$  is the angle that the incident rays make to the normal and  $\theta_t$  is the angle that the refracted angle makes to the normal direction.

The angle of the refracted ray can be calculated by means of Snell's Law:

$$\frac{n_1}{n_2} = \frac{\sin \theta_t}{\sin \theta_i} \quad (4.2)$$

The cones are made of a transparent or translucent material and it is characterized by its transmittance ( $Tr$ ). Finally, the cone's material has been considered as a mixed specular-diffuse reflector, thus a specular factor ( $S$ ) has been attributed to it, representing the fraction of light that is reflected as specular light, while the rest is reflected as diffuse light.

Taking into account the geometrical and trigonometrical relations between the shape of the cone and the reflected beams direction, the depth of the cone ( $L_R$ ) where reflected radiation hits can be calculated as follows:

---


$$L_R = \frac{D}{(\cos \varphi)(\tan 2\varphi + \tan \varphi)}$$

being  $D$  the diameter of the cone and  $\varphi$  is half of the aperture angle of the cone. Depending on the depth of the cone and its aperture angle, successive reflections can be produced, reaching a depth that is calculated like  $L_R$  but taking into account the relation between  $D$  and the diameter of the cone at the height of  $L_{R_{(n-1)}}$ .

$$L_{R_n} = \frac{D - 2(L_{R_{(n-1)}} \sin \varphi)}{(\cos \varphi)(\tan 2n\varphi + \tan \varphi)} + L_{R_{(n-1)}}$$

The directions of the reflections coming from the solar beam that hits the upper part of the cone with the depths at which these reflections are produced are shown in Figure 4.4. Solar beams hitting deeper parts of the cone will produce deeper reflections. Then, different depths of the cone receive different irradiance, demarcating the subdomains of the problem. A height of 0.20 m was kept between the apex of the cone and the bottom of the cylinder.

In the case of diffuse radiation, it is considered to come from any direction. For simplifying, the diffuse radiation over the cones base has been considered to be homogeneously distributed over the whole cones inner surface and that it is attenuated along the distance  $z$ .

Irradiance data were obtained from the Photovoltaic Geographical Information System (PVGIS) (European Commission 2012). The database provides irradiance data for real-sky conditions on a 2-axis tracking plane and on a horizontal surface throughout an average day of each month, as well as the ratio diffuse to global irradiation for a given geographical area. Real-sky conditions mean that data are calculated taking into account average cloud cover for each month. Data are provided for 15 minutes intervals along the day.

Irradiance data in the area of Santander (Spain, 43°27'44" North, 3°48'35" West, Elevation: 16 m a.s.l.) were taken as input data for the present model, and are show in Table 4.2.

It was considered that Photosynthetic Active Radiation (PAR) accounts for approximately 45 % of the total incident radiation.

#### 4. Model based feasibility evaluation of a novel photobioreactor

Solar time (h)	Jan	Feb	Mar	Apr	May	Jun	Jul	Aug	Sep	Oct	Nov	Dec	Average
4:52	0	0	0	0	0	93	81	0	0	0	0	0	15
5:07	0	0	0	0	18	149	143	0	0	0	0	0	26
5:22	0	0	0	0	148	199	202	0	0	0	0	0	46
5:37	0	0	0	81	200	247	255	0	0	0	0	0	65
5:52	0	0	0	149	247	290	303	69	0	0	0	0	88
6:07	0	0	0	210	290	330	346	132	87	0	0	0	116
6:22	0	0	129	264	328	366	384	193	164	0	0	0	152
6:37	0	0	215	311	362	398	418	249	233	0	0	0	182
6:52	0	0	280	352	393	428	449	299	297	105	0	0	217
7:07	0	93	334	388	420	454	476	343	353	178	0	0	253
7:22	0	157	380	420	445	477	500	383	402	237	0	0	283
7:37	0	211	418	448	466	498	522	418	446	289	103	0	318
7:52	132	257	451	473	486	517	540	449	484	335	156	129	367
8:07	183	296	479	494	502	533	557	477	517	373	199	188	400
8:22	222	331	503	513	517	547	571	501	546	407	236	236	428
8:37	256	360	524	529	530	560	583	522	571	436	267	272	451
8:52	285	385	542	543	541	570	594	541	593	461	295	302	471
9:07	309	407	557	555	550	580	602	557	612	483	318	327	488
9:22	330	426	570	565	558	587	610	571	628	501	338	348	503
9:37	347	442	581	574	565	594	616	583	642	517	356	365	515
9:52	363	456	591	581	570	599	621	593	654	531	370	380	526
10:07	375	468	598	587	575	603	625	602	664	543	383	393	535
10:22	386	478	605	592	578	607	629	609	672	552	394	403	542
10:37	395	486	610	596	581	610	631	615	678	560	402	412	548
10:52	402	493	614	599	583	612	633	620	684	566	409	418	553
11:07	408	498	617	601	585	614	635	624	688	571	415	424	557
11:22	412	502	619	603	586	615	636	627	691	575	419	428	559
11:37	414	504	621	604	587	616	636	629	693	577	422	430	561
11:52	416	505	621	604	587	616	637	631	694	579	423	431	562
12:07	416	505	621	604	587	616	637	632	694	579	423	431	562
12:22	414	504	621	604	587	616	636	632	693	577	422	430	561
12:37	412	502	619	603	586	615	636	632	691	575	419	428	560
12:52	408	498	617	601	585	614	635	632	688	571	415	424	557
13:07	402	493	614	599	583	612	633	631	684	566	409	418	554
13:22	395	486	610	596	581	610	631	629	678	560	402	412	549
13:37	386	478	605	592	578	607	629	627	672	552	394	403	544
13:52	375	468	598	587	575	603	625	624	664	543	383	393	537
14:07	363	456	591	581	570	599	621	620	654	531	370	380	528
14:22	347	442	581	574	565	594	616	615	642	517	356	365	518
14:37	330	426	570	565	558	587	610	609	628	501	338	348	506
14:52	309	407	557	555	550	580	602	602	612	483	318	327	492
15:07	285	385	542	543	541	570	594	593	593	461	295	302	475
15:22	256	360	524	529	530	560	583	583	571	436	267	272	456
15:37	222	331	503	513	517	547	571	571	546	407	236	236	433
15:52	183	296	479	494	502	533	557	557	517	373	199	188	407
16:07	17	257	451	473	486	517	540	541	484	335	156	14	356
16:22	11	211	418	448	466	498	522	522	446	289	15	8	321
16:37	0	157	380	420	445	477	500	501	402	237	9	0	294
16:52	0	14	334	388	420	454	476	477	353	178	0	0	258
17:07	0	7	280	352	393	428	449	449	297	15	0	0	223
17:22	0	0	215	311	362	398	418	418	233	7	0	0	197
17:37	0	0	129	264	328	366	384	383	164	0	0	0	168
17:52	0	0	9	210	290	330	346	343	87	0	0	0	135
18:07	0	0	0	149	247	290	303	299	5	0	0	0	108
18:22	0	0	0	81	200	247	255	249	0	0	0	0	86
18:37	0	0	0	6	148	199	202	193	0	0	0	0	62
18:52	0	0	0	0	90	149	143	132	0	0	0	0	43
19:07	0	0	0	0	9	93	14	13	0	0	0	0	11
19:22	0	0	0	0	0	10	7	5	0	0	0	0	2

Table 4.2: Irradiance data ( $\text{W m}^{-2}$ ) throughout an average day in Santander for each month and for a whole year on a 2-axis tracking plane. Source : Photovoltaic Geographical Information System (PVGIS) (European Commission 2012).

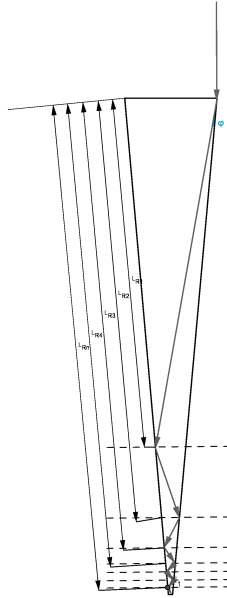


Figure 4.4: Reflections coming from the solar beam that hits the upper part of the cone with the depths at which these reflections are produced.

#### 4.2.2.2. Light gradients

As the model assumes that microalgae growth directly depends on local light intensity, knowing the fraction of light that arrives at any point of the culture is needed. The irradiance at any point of the culture depends on:

- the total incident radiation at the surface of the culture,
- the optical properties of the culture,
- the distance between that point and the irradiated surface.

Once the irradiance over the cone surface is known as the addition of direct radiation, diffuse radiation and reflected radiation; in order to predict the light intensity at

any distance of the irradiated surface, Lambert-Beer Law is the most widely applied expression:

$$I = I_0 e^{-K_a C_b z} \quad (4.3)$$

where  $I$  is the received light intensity ( $\mu\text{E m}^{-2} \text{s}^{-1}$ ) at a point situated at a distance  $z$  (m),  $I_0$  is the received light intensity over the irradiated surface of photobioreactor ( $\mu\text{E m}^{-2} \text{s}^{-1}$ ),  $K_a$  ( $\text{m}^2 \text{kg}^{-1}$ ) is the extinction coefficient and  $C_b$  ( $\text{kg m}^{-3}$ ) is the biomass concentration.  $K_a$  was experimentally determined as shown in Appendix A. The result was  $182 \text{ m}^2 \text{kg}^{-1}$ .

Although more complex expressions have been developed (Cornet 2009) in order to consider the light spreading by the solid particles, this phenomenon is usually negligible compared to the absorption by the biomass. Furthermore, when the extinction coefficient is experimentally determined, all these phenomena are directly affecting the measure, so they are already included in such coefficient.

In the case of the direct radiation, the light path between the cone's surface and the point  $P(x, y)$  is usually calculated according to the Sun position (Grima et al. 1999; Camacho et al. 1999). However, since in the case of the present reactor the cones tilt according to the Sun position in such a way that the direct radiation is always perpendicular to the cones base, the light path does not depend on the position of the Sun.

Light has been considered to be scattered once it reaches the culture suspension, being converted in diffuse radiation. Although a theoretic refraction angle, represented in Figure 4.5, has been calculated to know the fraction of refracted and transmitted radiation, in order to calculate the attenuation of light as it goes through the culture the distance in the direction perpendicular to the cones lateral wall ( $z$ ) has been considered instead of  $z_{\text{direct}}$ , which would be the path that an ideal direct beam would take.

According to the coordinates  $x$  and  $y$  of the point  $P$  within the modelled domain, its distance to the irradiated surface can be calculated as follows:

$$z = [(y \tan \varphi) - x] \cos \varphi \quad (4.4)$$

By substituting the equation for  $z$  (4.4) in the Lambert-Beer Law (4.3), the light intensity at a given point can be expressed as a function of its position  $P(x, y)$ .

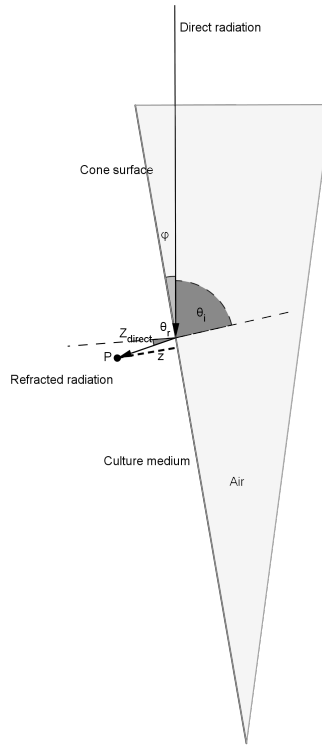


Figure 4.5: Scheme of the cone receiving direct radiation and refracting radiation in a theoretical direction  $z_{\text{direct}}$ .

#### 4.2.2.3. Local growth rate

The kinetic expression determines the specific production inside a bioreactor system as a function of the limiting factor. In light-limited cultures, the Monod-type model is a general kinetic model for describing the relationship between an organism growth and the concentration of the limiting factor, which in this case is the light. The use of this equation is valid when the light intensity inside the photobioreactor is under inhibitory levels.

$$\mu = \frac{\mu_{\max} I}{K_s + I}$$

where  $\mu_{\max}$  is the maximum specific growth rate,  $K_s$  is the half-saturation constant (the substrate concentration at which the specific growth rate is half of the maximum) and  $I$  is the received light intensity.

The following kinetic parameters shown in Table 4.3 were experimentally determined (procedure shown in Appendix A). In brief, growth rates were determined along 12:12 light-dark cycles, so biomass decrease due to dark respiration during the dark hours is included in these data. *Scenedesmus obliquus* was chosen as model strain.

Name	Abbreviation	Unit	Value
Maximum growth rate	$\mu$	$\text{d}^{-1}$	1.02
Half-saturation constant	$K_i$	$\mu\text{E m}^{-2}\text{s}^{-1}$	42.45

Table 4.3: Kinetic parameters

#### 4.2.2.4. Overall productivity

If the irradiance reaching a point  $P$  of the culture depends on its distance to the irradiated surface, which is the inner surface of the cone, homogeneously illuminated ring shaped volume units can be differentiated around the cone with its cross-section being an element of the mesh, as represented in Figure 4.6.

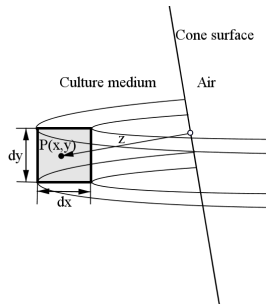


Figure 4.6: Homogeneously illuminated ring shaped volume with section  $dx \times dy$  and a point  $P(x, y)$  in the center of this section.

The volume of the ring shaped homogeneous element can be calculated as follows:

---


$$dV = \left\{ \left[ \frac{D}{2} - \left( x - \frac{dx}{2} \right) \right]^2 - \left[ \frac{D}{2} - \left( x + \frac{dx}{2} \right) \right]^2 \right\} dy \cdot \pi$$

Overall productivity in the photobioreactor unit can be calculated by integrating the productivity of these homogeneous units.

In the case of the pond, homogeneously illuminated volumes are horizontal layers parallel to the reactor surface.

Therefore, the overall productivity as grams of biomass per square meter and day (g biomass m<sup>-2</sup> d<sup>-1</sup>) can be calculated as follows:

$$P = \frac{\sum(\mu_i dV C)}{S}$$

being  $\mu_i$  the local growth rate (d<sup>-1</sup>),  $dV$  the volume of a homogeneously illuminated volume (m<sup>3</sup>),  $C$  the biomass concentration (kg m<sup>-3</sup>) and  $S$  the ground occupied surface of the photobioreactor unit (m<sup>2</sup>).

#### 4.2.3. Photosynthetic efficiency and biomass yield

Considering that photosynthesis needs 8 moles quanta to produce 30 g of biomass, the maximum biomass productivity was calculated according to the irradiance data in Santander. Then the photosynthetic efficiency could be calculated as the percentage of biomass produced in the photobioreactor unit in relation to the maximum productivity. The maximum productivity is calculated according to the irradiance over a two-axis tracking system in both —the novel photobioreactor and the open pond— cases.

Photosynthetic eff. (%) =

$$\frac{\text{Est. biomass productivity (g biomass m}^{-2} \text{ d}^{-1})}{\text{Max. theoretical biomass productivity (g biomass m}^{-2} \text{ d}^{-1})} \times 100$$

The biomass yield ( $Y_x$ ) on a PAR basis was calculated as:

$$Y_x = \frac{\text{Est. biomass productivity (g biomass m}^{-2} \text{ d}^{-1})}{\text{PAR photons (mol m}^{-2} \text{ d}^{-1})}$$



#### 4.2.4. Photobioreactor scale-up

The full-scale implementation of the photobioreactor would be carried out by repeating identical units. Under solar light utilization, the cones would incline to a certain angle  $\alpha$ , with respect to the horizontal, for each Azimuth angle in order to track the Sun. The arrangement of the cones limits their inclination since from a certain angle they will touch each other. A procedure to help in the decision of the distribution of the cones in the photobioreactor when it is scaled-up was carried out by modeling the working illuminated volume that provides a photobioreactor unit through the year. The distribution of the cones makes a grid whose nodes are the center of the upper base of the cones. The rhombus comprised among four nodes is characterized by the length of its side which is the distance between two contiguous cones ( $F_\beta$ ) and its angle which is twice the angle between a side of the rhombus and a reference direction that is the South ( $\beta$ ) as shown in Figure 4.7. These two parameters determine the maximum inclination angle of a cone for each Azimuth angle. Since the solar elevation at each Azimuth angle depends on the latitude of the location of the photobioreactor, both are essential factors in the design of the photobioreactor.

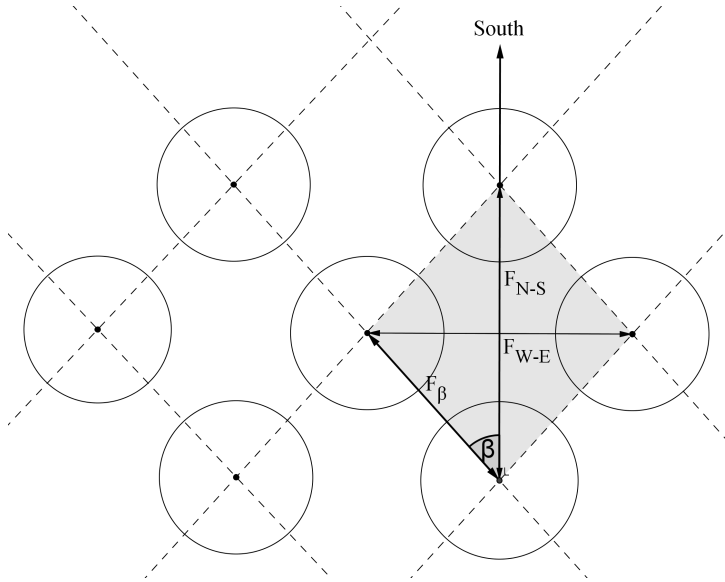


Figure 4.7: Top view of the cones distribution in the photobioreactor with the South direction as reference.

Once the diameter and the aperture angle of the cones have been optimized

according to the previously described model, there are three input variables that allows for the evaluation of the direct irradiance that a distribution allows to capture following the calculation scheme in Figure 4.8, whose main parameters are explained in the table Table 4.4. It is considered as captured irradiance the light entering into the cones perpendicularly to its base. The number of hours through the year that the cones are receiving direct radiation and the illuminated volume that they provide are also calculated.

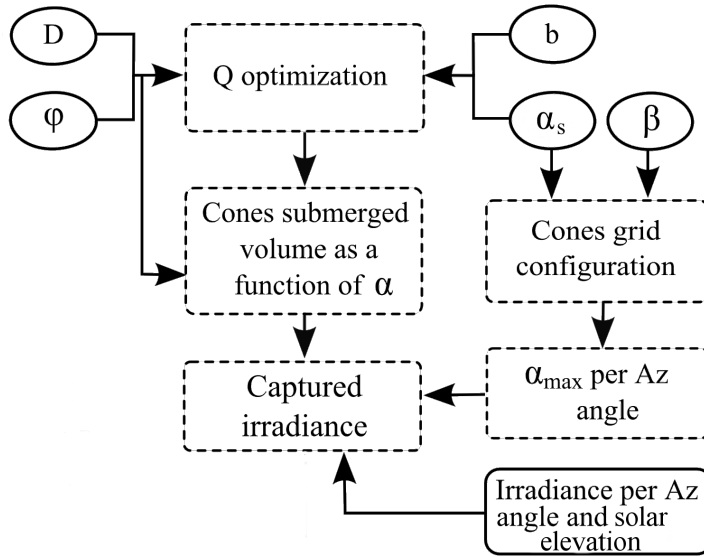


Figure 4.8: Calculation scheme.

The three input variables are:

**The pivot joint distance to the apex of the cone ( $b$ ):** The cones, acting as light distributors, are placed with its base in the upper side and its apex towards the bottom. However, the base cannot be placed at the water line level, since a minimum height ( $q$ ) above the water level must be fixed in order to avoid splashing over the cone's base. Furthermore, the cones base has to stand out above this fictitious line not only when they are in vertical position, but also

Variables		
Name	Abbreviation	Unit
Half of the aperture angle	$\varphi$	$^{\circ}$
Cone base diameter	$D$	m
Pivot joint distance to the apex of the cone	$b$	m
Inclination angle ( $Az = 0^{\circ}$ )	$\alpha_{\max}$	$^{\circ}$
Half of the rhombus angle	$\beta$	$^{\circ}$
Constants		
Height of the cones above the water level to avoid splashing	$q$	m
Other paramaters		
Height of the cones above the water level to avoid submersion	$Q$	m

Table 4.4: Variables, constants and other parameters of the model.

when they tilt in order to track the Sun. The cone inclination takes place over a pivot joint, which is located in a fixed point situated along the central axis of the cone. If the pivot joint is located in the base the value of  $b$  will be the height of the cone, taking into account the value of  $q$  and  $Q$ . On The contrary, if the pivot joint is in the apex, the value of  $b$  will be 0.

As a cone tilts from vertical position, the submerged fraction of the cone varies and therefore the water level rises or falls when the submerged volume decreases or increases respectively. In the case of the pivot joint in the base, the submerged volume firstly increases but from a certain angle it lowers because the part of the cone that stands out above the water is bigger than initially was, thus the water level decreases. Since the water level is lower as the cone tilts from certain angle, the distance between the water level when the cone is in vertical position and the base of the cone  $-Q-$  can be shorter; in other words, having into account the change in the water level, the cones can tilt more but  $Q$  does not need to be longer. However, in the case of the pivot joint in the apex the submerged volume always increases as the cone tilts, thus the water level always rises.

When the cones are inclined at a certain angle, the geometric figure that remains out of the water is a frusto cone with one of its bases being an ellipse. Then, the submerged volume ( $V_S$ ) in each moment can be determined by subtracting

this volume from the whole volume of the cone ( $V_T$ ). For each tilt angle it is possible to calculate the submerged volume, and therefore the variation of the water level  $a$  by dividing the difference of the cone volume that remains out of the water by the rhombus area. The submerged volume can be calculated as follows:

$$V_s = V_T - \left[ \left( \pi(R^2 + r^2 - Rr) \frac{h}{3} \right) - \frac{\pi r^3}{\cos \varphi \tan \alpha} \right]$$

$h$  and  $r$  parameters are identified in Figure 4.9. The procedure for  $V_s$ ,  $h$  and  $r$  calculation is specified in Appendix B.

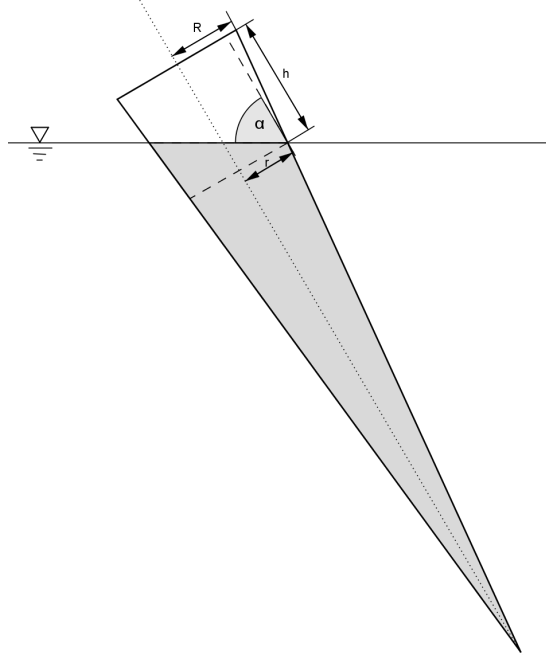


Figure 4.9: A cone inclined an angle  $\alpha$ . The shadowed area is the submerged fraction of the cone.

Therefore  $Q$  must be optimized by adjusting its value to make the distance between the base and the water level the minimum possible when the cones are tilted to its maximum angle and it depends on the situation of the pivot joint. The procedure followed to optimize  $Q$  is specified in Appendix B.

**Maximum inclination angle in the South direction ( $\alpha_S$ ):** This variable allows for the calculation of the first parameter that describes the grid, which is one of the diagonals of the rhombus, in other words the distance from one cone and the contiguous one in the South direction ( $F_{N-S}$ ).

The minimum distance between contiguous cones in any direction ( $F$ ) is determined from the maximum tilt angle that the cones can take in that direction ( $\alpha_{\max}$ ), which is also related to the base diameter through  $Q$ . This distance can be calculated from the trigonometric relations within the triangle that is observed in the longitudinal section of the cone tilted to the maximum (Figure 4.10), with its base just over the fictitious line  $q$ . The procedure is specified in Appendix B.

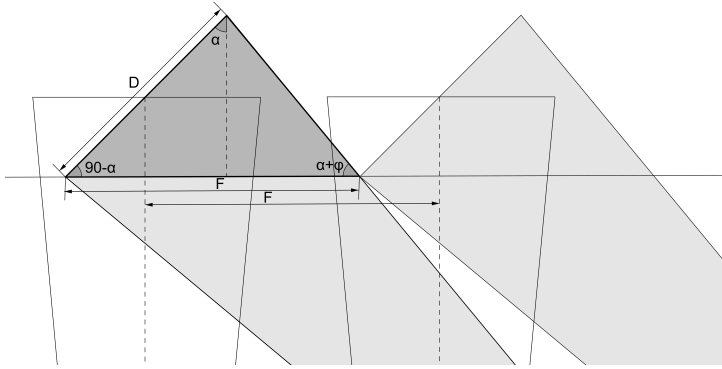


Figure 4.10: Minimum distance between adjoining cones.

The distance then can be calculated as follows:

$$F = D \sin \alpha + \frac{D \cos \alpha}{\tan (\varphi + \alpha)} = D \left( \sin \alpha + \frac{\cos \alpha}{\tan (\varphi + \alpha)} \right)$$

The optimal spatial distribution must provide the highest illuminated volume to occupied surface ratio over the year. The lower is the angle that the cones can reach when tracking the Sun, the higher is the solar irradiance that they can capture, however they must remain more separated one from each other and as a consequence, the number of cones is lower and the dark volume between them when they are nearly vertical is higher. Thus, there is an optimum maximum tilt angle, determining at the same time the separation between cones, which

---

provides the maximum illuminated volume to occupied surface ratio. In a given distribution, for each Azimuth angle there is a limiting tilt angle that avoids the cones to touch each other when they tilt in the plane of the Azimuth angle. The solar elevation —and as a consequence the tilt angle— depends on the geographical situation. Then, for each Azimuth angle, the elevation of the Sun can be calculated from the latitude, the earth declination and the hour angle. The equations (4.5) for its calculation are widely spread in bibliography.

$$\begin{aligned}\sin(90 - \alpha) &= \sin l \sin d + \cos l \cos d \cos H \\ \cos Az &= \frac{\sin l \sin(90 - \alpha) - \sin d}{\cos l \cos(90 - \alpha)}\end{aligned}\quad (4.5)$$

where  $90 - \alpha$  is the elevation of the Sun,  $l$  is the latitude,  $d$  is the declination angle,  $H$  is the hour angle and  $Az$  is the Azimuth angle. The declination angle is calculated as:

$$d = 23.45 \cdot \sin\left(360 \cdot \frac{284 + n}{385}\right)$$

where  $n$  is the number of day through the year (0 to 365).

The representation of the solar paths for each month in a Sun chart helps firstly to know the minimum elevation angle that the Sun takes in the South direction, and to have a preliminary rough idea about how much irradiance would be missed when limiting the cones tilt to a certain angle for each Azimuth. Since the relative position of the Sun with respect to the Earth takes its extreme situations in the solstices —about the 21st June and the 21st December—, a Sun chart (Figure 4.11) was elaborated for the 21st day of each month in the city of Santander (Spain), latitude  $43.46^\circ$  N.

Irradiance data for the simulations were obtained from the database PVGIS System (European Commission 2012). Since it provides irradiance data with time and time can be related with the solar position according to the equations proposed before, irradiance data were related to the solar position. Knowing the tilt limitations of each distribution it is possible to calculate the percentage of captured direct irradiance.

**Half of the rhombus angle ( $\beta$ ):** This is the second parameter needed to describe the grid. Once the diagonal in South direction is known ( $F_{N-S}$ ), the distance from one cone and the contiguous cone in  $\beta$  direction ( $F_\beta$ ) can be calculated.

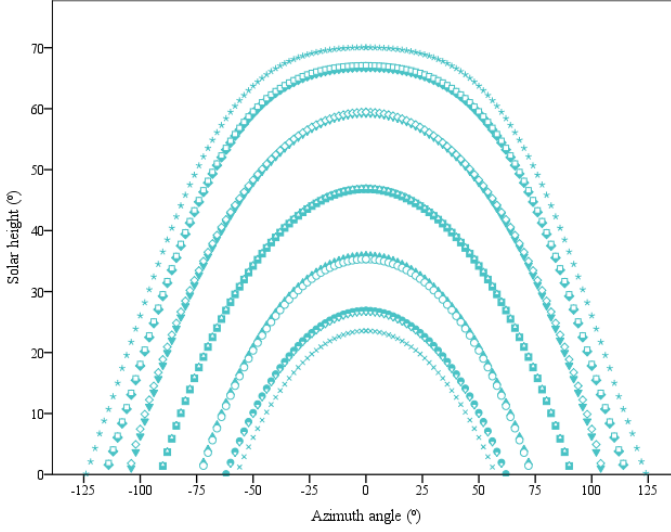


Figure 4.11: Solar elevation angle as a function of the Azimuth in Santander (Spain), latitude 43.46° for each month: January (●), February (▲), March (■), April (▼), May (◆), June (★), July (□), August (◇), September (△), October (○), November (▽) and December (×).

$$F_{\beta} = \frac{\frac{F_{N-S}}{2}}{\cos \beta}$$

Finally, the distance between one cone and the contiguous one in the East direction ( $F_{W-E}$ ) is calculated as:

$$F_{W-E} = F_{N-S} \tan \beta$$

These distances are represented in Figure 4.7.

Once the rhombus is described, in order to calculate the illuminated volume that a cone provides through the day, its maximum inclination angle for each Azimuth must be known. When the cones tilt in the direction that they are aligned, the limiting tilt angle is determined by the distance  $F$ , but for all the other Azimuth angles a new equation was developed. Figure 4.12 represents a situation in which the cones are aligned in a plane with an angle  $\beta$  with respect to the South but are inclined in the

---

plane of an Azimuth angle different than  $\beta$ . In this case the distance between the two bases,  $G$ , in the Azimuth direction limits the maximum tilt angle in this direction,  $\alpha$ , which can be calculated by means of the equation (4.6), where  $C$  is the chord of the base that gets in touch to the chord of the base of the contiguous cone in the Azimuth direction. The procedure to obtain this equation is shown in Appendix B.

$$G = C \left( \sin \alpha + \frac{\cos \alpha}{\tan(\varphi + \alpha)} \right) \quad (4.6)$$

The resolution of the equations above gives two main results for each distribution: the number of cones per unit surface and the maximum tilt angle for each Azimuth angle, which at the same time determines the irradiance captured by the cones.

Finally, in order to evaluate the distribution efficiency, the illuminated working volume per unit surface was calculated. The illuminated working volume has been defined as the culture volume that receives an intensity of light between the compensation point for photosynthesis and the saturation point. Then the working illuminated volume is considered as a margin that surrounds the submerged fraction of the cone in each moment. The width of this margin can be determined according to the previous model as a function of the biomass concentration and the light extinction coefficient of the species to be cultured. As explained before, the volume of the cone, and therefore the volume of the illuminated margin of the cone, that remains submerged for each inclination angle can be calculated. Therefore, the comparison variable for the different distributions is the working illuminated volume multiplied by the time during which this volume is maintained, per unit surface and per year ( $\text{m}^3 \text{ min m}^{-2} \text{ year}^{-1}$ ).

## 4.3. Results

### 4.3.1. Cone geometry and biomass concentration influence on areal productivity

Considering that light is the only limiting factor in the culture, there are several decision variables that influence volumetric and areal biomass productivity. Relating the geometry of the photobioreactor unit, the diameter of the cone as well as the aperture angle of the cone affects the areal productivity of the photobioreactor, since they determine the angle of the irradiated surface and the depth and occupied ground area of a unit. The largest is the base of the cone, the deeper can be the reactor but a higher distance must be maintained between two cones in order to avoid them to



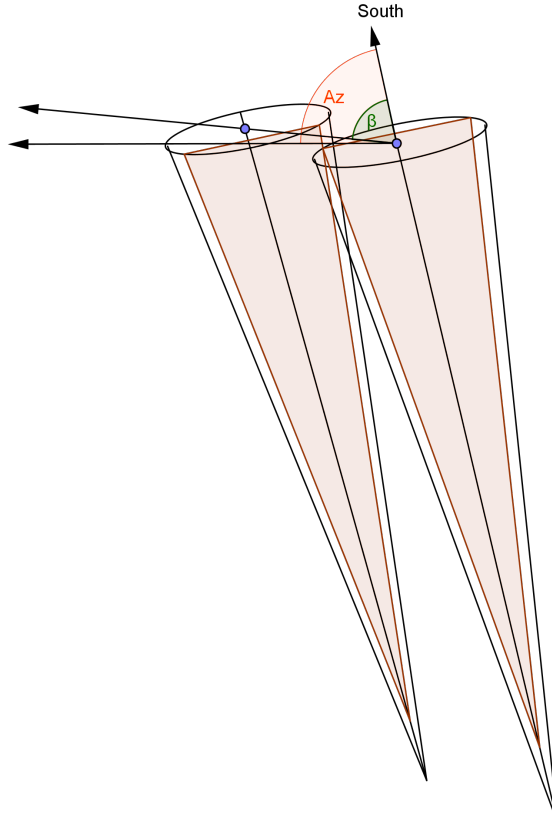


Figure 4.12: Two contiguous cones inclined in the  $Az$  direction. The red shadowed area represents the longitudinal section of the cone in  $Az$  direction.

touch each other when they are inclined, making dark areas larger. Furthermore, there will be fewer units per unit surface. Small dark areas are desirable in order to increase the light-dark cycles frequency.

According to the growth kinetics parameters of *S. obliquus*, to maintain the light intensity in the upper layers of the culture under saturation values, the aperture angle must be around  $10^\circ$  ( $\varphi = 5^\circ$ ). According to the Fresnel equations (4.1), in

Parameter	Unit	Photobioreactor	Open pond
Photobioreactor unit diameter	m	0.3	0.3
Cone diameter	m	0.3	
Cone height	m	1.63	
Photobioreactor unit height	m	1.83	0.3
Occupied surface	m <sup>2</sup>	0.07	0.07
Culture volume	m <sup>3</sup>	0.09	0.021
Illuminated surface to occupied surface ratio	m <sup>2</sup> m <sup>-3</sup>	11	1
Occupied surface to culture volume ratio	m <sup>2</sup> m <sup>-3</sup>	0.78	3.33
Illuminated surface to culture volume ratio	m <sup>2</sup> m <sup>-3</sup>	8.41	3.33

Table 4.5: Main dimensions and physical parameters of the photobioreactor unit and the open pond.

each reflection 61 % of the incident light is transmitted to the culture while 39 % is reflected.

For a certain aperture angle, the higher is the diameter of the cone, the lower is the illuminated surface to culture volume ratio. However, since the distance of the light path remains constant, above the optimal cone's base diameter the illuminated volume to the dark volume ratio decreases and below the optimal cone's base diameter the light path is restricted to the limits of the fictitious cylinder that contains the culture. 0.30 m has been seen as the optimal diameter for a sole photobioreactor unit. In a geometry with  $D = 0.30$  m and  $\varphi = 5^\circ$ , the farthest point to the irradiated surface keep a distance of 149 mm to it.

The dimensions and characteristics of the modellized photobioreactor unit and an open pond with the same ground surface occupancy are summarized in Table 4.5.

In the case of the open pond, the illuminated surface is equal to the ground occupied surface, while in the novel photobioreactor, the illuminated surface to occupied surface ratio is 11, complying with the recommendations for photobioreactor designing given by Posten et al. (Posten 2009). Furthermore, in the present design the occupied surface to culture volume ratio is 4.3 times lower than in the open pond.

Biomass concentration should be also optimized since it determines the optical length of the light through the culture. As can be seen in Figure 4.13, at very low concentrations, near the whole volume remains illuminated, however this too low concentration will predictably result in a low areal or volumetric productivity. Above a concentration of  $0.5 \text{ kg m}^{-3}$ , the illuminated distance from the irradiated surface is short and near constant. According to the proposed kinetics, above that concentration areal or volumetric productivity do not increase anymore, and even begin to decrease very slowly. However, working at high concentration is more beneficial for downstream processing.

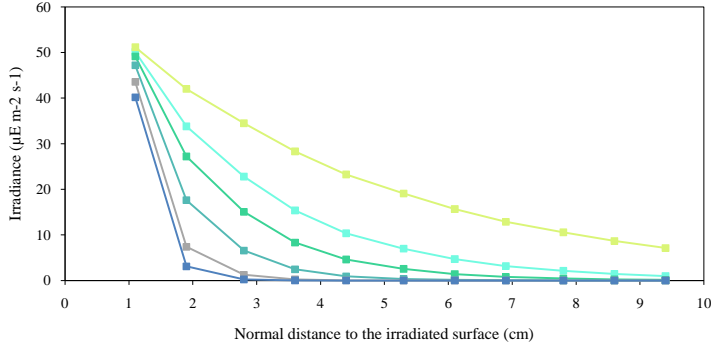


Figure 4.13: Variation of irradiance ( $\mu\text{E m}^{-2} \text{s}^{-1}$ ) with the normal distance (cm) to the irradiated surface as a function of the biomass concentration ( $\text{kg m}^{-3}$ ) in photobioreactor unit with  $D = 0.30 \text{ m}$  and  $\varphi = 5^\circ$  (■ 0.1, ■ 0.2, ■ 0.3, ■ 0.5, ■ 0.9, ■ 1.3).

#### 4.3.2. Hourly and seasonal variations in biomass productivity

The daily areal biomass productivity for three different scenarios was modelized in a photobioreactor unit with  $D = 0.30 \text{ m}$  and  $\varphi = 5^\circ$ . Biomass concentration was set to  $1 \text{ kg m}^{-3}$ . The three scenarios are, all of them under monthly average cloud cover, the most favorable one through the year (July daily average), the most unfavorable one (January daily average) and an average day through the whole year. In July the reactor receives light during 14.5 h per day, while in January it is only exposed to sunlight during 8.5 h. Results of areal productivity ( $\text{g m}^{-2} \text{d}^{-1}$ ) along the day are represented in Figure 4.14. The overall daily productivity, the average productivity during light hours, the photosynthetic efficiency and the biomass yield for a whole day are shown in Table 4.6.

Scenario	Daily areal productivity ( $\text{g m}^{-2} \text{d}^{-1}$ )	Avg. productivity during light hours ( $\text{g m}^{-2} \text{d}^{-1}$ )	Photosynthetic efficiency (%)	Biomass yield (g biomass/mol PAR photons)
January	15.17	42.83	8.75	0.76
July	34.57	56.25	7.73	0.67
Average	26.85	44.44	8.30	0.72

Table 4.6: Daily areal productivity ( $\text{g m}^{-2} \text{d}^{-1}$ ), the average productivity during light hours ( $\text{g m}^{-2} \text{d}^{-1}$ ), photosynthetic efficiency and biomass yield for the three scenarios in the novel photobioreactor.

Regarding the daily areal productivity, considerable differences can be appreciated

between the most favorable and the most unfavorable situations in the year. The productivity on an average day is higher than the average of the two other situations. Since models based on local light intensities and local growth rates tend to under-predict the productivity (Ogbonna and Tanaka 2000; Bosma et al. 2007), higher values of areal or volumetric productivity may be expected.

Photosynthetic efficiency values are in the range of reported data (Melis 2009). Biomass yield are similar to results referred to enclosed photobioreactors (Cuaresma et al. 2009; Richmond 2008). Both photosynthetic efficiency and biomass yield are higher in January than in July, which along with the plateau in the upper part of the daily areal productivity curve for July (Figure 4.14) suggest that some photosaturation is taking place during the summer days.

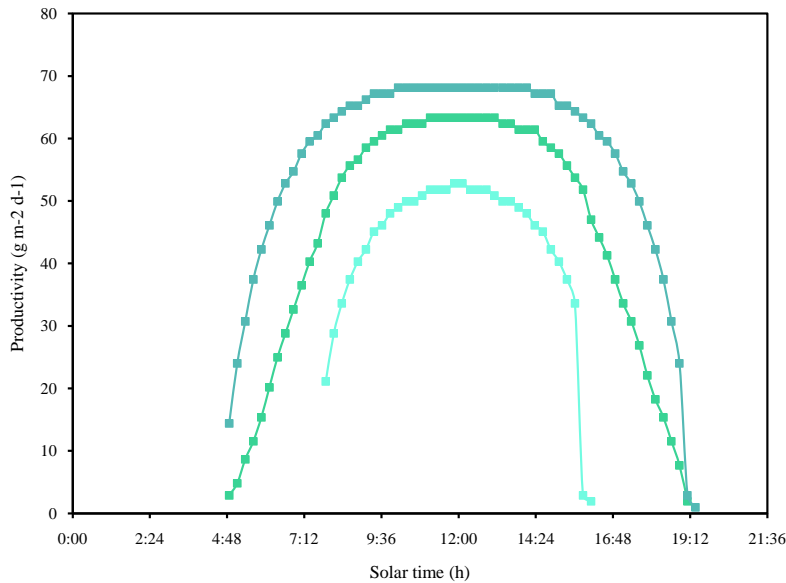


Figure 4.14: Daily areal productivity ( $\text{g m}^{-2} \text{d}^{-1}$ ) for the three different scenarios (■ most unfavorable month, ■ most favorable month, ■ average month).

Optimizing the cone properties in mid-latitudes where quite different Sun paths occur during the year leads to compromise the productivity in some part of the year. If the cone is optimized for summer conditions, a high dilution effect would compromise productivity during the winter. On the contrary, if winter conditions are used for optimization, high photosaturation will continue to occur during the summer. In

Scenario	Daily areal productivity ( $\text{g m}^{-2} \text{d}^{-1}$ )	Avg. productivity during light hours ( $\text{g m}^{-2} \text{d}^{-1}$ )	Photosynthetic efficiency (%)	Biomass yield (g biomass/mol PAR photons)
January	5.74	15.75	3.31	0.29
July	12.09	19.67	2.70	0.26
Average	10.08	16.41	3.11	0.27

Table 4.7: Daily areal productivity ( $\text{g m}^{-2} \text{d}^{-1}$ ), the average productivity during light hours ( $\text{g m}^{-2} \text{d}^{-1}$ ), photosynthetic efficiency and biomass yield for the three scenarios in an open pond.

this case, optimization has been carried out for an average day of the year, then some photosaturation takes place during the summer and some excessive dilution effect compromise productivity during the winter.

The results obtained for the modelling of an open pond are given in Table 4.7. Areal productivity values are in the range or reported results (Jimenez, Cossio, and Niell 2003). The predicted daily areal productivity for the three scenarios are, in average, 2.72 times higher in the novel photobioreactor than in the open pond.

#### 4.3.3. Photobioreactor scale-up

As stated before, the situation of the pivot joint as well as the maximum inclination angle of the cones are two main decision variables in the optimization of the cones distribution. In Figure 4.15 the two border cases are represented: the pivot joint in the base and the pivot joint in the apex. The deeper is the situation of the pivot joint (the nearer to the apex), the longer must be the distance between the cone base and the water level to tilt the same angle, thus the base is larger. As an example, both cones have been tilted to  $\alpha = 60^\circ$ , and both have the same submerged volume when they are in vertical position —the shading part in the the Figure 4.15. The one that has the pivot joint in the apex has a higher part over the water level — $Q$ —, resulting in a higher consumption of material for the construction of the cones and in a higher separation between adjacent cones. In contrast, since the apex remains static, the deep reached by the light is constant.

The working illuminated volume per cone and per unit surface were calculated for the two border cases from  $\alpha = 70^\circ$  which are the maximum solar elevation that takes the Sun in the latitude of this case study. Since the characteristics of the cone and therefore the variation of the water level depend on its maximum tilt angle, three cases were simulated:  $\alpha_{\max} = 20^\circ$ ,  $\alpha_{\max} = 35^\circ$  and  $\alpha_{\max} = 50^\circ$  for a cone with a diameter of 0.2 m at the height of the water level when it is in vertical position.

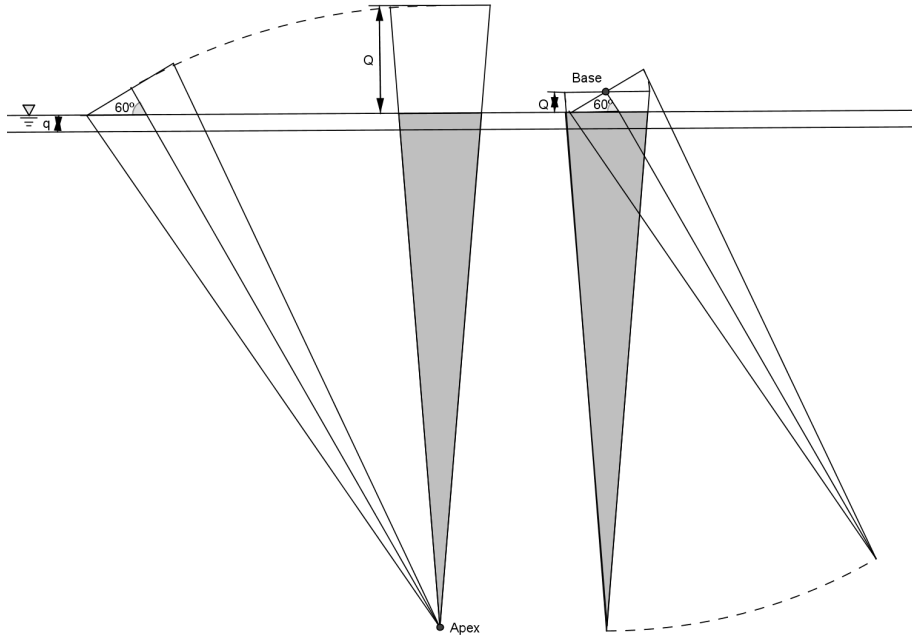


Figure 4.15: Scheme of the two extreme cases of situation of the pivot joint: in the apex and in the base. In both cases the cones are inclined  $30^\circ$ .

Results are represented in Figure 4.16 and Figure 4.17.

Placing the pivot joint in the apex results in a high illuminated working volume per cone but also requires a large  $Q$ , which makes the cones to be very distant one to each other, thus resulting in a low illuminated volume per unit surface. In the opposite case, when the pivot joint is in the base,  $Q$  takes its minimum value and the highest number of cones per unit surface is reached. This results in a high illuminated working volume and, as a consequence, in a low ratio dark volume to illuminated volume. As the height of the pivot joint along the axis of the cone decreases,  $Q$  is larger with respect to the situation in the base, and therefore the number of cones falls. However, the illuminated volume per cone is increased, but not enough to counteract the decrease of the number of cones. The optimum situation for the pivot joint is the base of the cones since it provides the highest illuminated working volume per unit surface and the lowest dark volume to illuminated volume ratio.

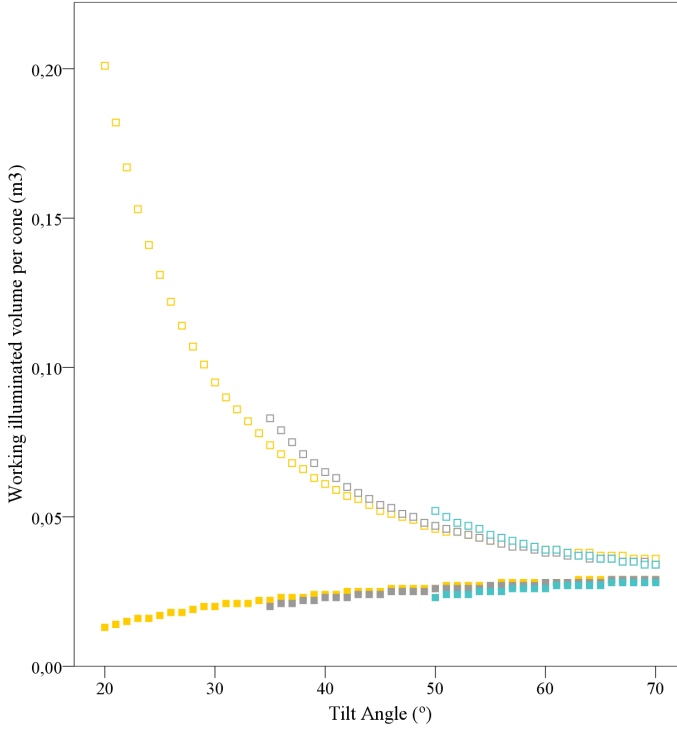


Figure 4.16: Variation of the working illuminated volume per photobioreactor unit with the tilt angle, for different situations of the pivot joint and different maximum tilt angle: (■) 50°; (■) 35°; (■) 20°. Filled symbols mean pivot joint in the base while white symbols mean pivot join in the apex.

With the pivot joint in the base of the cones, several cones distributions were compared. In all the cases  $\varphi$  took the value of  $5^\circ$  and the cones had fixed margin  $-q-$  of 0.10 m between the water level and  $Q$ .

Firstly two base diameters were compared for distributions in which the maximum inclination angle in the South direction is  $25^\circ$ . Although photobioreactor units with larger cones ( $D = 0.3$  m) have higher illuminated volume through the year, its value is lower when it is referred to the occupied ground surface. Larger cones provide larger illuminated volumes, but fewer cones can be installed per unit surface. Cones with lower base diameter ( $D = 0.2$  m) provide a higher illuminated volume per unit surface through the year. This is represented in Figure 4.18. Both diameters show a

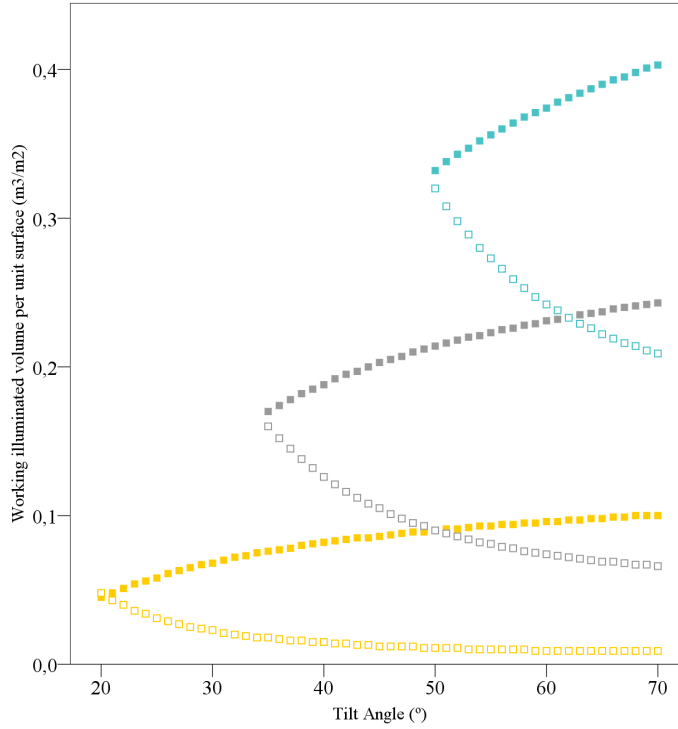


Figure 4.17: Variation of the working illuminated volume per unit surface with the tilt angle, for different situations of the pivot joint and different maximum tilt angle: (■) 50°; (■) 35°; (■) 20°. Filled symbols mean pivot joint in the base while white symbols mean pivot joint in the apex.

similar pattern in the variation of the illuminated volume-time per unit surface and per year with the angle  $\beta$ , presenting the maximum value when  $\beta = 45^\circ$ .

According to these results, the diameter of 0.2 m seems to result in higher photonic efficiency. Then, several cones distributions were compared for a cone with this diameter. As can be observed in Figure 4.19. The results of the simulations show that the highest illuminated volume-time per unit surface and per year occur for  $\alpha_S$  of  $25^\circ$  and  $\beta$  being  $45^\circ$ .

This configuration has 13 cones per square meter and makes a regular rhomboid grid with diagonals of 0.47 m. It allows for the capture perpendicularly to the base of the cones of the 67 % of the direct radiation falling over the photobioreactor unit.



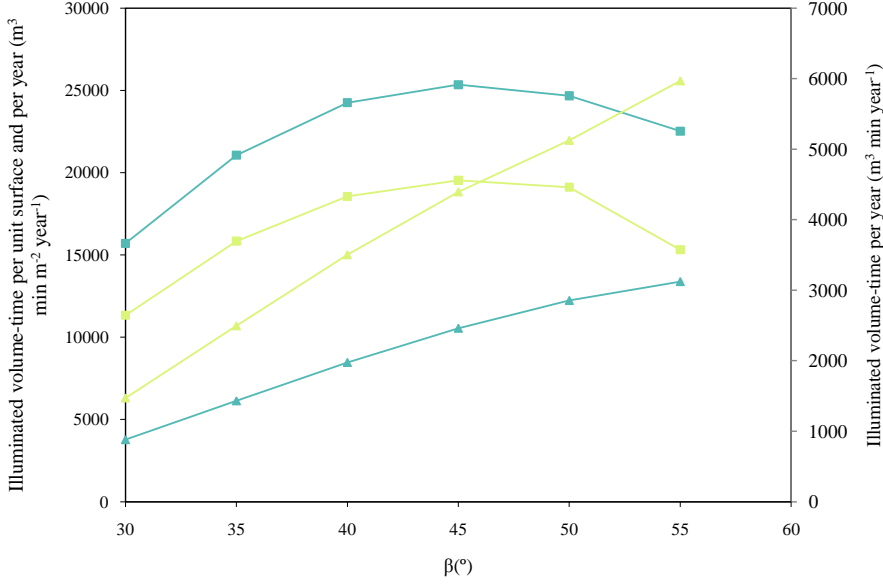


Figure 4.18: Variation of the illuminated volume-time per unit surface and per year ( $\text{m}^3 \text{ min m}^{-2} \text{ year}^{-1}$ ) and the illuminated volume-time per year ( $\text{m}^3 \text{ min year}^{-1}$ ) on the cones distribution. In all cases  $\alpha_S$  is  $25^{\circ}$ , and the abscissa axis represents  $\beta$ : ( $\blacksquare$ )  $\text{m}^3 \text{ min m}^{-2} \text{ year}^{-1}$  for a photobioreactor unit with a cone with diameter of 0.2 m at the height of the water level; ( $\blacksquare$ )  $\text{m}^3 \text{ min m}^{-2} \text{ year}^{-1}$  for 0.3 m of diameter; ( $\blacktriangle$ )  $\text{m}^3 \text{ min year}^{-1}$  for 0.2 m of diameter; ( $\blacktriangle$ )  $\text{m}^3 \text{ min year}^{-1}$  for 0.3 m of diameter

In Figure 4.20, the angle that limits the inclination of the cone for each Azimuth is represented, considering that  $0^{\circ}$  is the South direction. There is a first straight part which belongs to the central hours of the day where the inclination is not limited, since the lowest solar altitude in Santander in the South direction is  $25^{\circ}$  and this configuration allows the cones to tilt to this angle. The second part represents the angles limited by the cone which is located  $45^{\circ}$  to the Southwest or to the Southeast and with a separation of 0.23 m from the studied cone. The third part is the limitation by the cone situated  $90^{\circ}$  to the West or to the East.

However, several situations provide similar results. Then, another parameter should be used to evaluate the efficiency of those distributions. Since different situations allow for the introduction of a higher or a lower number of cones, they present different dark to illuminated volume ratios. Among the cases represented in Figure 4.19 that provide the highest illuminated volumes-time per unit surface and per

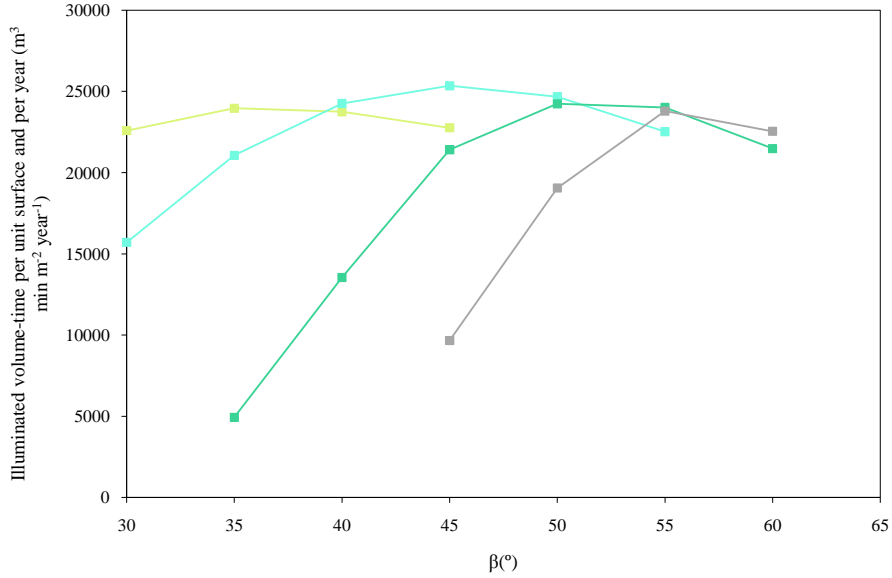


Figure 4.19: Variation of the illuminated volume-time per unit surface and per year ( $\text{m}^3 \text{ min m}^{-2} \text{ year}^{-1}$ ) on the cones distribution for a photobioreactor unit with a cone with diameter of 0.2 m at the height of the water level and different  $\alpha_S$ : (■) 20; (■) 25; (■) 30; (■) 35.

year ( $> 23.000 \text{ m}^3 \text{ min m}^{-2} \text{ year}^{-1}$ ), dark to illuminated volume ratios are between 6 and 11. Furthermore, the lowest ratios are due to the presence of a higher number of cones, thus a higher number of smaller dark volumes are placed among the cones, making the alternation between light and dark areas more frequent. Until the date, there is not a clear agreement on how the flashing light affects the microalgae growth although it seems that in general it is accepted that intermittent illumination enhances photosynthesis (Ogbonna, Yada, and Tanaka 1995; Sato, Yamada, and Hirabayashi 2010; Grobbelaar 2009). However, the duration of the L:D cycles do not depend only on the size of light and dark volumes, but also on the agitation and mixing grade.

The distribution that provides the lowest dark to illuminated volume ratio among those having a high illuminated volumes-time per unit surface and per year ( $> 23.000 \text{ m}^3 \text{ min m}^{-2} \text{ year}^{-1}$ ) allows the cones to tilt until  $25^{\circ}$  in South direction and has a  $\beta$  angle of  $40^{\circ}$ . According to these results, it can be deduced that configurations that limit the cones inclination in South direction cause notable energy losses.

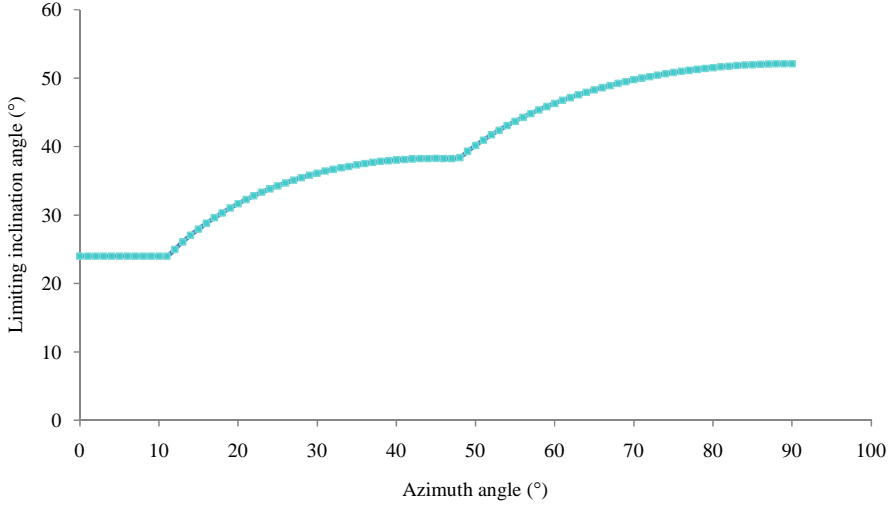


Figure 4.20: Limiting inclination angle for each Azimuth in a distribution with  $\alpha_S$  of 25° and  $\beta$  being 45°.

#### 4.4. Conclusions

A mathematical model of the novel photobioreactor for the culture of phototrophic organisms was built and the areal productivity in several scenarios was simulated with irradiance data of Santander. While conventional photobioreactors exposed to solar light usually receive an excessive amount of energy in the most external layers of the culture, the photobioreactor presented hereby takes advantage of the energy in excess distributing it over a higher surface, thus minimizing the photosaturation phenomenon and increasing the culture illuminated volume per occupied surface. Furthermore, the penetration of the cones in the culture medium drives the light deep into the tank, making possible the construction of photobioreactors in semi-buried tanks, which would make them more economical and easier to build than conventional closed photobioreactors.

The geometry of a unit of volume of the novel photobiorreactor was compared with a conventional open pond, showing that it multiplies by 11 the illuminated to occupied surface ratio.

Several decision variables when scaling-up the photobioreactor, being the situation of the pivot joint of the cones, the maximum inclination angle and the relative position

---

of the cones, play an important role in the yearly performance of the photobioreactor.

The areal productivity results provided by the model evidenced that, in a mid-latitude location, the longer is the duration of the day and the higher is the irradiance, the more advantage can be taken from this design. The illuminated volume through the year per unit surface is increased when the solar altitude along the day is high, thus suggesting that low latitudes are the most appropriate for this design.

## References

- An, J. Y and B. W Kim (2000). "Biological desulfurization in an optical-fiber photobioreactor using an automatic sunlight collection system". In: *Journal of Biotechnology* 80.1, pp. 35–44.
- Bosma, R. et al. (2007). "Prediction of volumetric productivity of an outdoor photobioreactor". English. In: *Biotechnology and bioengineering* 97.5, pp. 1108–1120.
- Camacho, F. G. et al. (1999). "Use of concentric-tube airlift photobioreactors for microalgal outdoor mass cultures". In: *Enzyme and microbial technology* 24.3-4, pp. 164–172.
- Cornet, J. F (2009). "Calculation of optimal design and ideal productivities of volumetrically lightened photobioreactors using the constructal approach". In: *Chemical Engineering Science* 65.2, pp. 985–998.
- Cuaresma, M. et al. (2009). "Productivity of *Chlorella sorokiniana* in a Short Light-Path (SLP) Panel Photobioreactor Under High Irradiance". In: *Biotechnology and bioengineering* 104.2, pp. 352–359.
- Cuaresma, M. et al. (2011). "Horizontal or vertical photobioreactors? How to improve microalgae photosynthetic efficiency". In: *Bioresource technology* 102.8, pp. 5129–5137.
- European Commission Joint Research Centre Institute for Energy, R. E. U. (2012). *Photovoltaic Geographical Information System (PVGIS)*.
- Evers, E. (1991). "A Model for Light-Limited Continuous Cultures: Growth, Shading, and Maintenance". In: *Biotechnology and bioengineering* 38, pp. 254–259.
- Fernández, F. G. A. et al. (1997). "A model for light distribution and average solar irradiance inside outdoor tubular photobioreactors for the microalgal mass culture". In: *Biotechnology and bioengineering* 55.5, pp. 701–714.
- Grima, E. M. et al. (1999). "Photobioreactors: Light regime, mass transfer, and scaleup". In: *Journal of Biotechnology* 70.1-3, pp. 231–247.
- Grobbelaar, J. U. (2009). "Upper limits of photosynthetic productivity and problems of scaling". In: *Journal of Applied Phycology* 21.5, pp. 519–522.
- Hsieh, C. H. and W. T. Wu (2009). "A novel photobioreactor with transparent rectangular chambers for cultivation of microalgae". In: *Biochemical engineering journal* 46.3, pp. 300–305.

- 
- Janssen, M. et al. (2003). "Enclosed outdoor photobioreactors: Light regime, photosynthetic efficiency, scale-up, and future prospects". In: *Biotechnology and bioengineering* 81.2, pp. 193–210.
- Jimenez, C., B. R. Cossio, and F. X. Niell (2003). "Relationship between physicochemical variables and productivity in open ponds for the production of *Spirulina*: a predictive model of algal yield". In: *Aquaculture* 221.1-4, pp. 331–345.
- Melis, A. (2009). "Solar energy conversion efficiencies in photosynthesis: Minimizing the chlorophyll antennae to maximize efficiency". In: *Plant Science* 177.4, pp. 272–280.
- Morweiser, M. et al. (2010). "Developments and perspectives of photobioreactors for biofuel production". In: *Applied Microbiology and Biotechnology* 87.4, pp. 1291–1301.
- Ogbonna, J. C., T. Soejima, and H. Tanaka (1999). "An integrated solar and artificial light system for internal illumination of photobioreactors". In: *Journal of Biotechnology* 70.1-3, pp. 289–297.
- Ogbonna, J. C. and H. Tanaka (2000). "Light requirement and photosynthetic cell cultivation - Development of processes for efficient light utilization in photobioreactors". In: *Journal of Applied Phycology* 12.3-5, pp. 207–218.
- Ogbonna, J. C., H. Yada, and H. Tanaka (1995). "Effect of cell movement by random mixing between the surface and bottom of photobioreactors on algal productivity". In: *Journal of Fermentation and Bioengineering* 79.2, pp. 152–157.
- Ogbonna, J. C. et al. (1996). "A novel internally illuminated stirred tank photobioreactor for large-scale cultivation of photosynthetic cells". In: *Journal of Fermentation and Bioengineering* 82.1, pp. 61–67.
- Posten, C. (2009). "Design principles of photo-bioreactors for cultivation of microalgae". In: *Engineering in Life Sciences* 9.3.
- Pulz, O. and W. Gross (2004). "Valuable products from biotechnology of microalgae". In: *Applied Microbiology and Biotechnology* 65.6, pp. 635–648.
- Qiang, H., D. Faiman, and A. Richmond (1998). "Optimal tilt angles of enclosed reactors for growing photoautotrophic microorganisms outdoors". In: *Journal of Fermentation and Bioengineering* 85.2.

- Rabe, A. E. and R. J. Benoit (1962). "Mean light intensity? a useful concept in correlating growth rates of dense cultures of microalgae". In: *Biotechnology and bioengineering* 4.4, pp. 377–390.
- Richmond, A. (2008). *Handbook of Microalgal Culture: Biotechnology and Applied Phycology*. John Wiley & Sons.
- Sato, T., D. Yamada, and S. Hirabayashi (2010). "Development of virtual photobioreactor for microalgae culture considering turbulent flow and flashing light effect". In: *Energy Conversion and Management* 51.6, pp. 1196–1201.
- Slegers, P. M. et al. (2011). "Design scenarios for flat panel photobioreactors". In: *Applied Energy* 88.10, pp. 3342–3353.
- Spolaore, P. et al. (2006). "Commercial applications of microalgae". In: *Journal of Bioscience and Bioengineering* 101.2, pp. 87–96.
- Ugwu, C. U., H. Aoyagi, and H. Uchiyama (2008). "Photobioreactors for mass cultivation of algae". In: *Bioresource technology* 99.10, pp. 4021–4028.
- Wijffels, R. H. and M. J. Barbosa (2010). "An outlook on microalgal biofuels". In: *Science* 329.5993, pp. 796–799.
- Yun, Y. S. and J. M. Park (2003). "Kinetic modeling of the light-dependent photosynthetic activity of the green microalga *Chlorella vulgaris*". In: *Biotechnology and bioengineering* 83.3, pp. 303–311.
- Zijffers, J. W. F. et al. (2008a). "Capturing sunlight into a photobioreactor: Ray tracing simulations of the propagation of light from capture to distribution into the reactor". In: *Chemical Engineering Journal* 145.2, pp. 316–327.
- Zijffers, J. W. F. et al. (2008b). "Design process of an area-efficient photobioreactor". In: *Marine Biotechnology* 10.4, pp. 404–415.





# 5

## **Photobioreactor for phototrophic organisms culturing**

This chapter includes an approximate translation of the following patent:

Tejero, I., Castrillo, M., Díez, R., Moreno-Ventas, X.E. Fotobiorreactor para el cultivo de organismos fotótrofos. ES2356653.

---

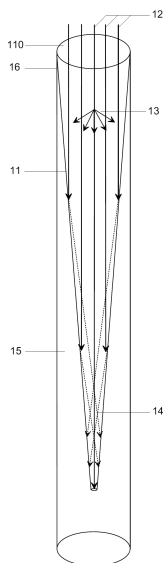


## Abstract

The invention relates to a photobioreactor for cultivating phototrophic organisms, said photobioreactor including a tank (15, 25, 35, 45, 55, 65) comprising a culture medium, and a biomass located inside the tank that is in contact with the culture medium. The photobioreactor additionally includes at least one transparent or translucent conical or frustoconical structure (11, 21, 31, 41, 51, 61) located entirely or partially inside the tank (15, 25, 35, 45, 55, 65) and through which visible radiation penetrates said tank.

## Resumen

La invención objeto de este capítulo consiste en un fotobiorreactor para el cultivo de organismos fotótrofos, que comprende un depósito (15, 25, 35, 45, 55, 65) que a su vez comprende un medio de cultivo y biomasa en el interior de dicho depósito y en contacto con dicho medio de cultivo. El fotobiorreactor comprende además al menos una estructura cónica o troncocónica transparente o translúcida (11, 21, 31, 41, 51, 61) situada total o parcialmente en el interior de dicho depósito (15, 25, 35, 45, 55, 65) a través de la cual o las cuales una radiación luminosa penetra en dicho depósito.



Basic unit of volume of the photobioreactor.



### 5.1. Field of invention

The present invention belongs to the field of phototrophic microorganisms culturing, like microalgae, for diverse industrial interesting products obtaining.

### 5.2. Description of prior art

During the last years there has been an increasing interest in microalgae culturing with a wide variety of objectives, such as their use in environmental remediation as well as with commercial aim in different industrial sectors (pharmaceutics, nutraceutics, aquaculture, etc). Among the wide variety of products that are obtained from microalgae, during the last decades it has been remarked its potential as oils producers that could be used as raw material for biofuel making.

Photobioreactors have been traditionally classified in two groups: open systems and closed systems. In the first type the culture is exposed to the atmosphere and it is usually contained in shallow ponds (15 cm to 30 cm deep). The culture is normally mixed and propelled by means of paddles. They usually need wide surfaces (500 m<sup>2</sup> to 5000 m<sup>2</sup>). As main advantages, their relative low cost and simplicity can be remarked, however they show several drawbacks like the easiness of contamination by other organisms, evaporation losses, large surface occupation, etc. Undoubtedly their main disadvantage is the low light utilization efficiency due to the scarce light penetration as a consequence of the light intensity attenuation as it goes through the culture.

With the aim of alleviate these drawbacks, the culture in closed systems or photobioreactors arose, where it is possible to have a better control of the operating conditions, enhancing the growth and the cell productivity and avoiding the contamination. These include vertical or horizontal photobioreactors, tubular, helical or thin panels among other designs. In spite of the several advantages that they show, they have important limitations related with the mass transfer, the control of temperature, oxygen accumulation, the control of light intensity, cleaning difficulties and energy consumption.

In spite of the progresses in this field, the production of phototrophic organisms is still expensive and it is only economically worthy when the final product has a high value, hardly for other products like fatty acids for biofuel production. This is why nowadays efforts in the field of microalgae cultivation are focused on the improving of biomass production systems, with the aim of obtaining a design meeting the criteria to make the biotechnological applications with this kind of organisms feasible.

---

The main problems in the culture of photosynthetic cells are related with the behavior of light when it goes through the culture, since very different light intensities appear among the different zones of the culturing device. In many configurations, some layers receive a very high light intensity, while as light goes through the culture; it is heavily attenuated reaching values under the minimum required for carrying out the photosynthesis. This is why the design of a photobioreactor must be based on a proper light supply, allowing a good biomass growth rate, minimizing photoinhibition and photosaturation. In a photobioreactor having a low optical density (low biomass concentration) and in a thin layer, approximately all the culture receives the same light intensity, but when talking about deep cultures or with a high biomass concentration, several phenomena produce different areas with different light intensities.

With the aim of achieving a good light distribution inside the photobioreactors, certain designs have been developed using artificial light sources. Lee et al. in their article "Photoacclimation of *Chlorella vulgaris* to Red Light from Light-Emitting Diodes Leads to Autospore Release Following Each Cellular División" (Lee and Palsson 1996) used LEDs, while Ogbonna et al. in their article "A Novel Internally Illuminated Stirred Tank Photobioreactor for Large-Scale Cultivation of Photosynthetic Cells" (Ogbonna et al. 1996) showed the use of fluorescent lamps.

However, the high cost of photosynthetic organisms producing mainly comes from the energetic consumption due to the use of artificial light and the mixing systems. For these reasons, more recently the use of solar light has been stated to be more proper, resulting in an economical and environmental advantage. Nowadays the only light source that could be considered to be economically viable in order to produce certain microalgae derived compounds, like oils for biofuel, is the solar light. The main problems related to its use are its cyclic variations and the excessive irradiation over the upper layers of the culture, resulting in photoinhibition occurring. In order to solve these problems, the possibility to capture, concentrate and distribute the light in a convenient way inside the culture has been considered. However, technologies using this technique are expensive and energy losses may be significant.

With the aim of introducing the light inside the photobioreactor volume, designs based on optical fiber, like the configuration presented by Ogbonna et al. in their article "An integrated solar and artificial light system for internal illumination of photobioreactors" (Ogbonna, Soejima, and Tanaka 1999), have been developed, but it requires a high economical and technological initial investment.

The photobioreactor presented in Hsieh and Wu in their article "A novel photobioreactor with transparent rectangular chambers for cultivation of microalgae" (Hsieh and Wu 2009) is also based on light distribution criteria and tries to guide the

light along the depth of open tanks. Light enters in a rectangular empty chamber where it is distributed, in form of diffuse light, through their lateral walls. However, this increase of the illuminated surface must be carefully done, since the optimization of productivity implies the control and knowledge of the culturing parameters and variables in order to monitor and model the process. This configuration is registered as patent US20090130747 (Wen-Teng and Hsieh 2009).

On the way to make use of all the solar incident irradiance over the reactor surface trying to avoid photoinhibition in the upper layers of the culture, Zijffers et al. show in their article “Capturing sunlight into a photobioreactor: Ray tracing simulations of the propagation of light from capture to distribution into the reactor” (Zijffers et al. 2008) another design that addresses the subject of driving the light deep into the reactor, in this case by means of solar concentrators and propagation of the concentrated beam along vertical plastic guides.

Other designs that attempt to distribute the light by means of an increase of the reception surface are those shown in the patent applications JP10304872 and JP10108665 for hydrogen producing bacteria culturing. They include elements driving and spreading the light towards the cell culture. The photobioreactor receives the light through a narrow opening in the upper part and it is distributed over a higher surface. The opening crosses a diffusing element that may be a rectangular or a triangular prism. The length of these structures is equal to the depth of the reactor tank, dividing the reactor in different chambers.

The patent ES 2238275 T3 (Brucker et al. 2005) presents also a photobioreactor that consists on a reaction chamber with transparent walls, where the illuminated surface is larger than the surface wrapping the reaction chamber. This is achieved by means of an undulating surface. Furthermore, the wall material would contain substances able to displace the wavelength of the incident radiation. In spite of achieving a higher irradiated surface with respect to other configurations, the direction of the incident beams is not optimized.

Finally, it is worth saying that not only lighting costs must be taken into account, also other maintenance costs such as cleaning and oxygen extraction in the case of closed systems where gases exchange hardly occur. Low ground surface occupancy is another valuable characteristic of an economically efficient photobioreactor.

### **5.3. Summary of the invention**

The present invention aims to solve the above mentioned drawbacks of phototrophic organisms culturing devices, enhancing the efficiency with respect to the

---

current culturing technologies.

The invention describes a photobioreactor being formed by a tank including a culture media with biomass growing on it. The culture medium, the biomass and the luminous radiation play a role inside this tank. At least one transparent conical structure is totally or partially submerged with its base in the upper part of the culture and the apex pointing to the bottom, driving the light to the culture in the tank.

In a possible embodiment of the invention, the luminous radiation is solar light and the invention includes a solar tracking system that allows the cones to tilt with its axis in the direction of the direct radiation in such a way that solar beams always enter into the cone perpendicularly to its base. In another possible embodiment of the invention, the luminous radiation is artificial light, where the invention includes a light source above the photobioreactor or inside at least one conical structure.

Preferably, the base of the cone is placed a distance above the water surface in order to avoid water splashing over the cone base. An additional height may be needed to avoid the base to be submerged when the cones are tilted. The cones are preferably made with transparent or translucent plastic. Furthermore, this plastic can contain substances able to select or even modify the wavelength of the light that goes through it. The plastic can constitute only the lateral walls of the cone, without base, or the whole cone. When the cones have not a plastic base, the whole photobioreactor should have a protective cover in order to avoid dirt to deposit on the cone's wall.

In a preferable implementation the photobiorreactor would include a system to inject and diffuse air in the form of bubbles to ensure the mixing in the reactor and to provide the CO<sub>2</sub> needed by the organisms. Furthermore, the air supplied can be CO<sub>2</sub> enriched, or even replaced by pure CO<sub>2</sub>.

Preferably, the photobioreactor also includes a harvesting and separation biomass system, which can be external or being integrated in the tank. Several configurations may be implemented when the system is inside the tank. In a possible embodiment, the separation system consists on the inclination of the bottom of the tank in order to favor the solids concentration. Alternatively, the photobioreactor contains a floating biomass separation system by means of surface scrapers.

Preferably, the photobioreactor comprises a nutrients and water supply system. The phototrophic organisms are preferably microalgae. The advantages of the invention are made evident in the following description.



#### 5.4. Brief description of the drawings

For a better understanding of the characteristics of the invention and complementing the description, a set of drawings accompanies this document in accordance to a preferable example of embodiment. These drawings are:

**Figure 5.1** represents the scheme of an elemental unit of this photobioreactor in accordance to an embodiment of the present invention.

**Figure 5.2** shows a scheme of the photobioreactor in accordance to an embodiment of the present invention, in which the transparent conical structures remain in vertical position.

**Figure 5.3** shows a scheme of the photobioreactor in accordance to an embodiment of the present invention, in which the transparent conical structures remain in inclined position.

**Figure 5.4** shows an example of the photobioreactor with a biomass separation system consisting on an external solid-liquid separation system, in accordance to an embodiment of the present invention.

**Figure 5.5** shows another example of the photobioreactor with a biomass separation system by means of solids concentration in the same photobioreactor, in accordance to an embodiment of the present invention.

**Figure 5.6** shows another example of the photobioreactor with a biomass separation system by means of flotation and solids concentration in one side of the same photobioreactor, in accordance to an embodiment of the present invention.

#### 5.5. Detailed description of the invention

Some preferable embodiments in accordance to the present invention are described below, without limiting other possible embodiments or combination of embodiments different than those described.

In order to achieve high biomass productivity, the optimization of the environmental factors and operational conditions are needed. Some of them are relatively easy to control, like temperature and nutrients supply, not occurring the same in the case of light supply, which is one of the hardest to control. From this point of view, internally illuminated photobioreactors are an interesting alternative to conventional systems, since on the one hand they meet most of the advantages of open systems and, on the

---

other hand, they allow for some control of the culture conditions. In addition, guiding the light deeper allows for more compact—in terms of ground surface occupancy—photobioreactors.

In this document a photobioreactor comprising a tank with introduction of light by means of inverted transparent conical structures is described. The aforementioned structures are placed in such a way that their base is above the culture level and their apex is submerged. So as to simplify, in this text the photobioreactor may be called reactor, having both terms the same meaning.

The described photobioreactor allows for phototrophic organisms culturing, especially microalgae. Non limiting examples of microalgae that could be cultured in this reactor are *Chlorella vulgaris*, *Isochrysis galbana*, *Pavlova lutheri*, etc.

Figure 5.1 shows a unit of volume of the present photobioreactor. The unit of volume can be defined as a cone with its field of influence. In this figure, the cone (11) is housed in a fictitious cylinder (16) that retains the volume of culture included in this unit of volume. In other words, a photobioreactor would contain a certain number of identical units of volume, each one comprising a cone and a portion of culture media and biomass. In the case of the unit of volume, the base of the cone (110) coincides with the upper base of the cylinder. Alternatively, the cone could be substituted by a truncated cone if it is preferred due to constructive reasons. The arrangement of these conical structures in the photobioreactor depends on intrinsic characteristics of the species to be cultured and the selected illumination system. In the case of solar light, the arrangement should be optimized for the geographical place where the photobioreactor is going to be implemented. The tank (15) comprises the culture medium.

This conical structure would be built with a transparent or translucent material, whose transmittance should be as high as possible. Some examples of plastics are Low Density Polyethylene (LDPE) or Ethylene Vinyl Acetate (EVA) and examples or additional substances that can be added to improve the quality of the light are transition elements.

In Figure 5.1 the space between the cone (11) and the fictitious cylinder (16) contains the culture medium, which is composed by the required nutrients for the growing of the cultured biomass. This biomass receives the solar light composed by the direct (12), the diffuse (13) and the reflected (14) radiation that hits the wall of the cone or the artificial light. The light is transferred to the culture medium after going through the walls of the cone (11). Once in the culture, light is captured by the cells and it is utilized in the photosynthesis process, where microorganisms use CO<sub>2</sub>, water and light, together with the supplied nutrients, in order to produce biomass.

Due to this configuration, the photobioreactor has an enlarged illuminated surface to culture volume ratio in comparison to other previously mentioned geometries. This is achieved by distributing the light that would irradiate the base of the cone throughout the inner surface of the cone. As a consequence, it is possible to increase the photobioreactor depth, thus for a given volume the occupied ground surface is smaller.

The base (110) of the cone (11) when they are in vertical position is placed above the water level, at a distance that allows the cones to tilt to a given angle while their base remains always over the water level and the possible splashing due to the turbulence of the medium. The conical or frustoconical structure may have the upper base or be open. In case of an open cone, the photobioreactor will be preferably covered with a transparent or translucent surface.

The photobioreactor can work with solar or artificial light. When an artificial light source is used, the cones remain static and in vertical position, as shown in Figure 5.2. In this case, they receive the light from one or several sources situated on top of the reactor (not shown in the drawing). As represented in Figure 5.2, the cones (21) are submerged in a reaction chamber (25) that contains the culture medium. As indicated, the base of the cone (21) is placed above the minimum margin (29) needed due to the turbulence of the medium. The submerged conical structures (21) are supported by a structure whose details are out of the scope of this patent.

When solar light is used, the conical structures (31) are tilted in the direction of the direct solar beams (32) as shown in Figure 5.3. For such a purpose the photobioreactor is equipped with a solar tracking system (not represented in the drawings) that makes the cones to tilt to a certain angle depending on the solar elevation and to move in the horizontal plane depending on the Azimuth angle. In this way, the irradiance supplied to the culture can be optimized on the way to avoid photoinhibition and photolimitation phenomena. The submerged conical structures (31) are supported by a structure whose details are out of the scope of this patent.

Furthermore, when the photobioreactor is going to be used with solar light, as in Figure 5.3, an additional margin (332) must be considered in order to avoid the base of the cone (31) to be submerged when the cones are tilted to their maximum angle. The tilting angle coincides with the solar elevation angle, which depends on the hour and the day of the year as well as on the latitude. At the same time, the margin (332) determines the minimum distance that must be kept between a cone and the nearest one to avoid them to touch each other when they are inclined.

When the cone receives solar irradiance, the light intensity over its inner surface is homogeneous and proportional (by means of the Lambert's Cosine Law) to the

---

irradiance over a horizontal surface of the geographical place where the reactor is located. Then, the incident irradiance depends on the angle of the lateral wall of the cone (half of the aperture angle) which means that the irradiance over the culture can be adjusted as a function of the species to be cultured and the irradiance of the geographical place by optimizing this angle.

The irradiance that reaches the inner surface of the cone is not totally transmitted; there is a fraction that is reflected, to a higher or a lower extent, depending on the angle of incidence and the refraction index of the material of the cone. Part of the radiation can be reflected as diffuse radiation while other part can be reflected as direct radiation. The portion that is reflected as direct radiation is directed towards a deeper part of the cone, establishing different cone's sections with different received irradiance. Due to the shape and the arrangement of the cones (31), most of the reflected irradiance is directed towards the bottom of the reactor, minimizing the energy loss.

In both cases —with solar or artificial light— carbon dioxide is needed for phototrophic organisms' growth. It can be supplied by means of several methods: by diffusion from atmospheric air, by an air flow or a CO<sub>2</sub> enriched air flow injection or by means of both methods simultaneously. The convenience of using simply air or CO<sub>2</sub> enriched air depends on the metabolic requirements of the species to be cultured and the goal of the culture. The injection of air or CO<sub>2</sub> enriched air is achieved by means of diffusers (28 and 38) located in the lower part of the reactor that supply bubbles that go up through the culture volume. Aeration, besides acting as carbon supply, favors the mixing and shaking of the culture, thus allowing for a proper homogenization of the content of the tank. In case of need, agitators (220 and 320) may be placed inside the reactor in order to increase the mixing intensity.

Figure 5.4 shows a possible embodiment of the present invention that includes an external solid-liquid separation system —or biomass-water separation— allowing for biomass extraction. This system may be applied to solar or artificial light photobioreactors. The solid-liquid separation system shown in Figure 5.4 is implemented by means of an external unit (440) and can employ a method like decantation, flotation, centrifugation, filtration or others. Afterwards biomass is extracted (445). In this case, the liquid effluent of the solid-liquid separation unit (440) returns through a pipe (445) to the photobioreactor, contributing to nutrient and water supply. Furthermore, the supply of water (442) and nutrients (443) may be alternatively carried out by means of direct dosage. The embodiment shown in Figure 5.4 presents also the inlet air or CO<sub>2</sub> enriched air piping (444) and the injection devices (48).

Alternatively, the photobioreactor can contain the harvesting system in the cultur-

ing tank. Examples are showed in Figure 5.4 and Figure 5.5, where the photobioreactor are configured to extract the biomass by sedimentation or by flotation respectively.

In accordance with another embodiment of the invention, as illustrated in Figure 5.5, the solid-liquid separation system is located inside the photobioreactor. As can be observed, this system is implemented by means of inclined walls in the bottom (559) in order to favor solids accumulation. The solid-liquid separation in this case is the decantation of microalgal biomass. Due to the force of gravity, particles with higher density than water settle and are accumulated thanks to the inclined walls. The extraction system (560) allows for biomass harvesting. For such a purpose, in the lower part of the solids concentration volume there is a pipe for biomass extraction, either by gravity or by pumping. Air diffusers (520), in case of existing, must be located at a height above the solids concentration volume (550) in order not to disturb this area. The implementation of Figure 5.5 shows also the inlet air or CO<sub>2</sub> enriched air piping (544) and the injection devices (58).

Figure 5.6 illustrates another embodiment of the photobioreactor, in this case with a solid separation system by means of a skimmer rake. In this case the harvesting principle is flotation, which is characteristic of light biomass (less dense than water) and favored by the aeration that takes places by means of the inlet air or CO<sub>2</sub> enriched air piping (644) and the injection devices (68). The skimmer rake is located in a quiet area; that is to say in a place out of the influence of the cones and the turbulence caused by the mixing. The skimmer rake comprises a system composed by scrapers, chains and a pulley that goes through the water surface with the scrapers partially submerged. In this way the scum is transported to a hopper. The pulley chain allows the scrapers to return to their initial position above the water. Alternatively, other systems meeting the same role may be implemented. Additionally, in the embodiment shown in Figure 5.6 the photobioreactor comprises the floating biomass extraction system (661) as well as the extraction system (660) from the solids concentration volume (650) placed in the bottom of the tank. Both systems may work simultaneously or alternatively.

Although in Figure 5.4 Figure 5.5 and Figure 5.6 the cones (41, 51 and 61) are vertically placed as in a photobioreactor using artificial light, the different solid-liquid separation systems described here could be used as well in a solar light photobioreactor.

---

## 5.6. Claims

1. A photobioreactor for phototrophic organisms culturing that comprises a tank (15, 25, 35, 45, 55, 65) containing a culture media and biomass inside the tank and in contact with said culture media,  
**characterized by** the existence of at least one transparent or translucent, conical or frustoconical structure (11, 21, 31, 41, 51, 61) partially or totally placed inside the mentioned tank (15, 25, 35, 45, 55, 65), through which the luminous radiation enters into the tank.
2. The photobioreactor of Claim 1, wherein said radiation is solar radiation and wherein the photobioreactor comprises a solar tracking system configured to orientate at least one conical or frustoconical structure (31) in the direction of said solar incident radiation.
3. The photobioreactor of Claim 1, wherein said radiation is artificial radiation and wherein the photobioreactor comprises at least one artificial light source above said photobioreactor or inside said at least one conical or frustoconical structure (21).
4. The photobioreactor according to any of the preceding claims wherein the largest base of said at least one conical or frustoconical structure (11, 21, 31, 41, 51, 61) is placed at a height (29, 332) above the maximum culture medium level (27, 37) comprised in the tank (25, 35).
5. The photobioreactor according to any of the preceding claims wherein said conical or frustoconical structure (11, 21, 31, 41, 51, 61) is made of a transparent or translucent plastic material.
6. The photobioreactor of Claim 5, wherein said transparent or translucent plastic material comprises at least one substance able to displace the wavelength of the received radiation.
7. The photobioreactor according to any of the preceding claims wherein said conical or frustoconical structure (11, 21, 31, 41, 51, 61) has its largest base open and is covered by a transparent or translucent plastic surface at certain height above the same.
8. The photobioreactor according to any of the preceding claims that also comprises a system to inject and diffuse the air (28, 38, 48, 58, 68) that provides an additional carbon supply.

9. The photobioreactor of Claim 8 wherein said injection and diffusion system (28, 38, 48, 58, 68) supplies CO<sub>2</sub> enriched air.
10. The photobioreactor according to any of the preceding claims comprising a biomass-liquid separation system consisting on an external device (440) for biomass extraction (445) and liquid recirculation (444) to the tank (45).
11. The photobioreactor according to any of Claims 1 through 9, comprising a biomass-liquid separation system, integrated in said photobioreactor.
12. The photobioreactor of Claim 11, wherein said biomass-liquid separation system, integrated in said photobioreactor, is based on the tank walls (550) inclination in order to favor biomass concentration in the bottom of the tank.
13. The photobioreactor of Claim 11, wherein said biomass-liquid separation system, integrated in said photobioreactor, comprises at least one device (660) for the extraction of floating biomass in the culture surface.
14. The photobioreactor according to any of the preceding claims, comprising a nutrients supply system (443, 543, 643) and a water supply system (442, 542, 642).
15. The photobioreactor according to any of the preceding claims, wherein said phototrophic organisms are microalgae.

---

# 5.7. Drawings

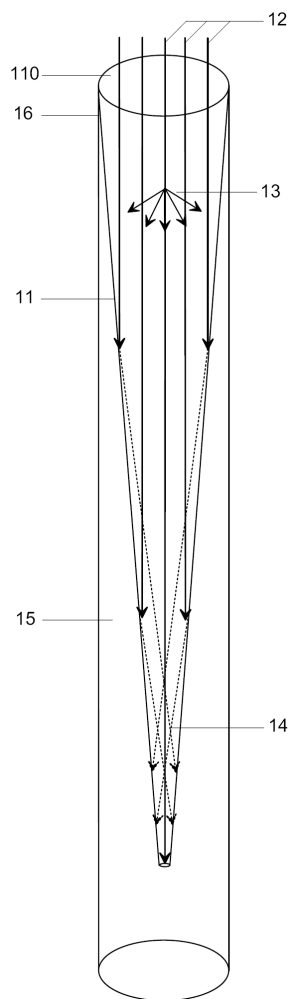


Figure 5.1: Basic unit of volume of the photobioreactor.



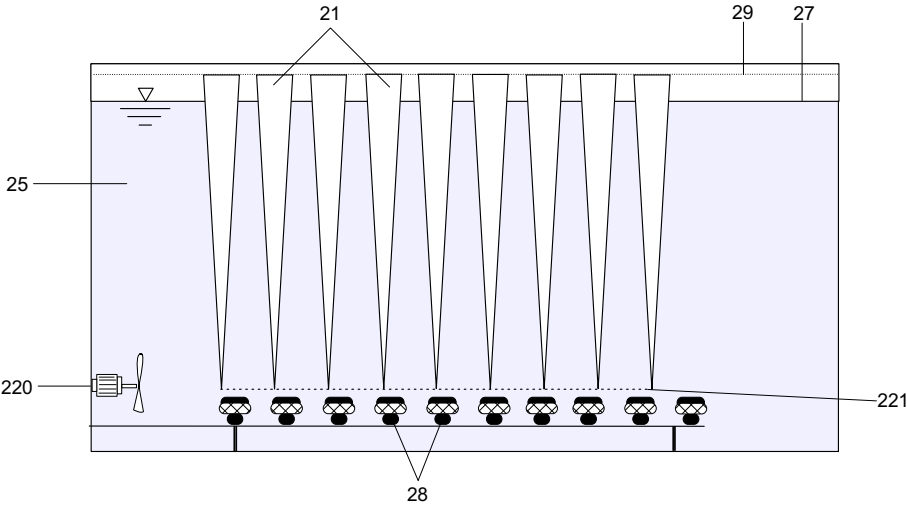


Figure 5.2: Implementation of the photobioreactor with the cones vertically placed.

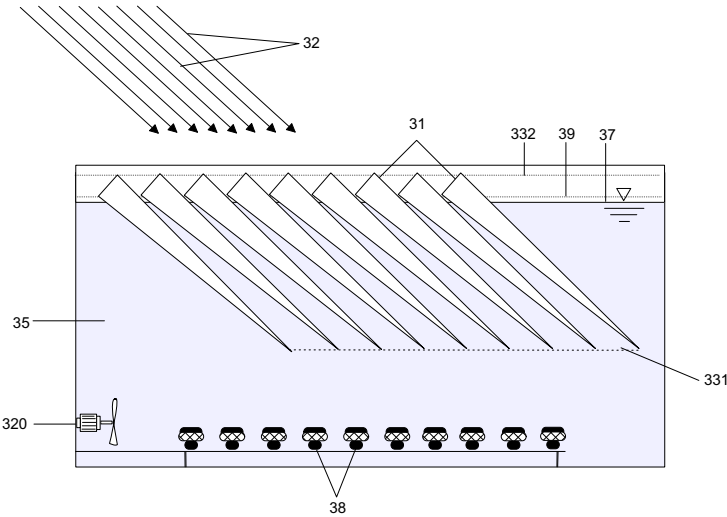


Figure 5.3: Implementation of the photobioreactor with the cones tilted in the direction of the direct solar radiation.

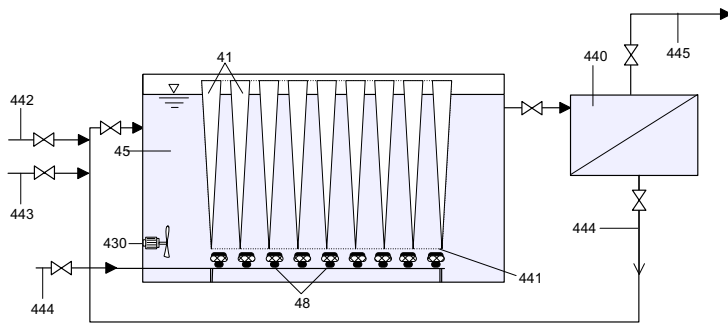


Figure 5.4: Possible implementation with an external harvesting system.

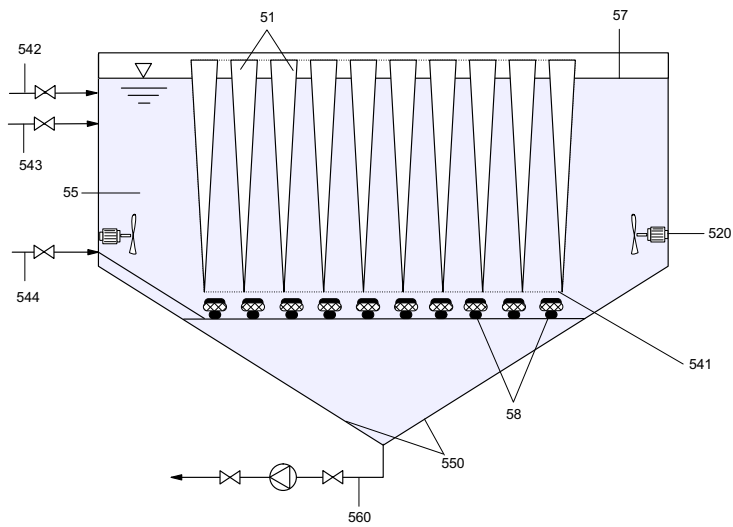


Figure 5.5: Possible implementation with the sedimentation clarifier in the culturing tank.

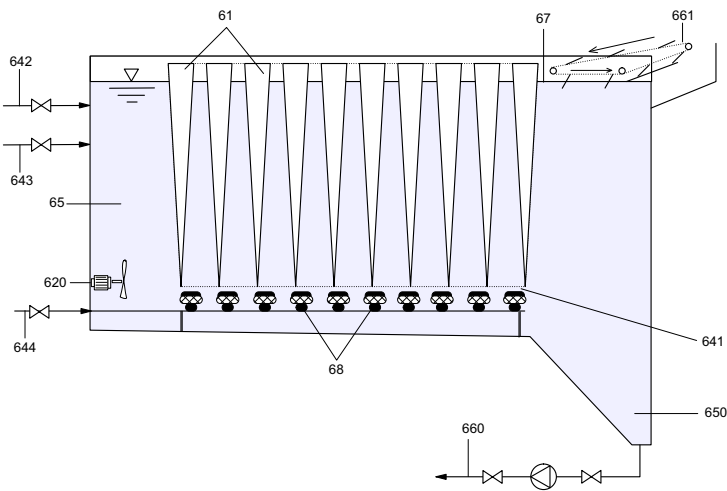
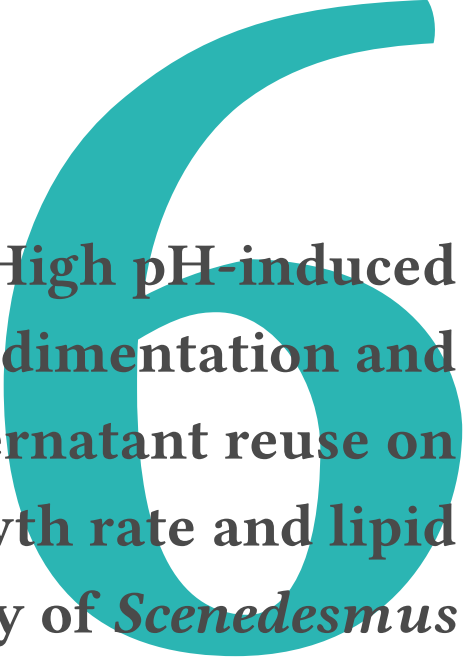


Figure 5.6: Possible implementation with sweeping device and lower concentrator.

---

## References

- Brucker, F. et al. (2005). *Photobioreactor with improved supply of light by surface enlargement, wavelength shifter bars or light transport*.
- Hsieh, C. H. and W. T. Wu (2009). "A novel photobioreactor with transparent rectangular chambers for cultivation of microalgae". In: *Biochemical engineering journal* 46.3, pp. 300–305.
- Lee, C. G. and B. Ø. Palsson (1996). "Photoacclimation of *Chlorella vulgaris* to red light from light-emitting diodes leads to autospore release following each cellular division". In: *Biotechnology progress* 12.2, pp. 249–256.
- Ogbonna, J. C., T. Soejima, and H. Tanaka (1999). "An integrated solar and artificial light system for internal illumination of photobioreactors". In: *Journal of Biotechnology* 70.1-3, pp. 289–297.
- Ogbonna, J. C. et al. (1996). "A novel internally illuminated stirred tank photobioreactor for large-scale cultivation of photosynthetic cells". In: *Journal of Fermentation and Bioengineering* 82.1, pp. 61–67.
- Wen-Teng, W. and C. Hsieh (2009). *System and Method of Enhancing Production of Algae*.
- Zijffers, J. W. F. et al. (2008). "Capturing sunlight into a photobioreactor: Ray tracing simulations of the propagation of light from capture to distribution into the reactor". In: *Chemical Engineering Journal* 145.2, pp. 316–327.



# 6

## High pH-induced flocculation-sedimentation and effect of supernatant reuse on growth rate and lipid productivity of *Scenedesmus obliquus* and *Chlorella vulgaris*

Part of this chapter has been published as: Castrillo, M.; Lucas-Salas, L.M.; Rodríguez-Gil, C.; Martínez D. High pH-induced flocculation-sedimentation and effect of supernatant reuse on growth rate and lipid productivity of *Scenedesmus obliquus* and *Chlorella vulgaris*. Bioresour Technol 128 (2013) 324-329

---



## Abstract

High pH-induced flocculation-sedimentation of *Scenedesmus obliquus* and *Chlorella vulgaris* was studied with the objective of improving the efficiency of microalgae harvesting, since it is one of the most expensive steps of production of microalgae. Desired pH values were achieved by addition of NaOH and  $\text{Ca(OH)}_2$ . Growth rate and lipid productivity in fresh media prepared with tap water and with analytical-grade water, and in reused media prepared with culture centrifuged supernatant and the supernatant from high pH-induced flocculation-sedimentation were compared. Since the growth rates for reused media were about 1.7 times higher than in fresh media, and the lipid productivities were about  $25 \text{ mg L}^{-1} \text{ d}^{-1}$  and  $26 \text{ mg L}^{-1} \text{ d}^{-1}$  in flocculated and centrifuged reused media respectively, medium reuse is a suitable method of saving water and nutrients contributing to the sustainability of the microalgae culturing process.

## Resumen

La floculación-sedimentación producida por aumento de pH fue estudiada con las especies de microalgas *Scenedesmus obliquus* y *Chlorella vulgaris*, con el objetivo de mejorar la eficiencia del proceso de recogida de las microalgas, la cual es una de las etapas que supone un mayor coste económico dentro del cultivo de estos organismos. Los valores de pH deseados se alcanzaron mediante adición de NaOH y  $\text{Ca(OH)}_2$ . Se compararon las tasas de crecimiento y las productividades lipídicas obtenidas en cultivos en medio fresco preparado tanto con agua de grifo como con agua destilada, y con medio reutilizado preparado con el sobrenadante del medio centrifugado y con el sobrenadante del medio clarificado mediante sedimentación-floculación por aumento de pH. Ya que las tasas de crecimiento para el medio reutilizado fueron aproximadamente 1,7 veces mayores que para medio fresco, y las productividades lipídicas  $25 \text{ mg L}^{-1} \text{ d}^{-1}$  y  $26 \text{ mg L}^{-1} \text{ d}^{-1}$  para sobrenadante de floculación y centrifugación respectivamente, la reutilización de medio de cultivo se mostró como un método viable para el ahorro de agua y nutrientes, contribuyendo a la sostenibilidad del cultivo de microalgas.





## 6.1. Introduction

Lipids produced by microalgae are viewed as a good alternative for fossil fuels (Chisti 2007); however, large-scale production of microalgae-derived fuels is not yet cost-effective on a large scale (Wijffels and Barbosa 2010). The cost of microalgae biomass harvesting strongly influences the cost of the final product, and may be between 20 % to 30 %, or even up to 60 % for certain compounds as final products, of the total cost of biofuel or other extracted chemicals (Grima et al. 2003). There are several problems that make microalgae recovery process difficult, such as the small size of the cells and electrostatic repulsion due to their negative surface charge (Papazi, Makridis, and Divanach 2010).

Furthermore, biomass contents usually are in the range of  $0.1 \text{ g L}^{-1}$  to  $1 \text{ g L}^{-1}$ , requiring handling of big volumes to harvest a small amount of biomass. An optimal harvesting technique should be independent of the cultured species, consume little energy and chemicals and not be harmful to the valuable products extracting process (Chen et al. 2011). Centrifugation, filtration and gravity settling are current harvesting methods. These processes may be preceded by a flocculation step. Centrifugation is the most rapid and reliable method, but due to its high cost, its implementation at large-scale is not considered (Christenson and Sims 2011). Flocculation-sedimentation is assumed to be more effective than centrifugation and gravity settling, since it allows treating large culture volumes and does not consume much energy. It can be also considered as a step for improving centrifugation or filtration yields (Lee et al. 2012). Several cell coagulants have been proposed, among them a wide variety of salts (Papazi, Makridis, and Divanach 2010) chitosan (Morales, Noüe, and Picard 1985; Ahmad et al. 2011) and starch (Vandamme et al. 2010).

Flocculation by using a flocculating microalgae to concentrate a non-flocculating microalgae has also been proposed as an effective and sustainable method (Salim et al. 2011). Microalgae flocculation induced by a high pH is also feasible (Vandamme et al. 2012). In the current study, flocculation of *Scenedesmus obliquus* and *Chlorella vulgaris* induced by the addition of NaOH or  $\text{Ca}(\text{OH})_2$  was studied. The latter forms calcium carbonate and precipitates at pH 9.1 to 9.5 acting as the sweep mechanism responsible (Leentvaar and Rebhun 1982). The presence of  $\text{CaCO}_3$  in the microalgae pellet adds value to the application of microalgae in animal feed, since most types of cattle fodder are supplemented with this compound. NaOH-induced precipitation requires the presence of calcium or magnesium (Semerjian and Ayoub 2003) and therefore, the magnesium concentration was measured before each assay.

In order to avoid the use of pure water, which would be unfeasible at large

---

scale, growth rate and lipid productivity were also studied using tap water and the supernatant of cultures after centrifugation and high pH-induced flocculation, since it could help to make microalgae culturing more sustainable. Supernatant reuse would become especially important since it also makes water and nutrients saving possible. A previous study (Kim et al. 2011) on the growth yield when using flocculated medium for subsequent algal cultivation found a decrease in growth yield of 8 % per cycle of flocculation and cultivation during 16 d in comparison with cultures in fresh and sterilized BG11. A yield increase by 10.3 % and 11.9 % was obtained when 20 % and 50 % of fresh BG11 medium was added, respectively. Wu et al. 2012 obtained similar biomass growth with reused medium and fresh medium. Lee et al. 1998 found no remarkable differences in lipid production yield when *Botryococcus braunii*, a green microalgae strain, was harvested by high pH and chemical treatments.

## 6.2. Methods

*S. obliquus* (CCAP 276/3A) and *C. vulgaris* (Beijerinck CCAP 211/ 11B) were supplied by the Culture Collection of Algae and Protozoa in Scotland, UK. High pH-induced flocculation-sedimentation experiments were carried out with both species, while supernatant reuse was only studied with *S. obliquus*.

### 6.2.1. Culture conditions

Microalgae cells for flocculation-sedimentation assays were cultivated in a 70 L photobioreactor, aerated with air enriched with 2 % CO<sub>2</sub> at a flow rate of 0.027 vvm and illuminated for 12 h per day with a Philips Master HPI Plus 400 W/767 lamp. Culture medium was BG11, which contained (g L<sup>-1</sup>): NaNO<sub>3</sub>, 1.5; K<sub>2</sub>HPO<sub>4</sub>, 0.04; MgSO<sub>4</sub>·7H<sub>2</sub>O, 0.075; CaCl<sub>2</sub>·2H<sub>2</sub>O, 0.036; citric acid, 0.006; green ammonium Fe<sup>3+</sup> citrate, 0.006; EDTANa<sub>2</sub>, 0.10; Na<sub>2</sub>CO<sub>3</sub>, 0.02; H<sub>3</sub>BO<sub>3</sub>, 0.0029; MnCl<sub>2</sub> · 4 H<sub>2</sub>O, 0.0018; ZnSO<sub>4</sub> · 7 H<sub>2</sub>O, 0.0002; Na<sub>2</sub>MoO<sub>4</sub> · 2 H<sub>2</sub>O, 0.0003; CuSO<sub>4</sub> · 5 H<sub>2</sub>O, 0.08 × 10<sup>-3</sup> and Co(NO<sub>3</sub>)<sub>2</sub> · 6 H<sub>2</sub>O, 0.05 × 10<sup>-3</sup> dissolved in distilled water. The pH of the medium was adjusted to 7.1. The microalgae cells were harvested after reaching stationary phase.

### 6.2.2. Flocculation-sedimentation assays

Flocculation-sedimentation was studied by adjusting the pH of cultures to 10, 10.4, 10.8, 11.2, 11.6 and 12 with 1 M NaOH and a suspension of Ca(OH)<sub>2</sub>. Before the assays, the magnesium concentration and dry weight were measured. For the dry weight analysis, the samples were filtered through a previously dried Whatman

paper filter GF/C 47 mm and dried at 103 °C until constant weight. The absorbance was measured at 685 nm with a spectrophotometer (DR3800 Hach Lange). Assays were carried out in triplicate in 50 mL Falcon tubes (Figure 6.1). After pH adjustment, the cultures were shaken using a vortex during 30 s and left undisturbed for 60 min in the dark at room temperature.

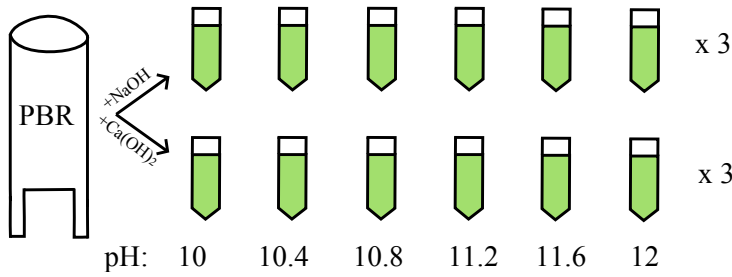


Figure 6.1: Flocculation-sedimentation assays scheme.

Recovery efficiency was calculated based on optical density measurements (Lee, Lewis, and Ashman 2009):

$$\text{Recovery efficiency (\%)} = 1 - \frac{ABS_i}{ABS_f} \cdot 100$$

where  $ABS_f$  is the absorbance of the sample taken at the end of the experiment and  $ABS_i$  is the absorbance of the sample taken at the beginning of the experiment.

### 6.2.3. Supernatant reuse assay

Growth and lipid productivity were compared in cultures prepared with the supernatants of centrifugation and flocculation-sedimentation and in cultures prepared with tap water and analytical grade water. For preparing the supernatant media, volumes of 4.5 L were recovered from a culture of *S. obliquus*, grown in a photobioreactor, by NaOH-induced flocculation-sedimentation at pH 12 and by centrifugation at 3852 58g for 10 min, respectively. The supernatant were filtered using 0.45 µm polycarbonate filters. Essential nutrients ( $\text{NO}_3\text{-N}$  and  $\text{PO}_4\text{-P}$ ) concentrations were determined by photometric analyses (Spectroquant Nitrate Test 1.14773.0001 and Spectroquant Phosphate Test 1.14848.0002 respectively) using a spectrophotometer DR 3800 Hach Lange after filtration and those nutrients that were in shortage were added in the form of  $\text{NaNO}_3$  and  $\text{K}_2\text{HPO}_4$  to achieve concentrations of  $34 \text{ mg L}^{-1}$

---

$\text{NO}_3\text{--N}$  and  $3.4 \text{ mg L}^{-1} \text{ PO}_4\text{--P}$ , which have been seen as suitable for lipid production by *S. obliquus* in previous studies (unpublished data). The pH was adjusted to 7.1 with 1 M HCl. The two media were sterilized in an autoclave (Presoclave-II, Selecta) at  $121^\circ\text{C}$  and 1.2 atm during 20 min, inoculated with *S. obliquus* and divided between three identical flasks. The two other case studies were performed with the same conditions but using tap water and analytical-grade water provided by an Elix Advantage System (Millipore), in triplicate too. The cultures were placed in a growth chamber, aerated with air enriched with 2%  $\text{CO}_2$  at a flow rate of 0.027 vvm and shaken at 350 rpm. The temperature was  $22.0 \pm 0.2^\circ\text{C}$  and the light intensity was  $145 \mu\text{E m}^{-2} \text{ s}^{-1}$ . Both aeration and light were supplied for 12 h per day.

Biomass growth was measured by the absorbance at 685 nm with a spectrophotometer DR3800 Hach Lange. The number of cells was counted with the aid of a Thoma counting chamber. Dry weight was measured as described in Section 6.2.2. Essential nutrients were monitored by the photometric analyses specified in the previous paragraph.

Biomass was harvested when cultures had remained 7 d under nitrogen stress ( $\text{NO}_3\text{--N}$  under  $7 \text{ mg L}^{-1}$ ) half volume by centrifugation at 3852 28g for 5 min and half volume by flocculation with 1 M Na(OH) at pH 11.4 for 2 h (analytical-grade water medium was harvested by centrifugation only). The harvested algae were stored at  $30^\circ\text{C}$ .

An scheme of the developed assays is shown in Figure 6.2.

#### 6.2.4. Lipid extraction and screening

The microalgae samples were previously freeze-dried (Virtis Benchtop K, SP Scientific Inc.), sonicated for 15 min (Vibra-Cell™ Ultrasonic Processor) and dried at  $60^\circ\text{C}$  over-night. The resulting microalgae powder was hydrolysed with 4 M HCl in a hydrolysis unit (B-411/E-416 Büchi, Switzerland). Lipids were extracted by warm Soxhlet method by an extraction system B-811 (Büchi, Switzerland). Lipid percentage was calculated for each replicate. Afterwards lipid samples were put together by treatment in order to have enough quantity to carry out the lipid profile screening. The fatty acid composition was analyzed by an external laboratory. The employed method was GC-MS preceded by derivatization with trimethylsulfonium hydroxide (TMSH), according to the method described in EN ISO 12966-3:2009 (12966 2009). Fatty acid composition was calculated as the percentage of each fatty acid methyl ester (FAME) in the samples.

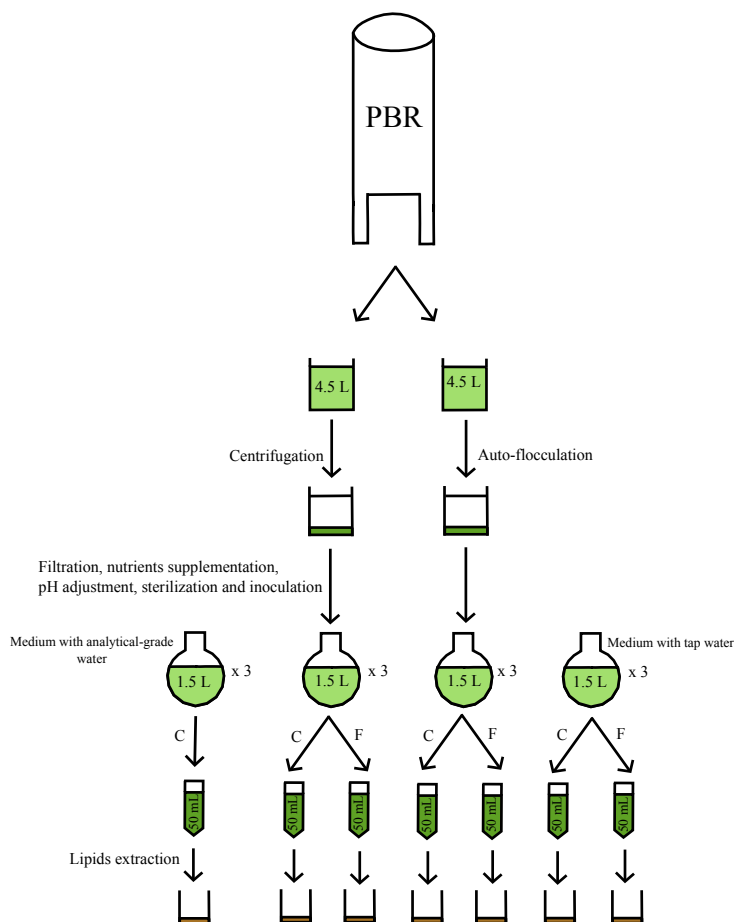


Figure 6.2: Supernatant reuse assays scheme.

### 6.2.5. Statistical analyses

Statistical analyses of the data were carried out with IBM SPSS Statistic 19. Results were considered highly significant when  $\alpha < 0.01$  or significant if  $0.01 < \alpha < 0.05$ . In order to compare results, data were analyzed with t-Student or ANOVA and DHS Tukey post hoc analyses as parametric and Kruskal-Wallis and Mann-Whitney U-tests with Bonferroni correction as non-parametric tests. In charts, error bars show 95 %

confidence intervals of the mean.

## 6.3. Results and discussion

### 6.3.1. Flocculation-sedimentation assays

The assays for *S. obliquus* and *C. vulgaris* were carried out at biomass concentrations of  $0.428 \text{ g L}^{-1}$  and  $0.450 \text{ g L}^{-1}$  respectively. The magnesium concentrations in the medium prior to base additions were under the detection limit ( $5 \text{ mg L}^{-1}$ ) and  $6.6 \text{ mg L}^{-1}$  for *S. obliquus* and *C. vulgaris*, respectively. No significant differences were detected between assays carried out with the same species but highly significant differences were seen when comparing assays with different microalgae, except in the comparison between *S. obliquus* with  $\text{Na(OH)}$  and *C. vulgaris* with  $\text{Ca(OH)}_2$ .

Absorbance results for flocculation-sedimentations are showed in Table 6.1 and Table 6.2.

pH	<i>S. obliquus</i> with $\text{Na(OH)}$			<i>S. obliquus</i> with $\text{Ca(OH)}_2$		
	$ABS_0$	$ABS_f$	RE (%)	$ABS_0$	$ABS_f$	RE (%)
10	1.36	1.156	15.00	1.428	1.308	8.40
	1.36	1.218	10.44	1.428	1.296	9.24
	1.36	1.238	8.97	1.428	1.338	6.30
10.4	1.36	1.132	16.76	1.428	0.895	37.32
	1.36	1.156	15.00	1.428	0.863	39.57
	1.36	1.284	5.59	1.428	1.105	22.62
10.8	1.36	0.652	52.06	1.428	0.385	73.04
	1.36	0.632	53.53	1.428	0.359	74.86
	1.36	0.736	45.88	1.428	0.363	74.58
11.2	1.36	0.518	61.91	1.428	0.344	75.91
	1.36	0.561	58.75	1.428	0.383	73.18
	1.36	0.555	59.19	1.428	0.386	72.97
11.6	1.36	0.282	79.26	1.428	0.301	78.92
	1.36	0.298	78.09	1.428	0.31	78.29
	1.36	0.293	78.46	1.428	0.307	78.50
12	1.36	0.292	78.53	1.428	0.139	90.27
	1.36	0.256	81.18	1.428	0.157	89.01
	1.36	0.268	80.29	1.428	0.148	89.64

Table 6.1: Initial and final absorbance and calculated recovery efficiency in assays with *S. obliquus*.

## 6. High pH-induced flocculation-sedimentation and effect of supernatant reuse

pH	<i>C. vulgaris</i> with Na(OH)			<i>C. vulgaris</i> with Ca(OH) <sub>2</sub>		
	<i>ABS</i> <sub>0</sub>	<i>ABS</i> <sub>f</sub>	RE (%)	<i>ABS</i> <sub>0</sub>	<i>ABS</i> <sub>f</sub>	RE (%)
10	2.016	1.947	3.42	2.016	1.935	4.02
	2.016	1.929	4.32	2.016	1.962	2.68
	2.016	1.92	4.76	2.016	1.959	2.83
10.4	2.016	1.935	4.02	2.016	1.785	11.46
	2.016	1.932	4.17	2.016	1.815	9.97
	2.016	1.941	3.72	2.016	1.809	10.27
10.8	2.016	1.902	5.65	2.016	1.896	5.95
	2.016	1.896	5.95	2.016	1.887	6.40
	2.016	1.911	5.21	2.016	1.89	6.25
11.2	2.016	1.845	8.48	2.016	1.524	24.40
	2.016	1.839	8.78	2.016	1.56	22.62
	2.016	1.845	8.48	2.016	1.596	20.83
11.6	2.016	1.554	22.92	2.016	0.96	52.38
	2.016	1.566	22.32	2.016	0.954	52.68
	2.016	1.569	22.17	2.016	0.918	54.46
12	2.016	1.284	36.31	2.016	0.55	72.72
	2.016	1.266	37.20	2.016	0.553	72.57
	2.016	1.239	38.54	2.016	0.601	70.19

Table 6.2: Initial and final absorbance and calculated recovery efficiency in assays with *C. vulgaris*.

Figure 6.3 shows the recovery efficiency of the microalgae biomass as a function of pH and type of base.

At pH values higher than 10.8, the effectiveness of the process rose with pH increase for both NaOH and Ca(OH)<sub>2</sub>, but considerably better results were obtained when Ca(OH)<sub>2</sub> was used. Smith and Davis 2012 found that the minimum Mg<sub>2</sub><sup>+</sup> concentration in the medium under ideal conditions should be between 1.5 % to 2.4 % of algal dry mass. These values may increase when organic matter is present in the medium. In the present experiments the relation between Mg<sub>2</sub><sup>+</sup> concentration and dry mass were 1.16 % and 1.5 % for *S. obliquus* and *C. vulgaris* respectively. Highly significant differences in the recovery efficiency for *C. vulgaris* and *S. obliquus*, when using NaOH were observed. In the case of *S. obliquus*, these results are in accordance with those of Smith and Davis 2012; however, the behavior of *C. vulgaris* was different as only very weak flocculation even at pH values higher than 11 were obtained, although magnesium had been detected in the sample.

The fact that *C. vulgaris* did not present a good flocculation-sedimentation using

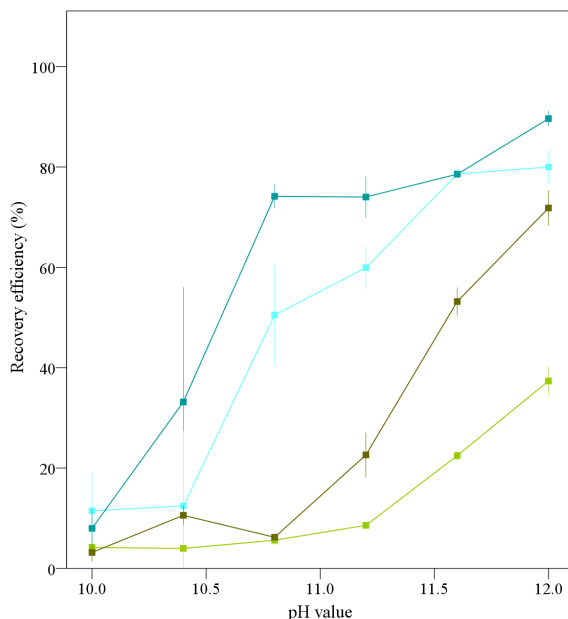


Figure 6.3: *S. obliquus* and *C. vulgaris* recovery efficiency as a function of pH achieved with different bases. (●) *S. obliquus* with NaOH; (■) *S. obliquus* with  $\text{Ca(OH)}_2$ ; (●) *C. vulgaris* with NaOH; (■) *C. vulgaris* with  $\text{Ca(OH)}_2$ . Error bars represent 95 % confidence intervals of the mean.

Na(OH) although magnesium was present, suggests that there is another factor governing its mechanisms. It is possible that *C. vulgaris* released polysaccharides that inhibited flocculation as observed by Wu et al. 2012 who noted a decrease in flocculation efficiency from 92 % to 7 % when  $70 \text{ mg L}^{-1}$  of polysaccharide were added to the medium. Furthermore, in the case of Vandamme et al. (Vandamme et al. 2012), where good results in flocculation of *C. vulgaris* were achieved, microalgae were resuspended in fresh medium, resulting in a removal of organic matter. This could have made the difference with the results of the present work.

Although  $\text{Ca(OH)}_2$  proved to be an efficient precipitating agent, the formation of  $\text{CaCO}_3$  precipitates that remain in the microalgal pellet causes trouble when lipids are extracted by means of acid hydrolysis using HCl due the reaction between  $\text{CaCO}_3$  and HCl. Therefore,  $\text{Ca(OH)}_2$  might be better suited for algae used in wastewater treatment and in animal feed rather than in biofuel production.



### 6.3.2. Supernatant reuse assay

#### 6.3.2.1. Biomass growth

Biomass growth is represented in Figure 6.4 and Figure 6.5 and doublings time in Figure 6.6. The statistical analyses showed that differences in cells count only existed between analytical-grade water and the other types of water, but not between different reused media or between them and tap water. No significant differences in algae dry weight were observed between analytical-grade water and tap water or between supernatant of flocculation and supernatant of centrifugation, but highly significant differences were noticed between fresh media and reused media, resulting in higher growth in the case of reused media. Maximum dry weight was about  $1.4 \text{ g L}^{-1}$  in fresh media while  $1.6 \text{ g L}^{-1}$  and  $1.7 \text{ g L}^{-1}$  were reached in supernatant of centrifugation and supernatant of flocculation respectively. Average doubling times were  $1.94 \pm 0.60 \text{ d}$  for cultures grown in medium prepared with analytical-grade water,  $2.05 \pm 0.60 \text{ d}$  with tap water and  $1.63 \pm 0.60 \text{ d}$  with recycled medium via centrifugation and  $1.66 \pm 0.60 \text{ d}$  with recycled medium via auto-flocculation.

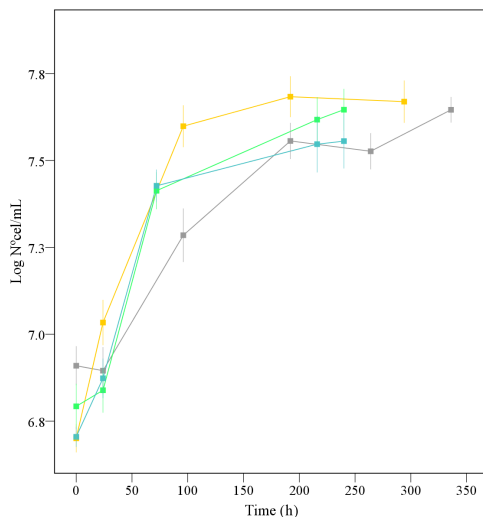


Figure 6.4: *S. obliquus* cells counts per mL of culture over time in (■) fresh medium made with analytical-grade water; (■) fresh medium made with tap water; (■) supplemented supernatant of flocculation by adding NaOH until pH 12; (■) supplemented supernatant of centrifugation at 3852.28g for 10 min. Error bars represent 95 % confidence intervals of the mean.

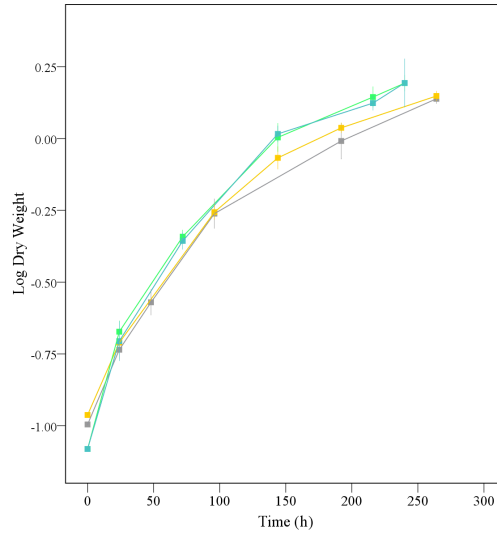


Figure 6.5: *S. obliquus* dry weight over time in (■) fresh medium made with analytical-grade water; (●) fresh medium made with tap water; (■) supplemented supernatant of flocculation by adding NaOH until pH 12; (■) supplemented supernatant of centrifugation at 3852.28g for 10 min. Error bars represent 95 % confidence intervals of the mean.

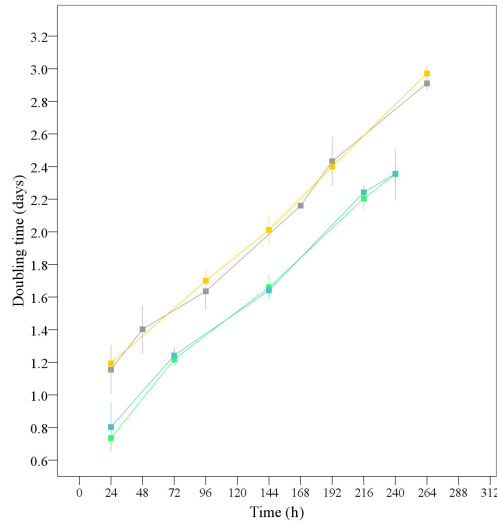


Figure 6.6: *S. obliquus* doubling time over time in (■) fesh medium made with analytical-grade water; (●) fresh medium made with tap water; (■) supplemented supernatant of flocculation by adding NaOH until pH 12; (■) supplemented supernatant of centrifugation at 3852.28g for 10 min. Error bars represent 95 % confidence intervals of the mean.

### 6.3.2.2. Lipid Production

Although the highest lipid content appeared in analytical-grade water medium, the productivity was higher in the two reused media due to the higher biomass productivity in reused media as concluded in the previous section. Lipid content (%), concentration ( $\text{g L}^{-1}$ ) and productivity ( $\text{mg L}^{-1} \text{d}^{-1}$ ) for the different types of water and different harvesting methods are shown in Table 6.3.

When the lipid productivities ( $\text{mg L}^{-1} \text{d}^{-1}$ ) were compared between samples obtained by centrifugation and samples obtained by flocculation with Na(OH), no significant differences were noticed except for cultures grown in tap water medium (Figure 6.7), however, significant differences were observed depending on the type of water of the culture media.

For samples collected by centrifugation, differences appeared between tap water and both –centrifuged and flocculated– reused media and between analytical-grade water and centrifuged media. For samples collected by flocculation, highly significant differences resulted when results for tap water and both reused media are compared.

In both cases the highest productivities were obtained for those cultures grown in medium with the supernatant of centrifugation, followed by those grown in medium with the supernatant of flocculation, while the lowest were those grown in tap water medium. This outcome may be due to the high volume of NaOH needed for reaching a pH value of 11.4 in medium prepared with tap water, which could have interfered in the later hydrolysis process.

Type of water	Harvesting method	Lipid content (%)		Lipid concentration ( $\text{g L}^{-1}$ )		Lipid productivity ( $\text{mg L}^{-1} \text{d}^{-1}$ )	
		M	SD	M	SD	M	SD
Analytical-grade	Centrifugation	18.147	0.789	0.250	0.013	22.689	1.196
Tap water	Centrifugation	16.884	0.000	0.237	0.004	21.591	0.354
	Flocculation	8.477	0.001	0.119	0.002	10.840	0.178
C. supernatant	Centrifugation	16.907	0.001	0.264	0.007	26.367	0.697
	Flocculation	16.708	0.000	0.261	0.007	26.056	0.689
F. supernatant	Centrifugation	16.547	0.002	0.259	0.021	25.884	2.051
	Flocculation	16.131	0.001	0.252	0.020	25.234	1.999

Table 6.3: *S. obliquus* lipid content (%), concentration ( $\text{g L}^{-1}$ ) and productivity ( $\text{mg L}^{-1} \text{d}^{-1}$ ) for the different types of water and different harvesting methods. M: mean; SD: Standard Deviation.

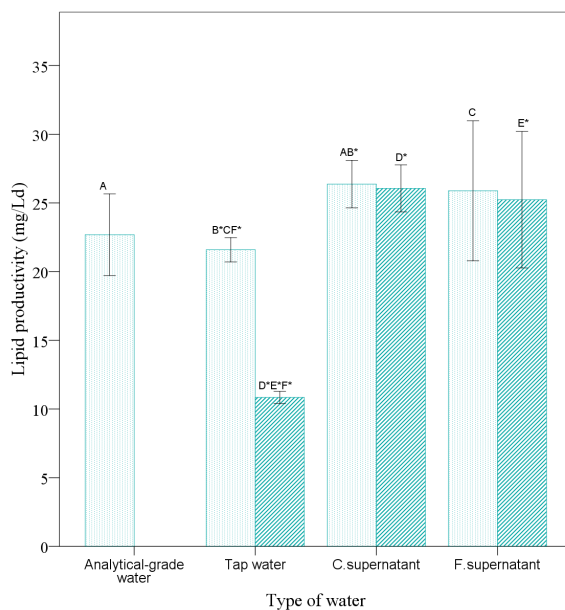


Figure 6.7: *S. obliquus* lipid productivity ( $\text{mg L}^{-1} \text{d}^{-1}$ ) after 7 d of N-stress and harvested by (dots) centrifugation at 3852 28g for 5 min; (lines) flocculation with NaOH at pH 11.4. Significant differences are indicated by means of pairs of capital letters, with an asterisk in the case of highly significant differences. Error bars represent 95 % confidence intervals of the mean.

### 6.3.2.3. Fatty acid profile

The fatty acids found in the samples are gathered in Table 6.4. Mean values of fatty acids productivity determined for each treatment are presented in Table 6.5.

Common name	Molecular formula	C:D
Palmitic acid	$\text{C}_{16}\text{H}_{32}\text{O}_2$	16:0
Palmitoleic acid	$\text{C}_{16}\text{H}_{30}\text{O}_2$	16:1
Hexadecadienoic acid	$\text{C}_{16}\text{H}_{28}\text{O}_2$	16:2
Hexadecatrienoic acid	$\text{C}_{16}\text{H}_{26}\text{O}_2$	16:3
Docosahexanoic acid	$\text{C}_{22}\text{H}_{42}\text{O}_2$	22:6
Stearic acid	$\text{C}_{18}\text{H}_{36}\text{O}_2$	18:0
Oleic acid	$\text{C}_{18}\text{H}_{34}\text{O}_2$	18:1
Linoleic acid	$\text{C}_{18}\text{H}_{32}\text{O}_2$	18:2
Linolenic acid	$\text{C}_{18}\text{H}_{30}\text{O}_2$	18:3

Table 6.4: Common name, molecular formula and C:D number of the fatty acids found in the microalgae biomass.

6. High pH-induced flocculation-sedimentation and effect of supernatant reuse

		16:0	16:1	16:2	16:3	22:6	18:0	18:1	18:2	18:3
Analytical grade water	M	6.103	0.227	0.272	0.272	0.771	0.885	9.507	2.496	2.133
Centrifugation	SD	0.322	0.012	0.014	0.014	0.041	0.047	0.501	0.132	0.112
Tap water	M	6.110 a*	0.281 b*	0.237 c*	0.151 d*	0.367 e*	0.993 f	9.759 g*	2.224 h*	1.490 i*
Centrifugation	SD	0.100	0.005	0.004	0.002	0.006	0.016	0.160	0.037	0.024
Tap water	M	5.236 a*	0.098 b*	c*	d*	e*	0.943 f	4.358 g*	0.206 h*	i*
Flocculation	SD	0.086	0.002				0.015	0.072	0.003	
C. supernatant	M	7.436	0.264	0.369	0.316 j*	0.870	1.081 k	10.07	3.480	2.452 l
Centrifugation	SD	0.197	0.007	0.010	0.008	0.023	0.029	0.266	0.092	0.065
C. supernatant	M	7.348	0.261	0.391	0.365 j*	0.912	0.990 k	9.797	3.361	2.606 l
Flocculation	SD	0.194	0.007	0.010	0.010	0.024	0.026	0.259	0.089	0.069
F. supernatant	M	7.196	0.259	0.311	0.336	0.958	1.035	9.991	3.106	2.718
Centrifugation	SD	0.570	0.021	0.025	0.027	0.076	0.082	0.792	0.246	0.215
F. supernatant	M	7.065	0.227	0.303	0.303	0.908	0.934	9.664	3.104	2.700
Flocculation	SD	0.560	0.018	0.024	0.024	0.072	0.074	0.766	0.246	0.214

Table 6.5: *S. obliquus* fatty acids productivity ( $\text{mg L}^{-1} \text{d}^{-1}$ ) after culture in media prepared with different types of water and harvesting by centrifugation at 3852 28g for 5 min and by flocculation with Na(OH) at pH 11.4. Pairs of identical lower case letters mean statistical significant differences ( $0.01 < \alpha < 0.05$ ) among different harvesting methods for each type of water. An asterisk is added when differences are highly significant.

In all cases more unsaturated than saturated fatty acids were found (average values of 66 % and 34 % respectively). Polyunsaturated fatty acids (PUFAs) accounted for 23 %. The docosahexaenoic acid (22:6) content exceeded the limit of 1 % stated in the requirements of fatty acid methyl esters (FAME) for diesel engines established by EN14214 (14214 2008). Linolenic (18:3) was always under 12 %, which is allowed by the standard. In order to study if the harvesting method had any influence on the productivity of each fatty acid, a t-Student test was applied to compare the productivities for centrifuged and flocculated samples in reused media and tap water (Figure 6.8 and Figure 6.9).

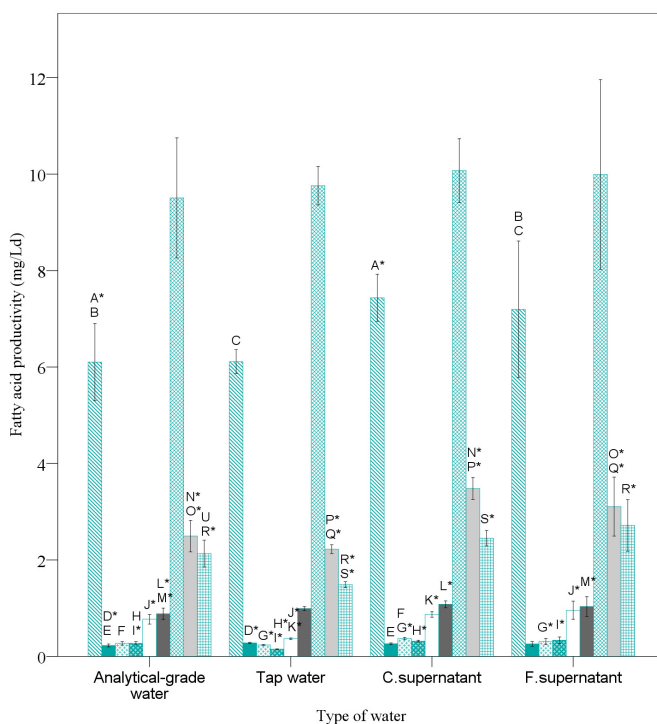


Figure 6.8: *S. obliquus* fatty acids productivities ( $\text{mg L}^{-1} \text{d}^{-1}$ ) in media prepared with fresh water, tap water and reused media when samples are harvested by centrifugation at 3852 28g for 5 min: (diagonal lines) palmitic, (plain blue) palmitoleic, (blue crosses) hexadecadienoic, (white crosses) hexadecatrienoic, (white) docosahexanoic, (dark grey) stearic, (diagonal grid) oleic, (light grey) linoleic and (straight grid) linolenic. Pairs of identical capital letters mean statistical significant differences ( $0.01 < \alpha < 0.05$ ) among different types of water. An asterisk is added when differences are highly significant ( $\alpha < 0.01$ ). Error bars represent 95 % confidence intervals of the mean.

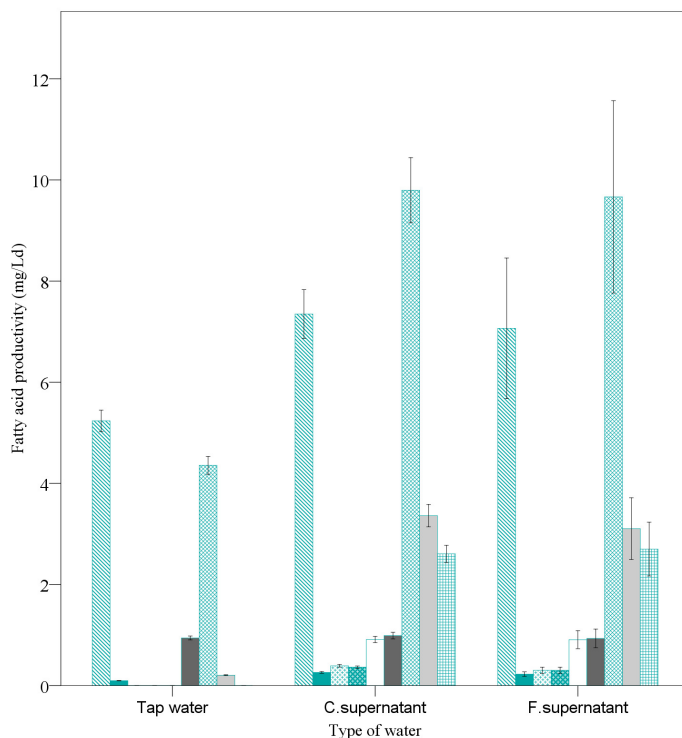


Figure 6.9: *S. obliquus* fatty acids productivities ( $\text{mg L}^{-1} \text{d}^{-1}$ ) in media prepared with fresh water, tap water and reused media when samples are harvested by flocculation with NaOH at pH 11.4: (diagonal lines) palmitic, (plain blue) palmitoleic, (blue crosses) hexadecadienoic, (white crosses) hexadecatrienoic, (white) docosahexanoic, (dark grey) stearic, (diagonal grid) oleic, (light grey) linoleic and (straight grid) linolenic. Pairs of identical capital letters mean statistical significant differences ( $0.01 < \alpha < 0.05$ ) among different types of water. An asterisk is added when differences are highly significant ( $\alpha < 0.01$ ). Error bars represent 95 % confidence intervals of the mean.

When the microalgae were cultured in medium recovered by flocculation no differences were observed between harvesting methods; however, when medium recovered by centrifugation was used, highly significant differences were noticed in hexadecatrienoic acid (16:3) and significant differences appeared in stearic acid (18:0) and linolenic acid. On the contrary, microalgae cultured using tap water showed a lipid profile that depended strongly on the harvesting technique. When samples were obtained by flocculation, the unsaturated fatty acids concentration decreased or even became undetectable while the saturated fatty acids concentration increased considerably with respect to samples obtained by centrifugation. PUFA concentrations

---

fell to an average value of 1.9 % in flocculated tap water medium while reaching 20.7 % in medium obtained by centrifugation. Palmitic acid (16:0) became the most abundant fatty acid in those samples and stearic acid reached 8.7 % while it was about 4 % in all other treatment. Only three unsaturated fatty acids were detected: palmitoleic (16:1), oleic (18:1) and linoleic (18:2).

Highly significant differences in PUFA concentration between algae obtained from tap water medium and the other media, while no differences were detected between those from reused media, whose average concentration of PUFA was 28.9 %. These results show that using tap water for microalgae culturing is not feasible when obtaining of nutritional compounds is the scope of the culture, since the concentration of PUFA, the more valuable fatty acids with nutritional purposes, is very low when using this water.

When microalgae were harvested by centrifugation, samples from both reused media only differed in hexadecadienoic acid (16:2), which was higher in the centrifuged reused medium. However, there was a large difference between samples from analyticalgrade water, tap water and reused media. Similar results were observed for samples collected by flocculation, since all the fatty acids presented highly significant differences between samples from tap water and both reused media, while only palmitoleic, hexadecadienoic and hexadecatrienoic (16:3) showed differences between reused media.

Neutral lipids, especially triacylglycerols, have been reported to be involved not only in energy storage, but also in adaptation to environmental conditions. Under optimal conditions of growth, algae synthesize fatty acids principally for esterification into glycerol- based membrane lipids, which constitute about 5 % to 20 % of their dry cell weight. Under unfavorable growth conditions, many algae alter their lipid biosynthetic pathways towards the formation and accumulation of neutral lipids, mainly in the form of triacylglycerol (TAG) (Hu et al. 2008). Among several stress factors, salt stress has been reported to induce the synthesis of lipids as a strategy of physiological resistance (Lu et al. 2012). Furthermore, the presence of organic matter is considered also a stress factor, especially during nitrogen starvation (Solovchenko 2012). Medium reuse could have exposed the algae to increased salinity and organic matter. The increase in PUFAs in algae grown in reused media could also be a sign of stress, as fatty acid unsaturation has been also recognized as a mechanism of adaptation to environmental conditions. It has been suggested that microalgal TAG could have a role as a depot of PUFA, which can be mobilized for the construction of chloroplastic membranes under certain environmental conditions (Khozin-Goldberg, Shrestha, and Cohen 2005). The accumulation of organic matter, despite its possible



positive effect on lipid productivity, may be detrimental to the overall medium reuse due to its negative influence on the flocculation-sedimentation and the excessive accumulation of PUFAs. It may be necessary to dilute the recycled water with fresh medium, something that might have to be done in large-scale plants anyway as water loss during biomass harvesting will occur.

#### 6.4. Conclusions

High microalgal biomass recovery efficiencies can be achieved by high pH-induced flocculation-sedimentation, however further research should be conducted to clarify the flocculation mechanisms. The experiments conducted in this work demonstrate that magnesium is not the sole factor influencing high pH induced flocculation with Na(OH). A suggested explanation is the possible accumulation of organic matter.

According to the presented results, recovery of *C. vulgaris* using high pH-induced flocculation-sedimentation is not as efficient as the recovery of *S. obliquus*, specially when using Na(OH). In the case of *S. obliquus* recovery efficiencies around 80 % can be achieved, but it is worth taking into account that CaCO<sub>3</sub> precipitates when using Ca(OH)<sub>2</sub> may interfere during subsequent steps of downstream processing, thus the final quality of the products must be a criterion when selecting the harvesting method.

The current results reveal that the limiting factor in the reuse of flocculated microalgal culture medium is the depletion of nutrients, and supplementation with nutrients will be necessary to achieve higher growth yields than can be with fresh medium. The fatty acids from microalgae grown in reused media had more desirable nutritional qualities than those from algae grown in fresh media. The fatty acid composition of algae grown in reused media was suitable for biofuel production. These findings are of special importance to microalgae culture in areas with a scarcity of fresh water that usually are those with better solar irradiance.

---

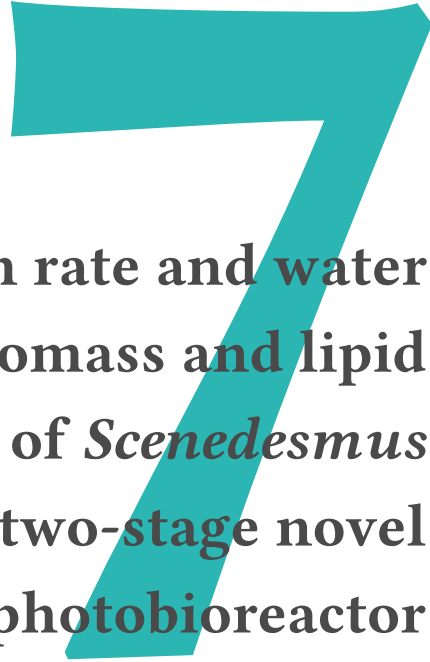
## References

- 12966, E. S. E. I. (2009). *Animal and vegetable fats and oils - Gas chromatography of fatty acid methyl esters - Part 3: Preparation of methyl esters using trimethylsulfonium hydroxide (TMSH)*.
- 14214, E. S. E. I. (2008). *Automotive fuels - Fatty acid methyl esters (FAME) for diesel engines - Requirements and test methods*.
- Ahmad, A. L. et al. (2011). "Optimization of microalgae coagulation process using chitosan". English. In: *Chemical Engineering Journal* 173.3, pp. 879–882.
- Chen, C.-Y. et al. (2011). "Cultivation, photobioreactor design and harvesting of microalgae for biodiesel production: A critical review". In: *Bioresource technology* 102.1, pp. 71–81.
- Chisti, Y. (2007). "Biodiesel from microalgae". English. In: *Biotechnology Advances* 25.3, pp. 294–306.
- Christenson, L. and R. Sims (2011). "Production and harvesting of microalgae for wastewater treatment, biofuels, and bioproducts". In: *Biotechnology Advances* 29.6, pp. 686–702.
- Grima, E. M. et al. (2003). "Recovery of microalgal biomass and metabolites: process options and economics". In: *Biotechnology Advances* 20.7-8, pp. 491–515.
- Hu, Q. et al. (2008). "Microalgal triacylglycerols as feedstocks for biofuel production: Perspectives and advances". In: *Plant Journal* 54.4, pp. 621–639.
- Khozin-Goldberg, I., P. Shrestha, and Z. Cohen (2005). "Mobilization of arachidonyl moieties from triacylglycerols into chloroplastic lipids following recovery from nitrogen starvation of the microalga *Parietochloris incisa*". In: *Biochimica Et Biophysica Acta-Molecular and Cell Biology of Lipids* 1738.1-3, pp. 63–71.
- Kim, D.-G. et al. (2011). "Harvest of *Scenedesmus* sp. with bioflocculant and reuse of culture medium for subsequent high-density cultures". In: *Bioresource technology* 102.3, pp. 3163–3168.
- Lee, A. K., D. M. Lewis, and P. J. Ashman (2009). "Microbial flocculation, a potentially low-cost harvesting technique for marine microalgae for the production of biodiesel". In: *Journal of Applied Phycology* 21.5, pp. 559–567.
- Lee, D.-J. et al. (2012). "Coagulation-membrane filtration of *Chlorella vulgaris*". In: *Bioresource technology* 108.0, pp. 184–189.

- Lee, S. et al. (1998). "Effects of harvesting method and growth stage on the flocculation of the green alga *Botryococcus braunii*". English. In: *Letters in applied microbiology* 27.1, pp. 14–18.
- Leentvaar, J. and M. Rebhun (1982). "Effect of Magnesium and Calcium Precipitation on Coagulation-Flocculation with Lime". English. In: *Water research* 16.5, pp. 655–662.
- Lu, N. et al. (2012). "Regulation of lipid metabolism in the snow alga *Chlamydomonas nivalis* in response to NaCl stress: An integrated analysis by cytomic and lipidomic approaches". In: *Process Biochemistry* 47.7, pp. 1163–1170.
- Morales, J., J. de la Noüe, and G. Picard (1985). "Harvesting marine microalgae species by chitosan flocculation". In: *Aquacultural Engineering* 4.4, pp. 257–270.
- Papazi, A., P. Makridis, and P. Divanach (2010). "Harvesting *Chlorella minutissima* using cell coagulants". English. In: *Journal of Applied Phycology* 22.3, pp. 349–355.
- Salim, S. et al. (2011). "Harvesting of microalgae by bio-flocculation". In: *Journal of Applied Phycology* 23.5, pp. 849–855.
- Semerjian, L. and G. Ayoub (2003). "High-pH magnesium coagulation-flocculation in wastewater treatment". English. In: *Advances in Environmental Research* 7.2, pp. 389–403.
- Smith, B. T. and R. H. Davis (2012). "Sedimentation of algae flocculated using naturally-available, magnesium-based flocculants". In: *Algal Research-Biomass Biofuels and Bioproducts* 1.1, pp. 32–39.
- Solovchenko, A. E. (2012). "Physiological Role of Neutral Lipid Accumulation in Eukaryotic Microalgae under Stresses". In: *Russian Journal of Plant Physiology* 59.2, pp. 167–176.
- Vandamme, D. et al. (2010). "Flocculation of microalgae using cationic starch". In: *Journal of Applied Phycology* 22.4, pp. 525–530.
- Vandamme, D. et al. (2012). "Flocculation of *Chlorella vulgaris* induced by high pH: Role of magnesium and calcium and practical implications". In: *Bioresource technology* 105, pp. 114–119.
- Wijffels, R. H. and M. J. Barbosa (2010). "An outlook on microalgal biofuels". In: *Science* 329.5993, pp. 796–799.

---

Wu, Z. et al. (2012). "Evaluation of flocculation induced by pH increase for harvesting microalgae and reuse of flocculated medium". In: *Bioresource technology* 110.0, pp. 496–502.



# Effects of dilution rate and water reuse on biomass and lipid production of *Scenedesmus obliquus* in a two-stage novel photobioreactor

Part of this chapter has been published as: Lucas-Salas, L.M.; Castrillo, M.; Martínez, D. Effects of dilution rate and water reuse on biomass and lipid production of *Scenedesmus obliquus* in a two-stage novel photobioreactor. Bioresour Technol 143 (2013) 344-352

---



## Abstract

Continuous culture of fresh water microalgae *Scenedesmus obliquus* was developed in a two-stage photobioreactor, avoiding the intermediate harvesting step to achieve a half-way point between the progressive and the sudden N-starvation strategies, guaranteeing light limited conditions in the first stage and N-stress conditions in the second stage. This methodology resulted in biomass productivity values at the best dilution rate ( $0.118 \text{ d}^{-1}$ ) of  $15.25 \pm 1.06 \text{ g m}^{-2} \text{ d}^{-1}$ , slightly higher than that expected according to batch experiment ( $12.90 \pm 0.75 \text{ g m}^{-2} \text{ d}^{-1}$ ). The dilution rate that maximized the lipid content was coincident with that for the maximum biomass productivity, resulting in an intensification of the lipid productivity. Microalgae can be successfully cultured in reused medium clarified by high pH flocculation-sedimentation and neutralized by bubbling the photobioreactors outlet  $\text{CO}_2$  current through it. Microalgae flocculation with NaOH does not result in a variation of the obtained lipid profile in comparison with the harvesting by centrifugation.

## Resumen

El cultivo en continuo de la microalga *Scenedesmus obliquus* en un reactor en dos fases ha sido desarrollado, evitando el paso intermedio de separación de la biomasa para lograr un término medio entre la privación progresiva y repentina de nitrógeno, garantizando condiciones de luz limitante en la primera fase y condiciones de estrés por falta de nitrógeno en la segunda fase. Esta metodología ha resultado en una producción de biomasa, a la mejor tasa de dilución ( $0.118 \text{ d}^{-1}$ ) de  $15.25 \pm 1.06 \text{ g m}^{-2} \text{ d}^{-1}$ , ligeramente mayor que la esperada de acuerdo con los experimentos desarrollados en batch  $12.90 \pm 0.75 \text{ g m}^{-2} \text{ d}^{-1}$ . La tasa de dilución que maximiza el contenido en lípidos coincidió con aquella que aportó la máxima productividad de biomasa, resultado en una intensificación de la productividad de lípidos. Las microalgas fueron cultivadas satisfactoriamente en medio reutilizado clarificado mediante floculación-sedimentación producida por aumento de pH y posterior neutralización por burbujeo de la corriente de  $\text{CO}_2$  de salida del reactor. La floculación con NaOH no produjo variaciones en el perfil lipídico, en comparación con la recogida de biomasa por centrifugación.





## 7.1. Introduction

Microalgae are nowadays considered as an attractive source of valuable biomass due to their wide variety of applications. Its utilization with environmental purposes like bioremediation and CO<sub>2</sub> fixation, as well as with commercial purposes in different industrial sectors has been reported (Mata, Martins, and Caetano 2010). Moreover, a new interest in microalgae culturing has grown in the last few years since the lipids that they produce are viewed as a good alternative to fossil fuels (Chisti 2007). However, they are not yet cost-efficient enough to be produced at large scale (Wijffels and Barbosa 2010).

More than twenty years ago the major economic bottlenecks to large-scale culture of microalgae were algal productivity, followed by labor and harvesting costs (Borowitzka 1992). Nowadays, the major drawbacks in the use of microalgae as oil producers for biofuel are still related with the cost of the process, especially the biomass harvesting and lipid extraction, and the biomass and lipid productivity yield, which depends on intrinsic characteristics of the selected species, but also on the existing culturing technologies (Rawat 2012). Both, development of microalgae culturing technologies and improving of the operation mode are still required to reduce the cost and be competitive with other energy sources. The number of works that study the biomass and lipid productivity, and more recently the lipid profile, under a wide variety of conditions is increasing, but most of them are developed under batch operating mode (Baky et al. 2012; Abomohra et al. 2012; Salama et al. 2013). In addition to the need of innovative designs that provide a better efficiency of light capturing, it has been recently highlighted the importance of understanding the steady-state behavior of microalgae cultures (Tang et al. 2012).

In nutrient-limited systems the limiting factor is a component of the medium, so it can be controlled by varying the dilution rate ( $D$ ). In light-limited systems, the limiting factor is not directly dependent of  $D$  and cannot be assumed to be distributed homogeneously in the photobioreactor (PBR) volume (Evers 1991). For this reason, it is difficult to extrapolate results from batch cultures to continuous cultures. Besides to adjust the nutrients concentrations in the input medium, the  $D$  must be adjusted to achieve the optimal light intensity.

In this work a two stage bench scale pilot plant of a novel design (Patent number ES2356653, (Tejero et al. 2011)) was used to study the effect of the  $D$  over *Scenedesmus obliquus* growth and lipid productivity under nitrogen stress (N-Stress) conditions. The improvement of lipid content under nutrient limitation is usually associated with low biomass productivity, then, it seems useful to separate the process in two

---

sub-processes. In the first stage growth conditions are set to maintain the algal cells in exponential growth, while the second stage is intended to increase the lipid productivity based on nutrient starvation conditions. The convenience of these conditions, especially with regard to triacylglycerol (TAG) production, has been previously reported (Mujtaba et al. 2012; Pruvost et al. 2009; Pruvost et al. 2011; Zhou et al. 2012).

The progressive N-starvation can be easily achieved in batch cultures, just waiting to nitrogen depletion. In large scale, continuous cultures are preferred rather than batch cultures, for this reason other methods like sudden starvation are being studied. However, the high cost of sudden N-starvation in comparison with the progressive method in a unique reactor is found as an important drawback due to the need of an intermediate harvesting process and cells resuspension in the N-deprived medium (Pruvost et al. 2009). This intermediate step is avoided in this work to achieve a half-way point between the progressive and the sudden N-starvation strategies, guaranteeing N-stress conditions in the second stage, since the inlet medium, that comes from the first PBR, is very poor in nitrogen. This requires an accurate calculation of the nutrients concentration in the inlet medium in the first PBR. Recently, other operating mode has been reported, consisting of a continuous PBR in one stage under low N-concentration (Klok et al. 2013). The lack of energy is compensated with a high supply of light in order to achieve biomass growth and TAG accumulation simultaneously. However, the necessity of that high light intensity could make it difficult to scale-up with a competitive areal productivity.

In the present work, before the continuous experimentation, a batch assay was carried out in order to estimate the more adequate operating parameters, especially  $D$ . If  $D$  is higher than the specific growth rate ( $\mu$ ), productivity becomes negative, since the biomass is washed out. Nutrients consumption rates must be also known at the working concentration, in order to calculate the composition of the inlet culture medium that assures N-stress conditions in the second stage. Furthermore, the influence of medium reuse, which has been previously studied at laboratory scale (Castrillo et al. 2013) was also analyzed at bench scale. The conceptual PBR configuration (Patent number ES2356653, (Tejero et al. 2011)) consists of a deep tank (between 1.2 m and 2 m approximately, depending on specific requirements and on local insolation conditions as explained in Chapter 4) that includes a series of conical structures made of a transparent material, such as plastic, with the base placed in the upper side over the water surface. These conical structures are submerged in the bulk liquid where microalgae biomass is cultivated.

Figure 7.1 shows a simple schematic diagram of the conical structures and their

role as light distributors. A sun tracking system would allow the cones to be positioned with its base in a perpendicular plane to the direct incident solar light, as shown in Figure 7.1b. Those conical structures guide the light downward since they receive the incident solar light on their base and spread it out through its lateral surface, thus conducting the light deeper into the culture. Since the light distribution area (cone lateral surface) is larger than the light receiving area (cone base), the layer of the culture close to the illuminated surface receives lower irradiance (according to Lambert's Cosine Law). Thanks to this design solution the photoinhibition phenomenon occurrence is reduced and the illuminated surface-to-occupied surface ratio is increased. As a result, areal productivity is enhanced even when doubling times are low due to low irradiances. Furthermore, as there are no vertical structures over the ground, shading phenomenon is eliminated, so there is no need of separation between reactors or reactor units to be scaled-up, improving once again the illuminated surface-to-occupied surface ratio. Once the optimum reactor unit characteristics are determined, the PBR could be scaled-up by increasing the number of reactor units. This scaling up method has been previously discussed by (Ogbonna et al. 1996). In spite of the several strengths mentioned in the previous paragraph, the indoor experimentation with this PBR has a weakness, which is the severe attenuation of the artificial light as it goes through the air, on the contrary to solar light (Figure 7.1). In outdoor experimentation solar light intensity would suffer no perceptible attenuation from the base of the cone to the apex (Irradiance in the base ( $I_b$ )  $\approx$  Irradiance in the apex ( $I_a$ )); therefore, light intensity through the whole cone inner surface would be homogeneous. In indoor assays irradiance varies along the cone height (data shown in Section 7.2.1), being too low in the bottom of the cone ( $I_b > I_a$ ), which is expected to result in a lower biomass productivity, compared to outdoor conditions. Despite this drawback, experimentation was carried out indoor since it allowed us to maintain irradiance and temperature values constant and under control. Although a brief description of the used PBR is made, the highlighted aspects of this work are not intrinsic of this design, since the two-stages operation mode would be implemented in any other configuration.

## 7.2. Methods

The microalgae selected for this study was *Scenedesmus obliquus* (CCAP 76/3A), which was supplied by the Culture Collection of Algae and Protozoa in Scotland, UK.

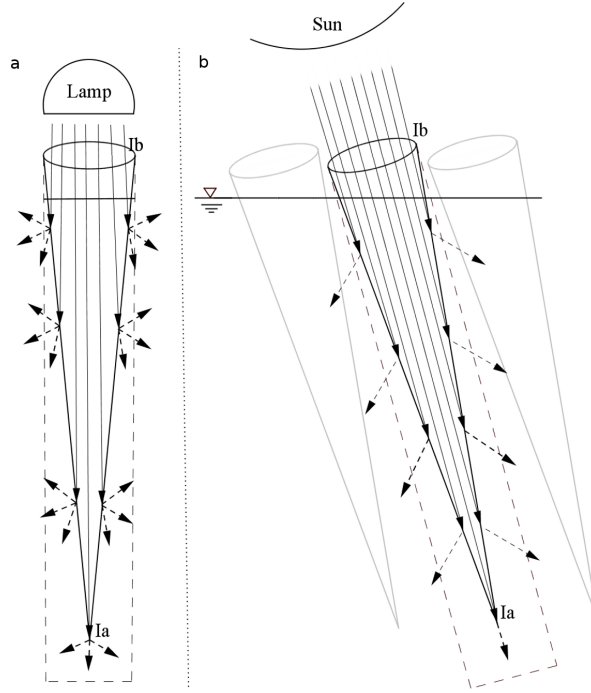


Figure 7.1: Radiation scheme in the indoor installation (a) and in the conceptual PBR (b), being  $I_b$  the incident radiation in the base of the cone and  $I_a$  the incident radiation that arrives to the apex. Continuous arrows represent incident radiation (artificial in a and solar in b) while dotted arrows represent refracted radiation.

### 7.2.1. Culture conditions

A bench scale plant based on the novel design was constructed and operated under diffuse light as a first approach. Figure 7.2 and Figure 7.3 shows a schematic diagram of the system, together with a real picture of the constructed prototypes. The bench scale plant consisted in two opaque cylindrical PBRs with diameter 0.30 m and 1.32 m high. A transparent PVC truncated cone with a large base (top base) diameter of 0.22 m, small base (bottom base) diameter of 0.03 m and 1.12 m high was placed inside. A light source (MASTER HPI Plus 400W/767) was placed 0.1 m above each PBR and operated in a 12:12 light-dark cycle. Light intensity values were measured by a quantum sensor Li-192 at several heights of the cone, revealing that light intensity is considerably attenuated as getting away from the light source. Light intensity values at 0 m, 0.11 m, 0.21 m, 0.31 m and 0.54 m from the cone base

were  $1000 \mu\text{E m}^{-2} \text{s}^{-1}$ ,  $800 \mu\text{E m}^{-2} \text{s}^{-1}$ ,  $626 \mu\text{E m}^{-2} \text{s}^{-1}$ ,  $380 \mu\text{E m}^{-2} \text{s}^{-1}$  and  $230 \mu\text{E m}^{-2} \text{s}^{-1}$ , respectively. 2 %  $\text{CO}_2$  enriched air was supplied at a flow of 0.028 vvm (gas volume per culture volume per minute) and injected by means of fine bubble spargers during the light hours. The aeration system allowed the complete mixing of the culture. Temperature was maintained at  $22.0 \pm 0.2^\circ\text{C}$ .

### 7.2.2. Batch assay

One of the PBRs previously described was filled at a working volume of 70 L of modified BG11 culture medium with the following composition ( $\text{g L}^{-1}$ ):  $\text{NaNO}_3$ , 0.135;  $\text{K}_2\text{HPO}_4$ , 0.018;  $\text{MgSO}_4 \cdot 7\text{H}_2\text{O}$ , 0.075;  $\text{CaCl}_2 \cdot 2\text{H}_2\text{O}$ , 0.036; citric acid, 0.006; green ammonium  $\text{Fe}^{3+}$  citrate, 0.006;  $\text{EDTANa}_2$ , 0.10;  $\text{Na}_2\text{CO}_3$ , 0.02;  $\text{H}_3\text{BO}_3$ , 0.0029;  $\text{MnCl}_2 \cdot 4\text{H}_2\text{O}$ , 0.0018;  $\text{ZnSO}_4 \cdot 7\text{H}_2\text{O}$ , 0.0002;  $\text{Na}_2\text{MoO}_4 \cdot 2\text{H}_2\text{O}$ , 0.0003;  $\text{CuSO}_4 \cdot 5\text{H}_2\text{O}$ ,  $0.08 \times 10^{-3}$  and  $\text{Co}(\text{NO}_3)_2 \cdot 6\text{H}_2\text{O}$ ,  $0.05 \times 10^{-3}$ , which provided a N:P ratio of 7. Initial  $\text{NO}_3\text{--N}$  concentration was  $22.2 \text{ mg L}^{-1}$  and  $\text{PO}_4\text{--P}$  was  $3.2 \text{ mg L}^{-1}$ . The culture was maintained until it reached the stationary phase.

### 7.2.3. Continuous experimentation

The photobioreactors were filled at a working volume of 70 L. The first PBR (PBR1) received fresh medium by means of an electromagnetic dosing pump (Seko AKE/L), while the second (PBR2) received the effluent of the first one. Four different assays were conducted. The main characteristics of the assays can be seen in Table 7.1. Since the two prototypes had the same volume, the different  $D_s$  were set by varying the flow rates. In this way, in the case of Assay 2, the flow rate between PBR1 and PBR2 was set by means of a bypass that evacuated out of the pipe the excess of flow. At an industrial scale  $D_s$  would be set by calculating the optimal PBRs volumes in order to assure a constant flow rate. The composition of the fresh medium was a modification of BG11 medium, which contained ( $\text{g L}^{-1}$ ):  $\text{NaNO}_3$ , 0.085;  $\text{K}_2\text{HPO}_4$ , 0.011;  $\text{MgSO}_4 \cdot 7\text{H}_2\text{O}$ , 0.075;  $\text{CaCl}_2 \cdot 2\text{H}_2\text{O}$ , 0.036; citric acid, 0.006; green ammonium  $\text{Fe}^{3+}$  citrate, 0.006;  $\text{EDTANa}_2$ , 0.10;  $\text{Na}_2\text{CO}_3$ , 0.02;  $\text{H}_3\text{BO}_3$ , 0.0029;  $\text{MnCl}_2 \cdot 4\text{H}_2\text{O}$ , 0.0018;  $\text{ZnSO}_4 \cdot 7\text{H}_2\text{O}$ , 0.0002;  $\text{Na}_2\text{MoO}_4 \cdot 2\text{H}_2\text{O}$ , 0.0003;  $\text{CuSO}_4 \cdot 5\text{H}_2\text{O}$ ,  $0.08 \times 10^{-3}$  and  $\text{Co}(\text{NO}_3)_2 \cdot 6\text{H}_2\text{O}$ ,  $0.05 \times 10^{-3}$ . Nutrients concentrations were low because they were calculated in accordance with the low cell densities found when working with artificial light. The  $\text{NO}_3\text{--N}$  concentration was calculated to achieve N-stress conditions in the second PBR ( $\text{NO}_3\text{--N}$  under  $7 \text{ mg L}^{-1}$ ). In assays 1, 2 and 3 the culture medium was prepared with analytical-grade water provided by an Elix Advantage System (Millipore) (fresh water experiments), and the pH of the medium was adjusted to 7.1 with 0.1 M HCl. In Assay 4, reused water was used to prepare the medium (clarified water experiments).

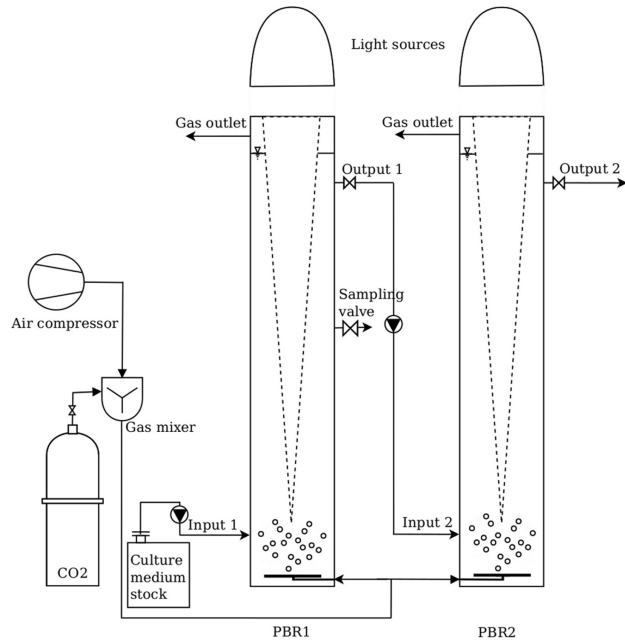


Figure 7.2: Operational scheme of the bench scale pilot plant.



Figure 7.3: Indoor installation.

In order to do this, the effluent from the second PBR was clarified by high pH-induced flocculation-sedimentation. Approximately  $0.24 \text{ g L}^{-1}$  NaOH were added to the medium (until pH reached a value of 11.2 to 11.4), then was left settling during 12 h. Afterwards, the supernatant was neutralized by bubbling  $\text{CO}_2$  enriched air from the gas outlet of the PBRs. pH values of the reused medium were  $7.68 \pm 0.10$ . As a little part of the microalgae remained in suspension, results obtained in Assay 4 are corrected for the remaining input biomass.

Assay	PBR	Input	Input flow rate ( $\text{m L min}^{-1}$ )	Unit $D$ ( $\text{d}^{-1}$ )	Accumulated $D$ ( $\text{d}^{-1}$ )	ST (d)
A1	1	Fresh medium	23	0.236	0.236	0
	2	PBR1 effluentc	23	0.236	0.118	4.2
A2	1	Fresh mediauma	23	0.236	0.236	0
	2	PBR1 effluentc	12	0.118	0.079	8.4
A3	1	Fresh mediauma	15	0.156	0.156	0
	2	PBR1 effluentc	15	0.156	0.078	6.4
A4	1	Clarified mediumb	18	0.185	0.185	0
	2	PBR1 effluentc	18	0.185	0.093	5.4

Table 7.1: Performance characteristics of the four continuous experiments: Type of input medium (Input); Input flow rate; Dilution rate for each PBR of the two operating in each assay (Unit  $D$ ); Accumulated dilution rate (Accumulated  $D$ ); Stress time (ST).

#### 7.2.4. Analytical methods

The biomass growth was controlled by absorbance at 685 nm using a spectrophotometer DR3800 Hach Lange, by number of cells that were counted with the aid of a Thoma counting chamber and by dry weight (DW) filtering the samples through a previously dried Whatman paper filter GF/C 47 mm and dried at  $103^\circ\text{C}$  until constant weight. Biomass productivity was calculated as the daily obtained dry weight per square meter of land occupied by one reactor unit ( $0.07 \text{ m}^2$ ) in case of PBR1 and two reactor units in case of PBR2, as they need the inlet culture media from PBR1. Nutrients monitoring was carried out by photometric analyses (Spectroquant Nitrate Test 1.14773.0001 and Spectroquant Phosphate Test 1.14848.0002 respectively) using the spectrophotometer DR 3800 Hach Lange. Nitrogen and phosphorous consumption were calculated as the daily consumed milligrams of the element (N, P) by gram of biomass DW. Absorbance measurements were done daily in order to ensure the correct performance of the assays (data not shown). Samples for the other analysis were taken every 2-3 days. Temperature and pH were continuously monitored with Crison Instruments sensors 6050 and 5333 respectively. The system was operated for at least a time higher than two hydraulic retention times (HRT), being  $\text{HRT} = D^{-1}$ , so

---

as to ensure steady-state conditions. Samples were taken at least in triplicate, through a sampling valve situated in the middle part of the PBR in the case of PBR1 and from the effluent in the case of PBR2. Since there was uniform mixing, no differences existed between the culture in the PBR and the effluent.

### 7.2.5. Lipid extraction and screening

Microalgae samples taken from PBR1 and PBR2 at the end of each experiment were centrifuged at 3852g for 10 min and washed three times with deionized water. The pellets were resuspended in deionized water and HCl was added so that the final solution was 4 M HCl. Then, this solution was hydrolyzed in a hydrolysis unit (B-411/E-416 Büchi, Switzerland). Lipids were n-hexane extracted by warm Soxhlet method using an extraction system B-811 (Büchi, Switzerland). This method is based on that proposed by BUCHI experts for the determination of total fat in a dehydrated vegetable food flakes samples (Application No. SAN 08-06, Copyright 2006 Büchi Labortechnik AG). Lipid percentage was calculated for each replicate. For some of the lipid samples a lipid profile screening was carried out. The fatty acid composition was analyzed by GC-MS preceded by derivatization with trimethylsulfonium hydroxide (TMSH), according to the method described in EN ISO12966- 3:2009 (12966 2009). Fatty acid composition was calculated as the percentage of each fatty acid methylester (FAME) in the samples.

### 7.2.6. Statistical analyses

Statistical analyses of the data were carried out with IBM SPSS Statistic 19. Results were considered highly significant when a  $\alpha < 0.01$  or significant if  $0.01 < \alpha < 0.05$ . In order to compare results, data were analyzed with t-Student or ANOVA and DHS Tukey post hoc analyses as parametric and Kruskal-Wallis and Mann-Whitney U-tests with Bonferroni correction as non-parametric tests. In charts, error bars show 95 % confidence intervals of the mean.

## 7.3. Results and discussion

### 7.3.1. Batch assay

The batch assay revealed that the highest biomass productivity ( $16.667 \pm 1.667 \text{ g m}^{-2} \text{ d}^{-1}$ ) takes place just before the stationary phase ( $time = 169 \text{ h}$ ,  $DW = 0.140 \pm 0.007 \text{ g}$ ), then it decreases dramatically, as can be seen in Figure 7.4 and Figure 7.5. Growth rate at 169 h was  $0.160 \pm 0.014 \text{ d}^{-1}$  while at 241 h



was  $0.110 \pm 0.033 \text{ d}^{-1}$ . Then, the  $D$  in continuous assays should be around these values to reach the steady-state. Nutrient monitoring showed that at 241 h nitrogen was available for the microalgae ( $\text{NO}_3\text{-N} > 7 \text{ mg L}^{-1}$ ) while  $\text{PO}_4\text{-P}$  was depleted, because *S. obliquus* consumes this nutrient as soon as it is supplied, as a consequence of the well-known process called luxury uptake of phosphorus, as it has been observed in previous assays (data not shown). Nitrogen and phosphorous consumption with time can be seen in Figure 7.6. Then, the limiting factor in the growth of *S. obliquus* from 241 h seems to be the light, which is highly attenuated through the culture.

During the period between 169 h and 241 h, the volumetric consumption rates of  $\text{NO}_3\text{-N}$  and  $\text{PO}_4\text{-P}$  were  $1.136 \text{ mg L}^{-1} \text{ d}^{-1}$  and  $0.014 \text{ mg L}^{-1} \text{ d}^{-1}$  respectively, corresponding to consumption rates per biomass unit (dry weight) of  $6.832 \text{ mg g}^{-1} \text{ d}^{-1}$  and  $0.086 \text{ mg g}^{-1} \text{ d}^{-1}$ .  $\text{PO}_4\text{-P}$  consumption rate was slow due to the low concentration at that time ( $0.065 \text{ mg L}^{-1}$  and  $0.022 \text{ mg L}^{-1}$  at 169 h and 241 h respectively) as a consequence of the way that microalgae consume it, as indicated above. These consumption rates were used to calculate the composition of the inlet medium in the continuous assay as a function of the  $D$  in PBR1 to guarantee N-stress conditions in PBR2. Higher  $\text{PO}_4\text{-P}$  consumption rates were expected in continuous assays due to the constant supply of this nutrient.

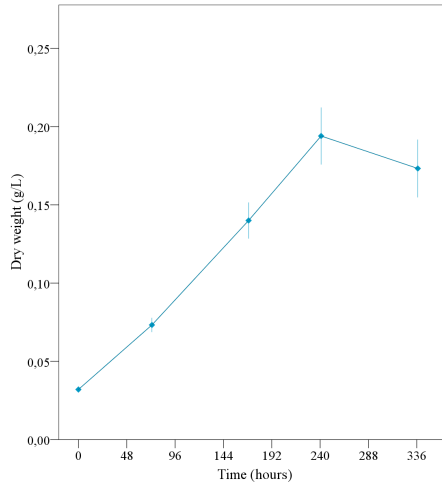


Figure 7.4: Dry weight ( $\text{g L}^{-1}$ ) versus time (hours) during the batch experiment. Error bars show 95 % confidence intervals of the mean.

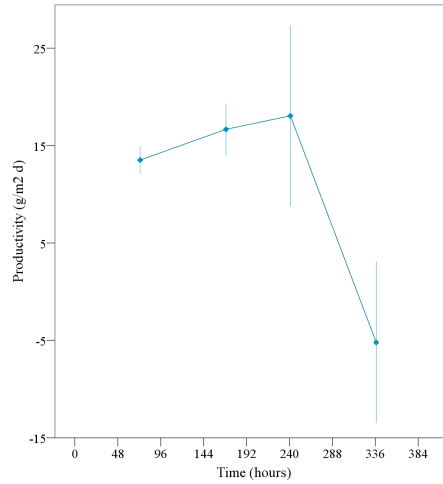


Figure 7.5: Biomass productivity ( $\text{g m}^{-2} \text{d}^{-1}$ ) versus time (hours) during the batch experiment. Error bars show 95 % confidence intervals of the mean.

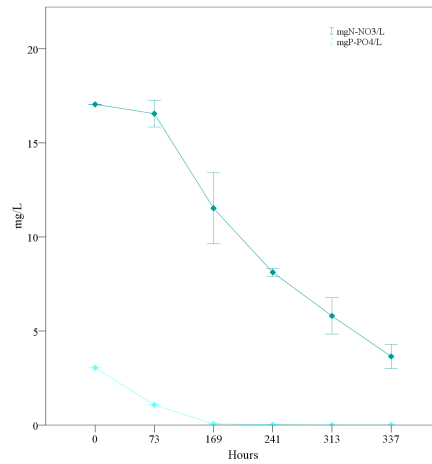


Figure 7.6: Nitrogen ( $\text{mg NO}_3\text{-N L}^{-1}$ ) and phosphorous ( $\text{mg PO}_4\text{-P L}^{-1}$ ) consumption versus time (hours) during the batch experiment. Error bars show 95 % confidence intervals of the mean.

### 7.3.2. Continuous assays

#### 7.3.2.1. Effect of dilution rate and water reuse on cell growth

An increase of  $D$  caused a decrease in the cell concentration in the nutrient rich PBRs (PBRs1) regardless of the type of water. In PBRs2 the same trend was observed, except for the lowest  $D$  ( $0.078 \text{ d}^{-1}$ ), when the number of cells decreased. However, no statistically significant differences were found between  $0.079 \text{ d}^{-1}$  and  $0.078 \text{ d}^{-1}$ .

Taking into account only the fresh water experiments it was possible to adjust a highly significant regression line between the cell number and  $D$  in both PBRs1 and PBRs2. Cell number predictions using the obtained regression model were compared with experimentally obtained data in the assays with clarified water. In the case of  $D = 0.185 \text{ d}^{-1}$ , both predicted and experimentally obtained data were statistically equal, whereas for  $0.093 \text{ d}^{-1}$ , predicted values were highly significant higher than the values experimentally obtained. These differences are attributed to the higher turbidity found when clarified water was used to prepare the culture medium. At the highest  $D_s$  in PBRs1 the optical density was low and the light attenuation due to this turbidity may be negligible, whereas at lower  $D_s$ , where higher optical densities were found, the turbidity of the clarified water might intensify the light stress factor, resulting in a decrease of cell division. In previous studies at laboratory scale (Castrillo et al. 2013), where light was not a stress factor, a better growth was found when using reused water.

#### 7.3.2.2. Effect of dilution rate and water reuse on dry weight and biomass productivity

Dry weight and biomass productivity values obtained for the different  $D_s$ , both in fresh and clarified water can be seen in Table 7.2.

Dry weight values reached in continuous cultures were lower than expected according to the batch assay, where  $(0.140 \pm 0.007) \text{ g L}^{-1}$  and  $(0.194 \pm 0.011) \text{ g L}^{-1}$  were obtained for growth rates of  $0.160 \text{ d}^{-1}$  and  $0.110 \text{ d}^{-1}$  respectively. Possible adaptation of microalgae cells to culture conditions, i.e. light attenuation during the culture, might allow them to reach higher DW values in batch assays. Figure 7.7 represents obtained DW values for the different  $D_s$  analyzed, in both fresh and clarified water experiments. A decrease in  $D$  resulted in a higher DW, as well as for the cell counts. Highly significant differences were found between the highest  $D$  ( $0.236 \text{ d}^{-1}$ ) and the other two experimented in nutrient rich PBRs, but no significant differences were obtained between  $0.185 \text{ d}^{-1}$  to  $0.156 \text{ d}^{-1}$ , corresponding to clarified and fresh water experiments respectively. A highly significant regression line was

Assay	PBR	Type of water	$D$ ( $\text{d}^{-1}$ )	DW ( $\text{g L}^{-1}$ )		BP ( $\text{g m}^{-2} \text{d}^{-1}$ )		LC (%)		LP ( $\text{g m}^{-2} \text{d}^{-1}$ )	
				Mean	SD	Mean	SD	Mean	SD	Mean	SD
A1/2 <sup>1</sup>	1	Fresh	0.236	0.057	0.012	13.357	2.758	5.627	0.142	0.886	0.125
A4	1	Clarified	0.185	0.082	0.013	15.001	2.365	5.617	0.489	0.963	0.143
A3	1	Fresh	0.156	0.087	0.011	13.587	1.741	3.558	0.469	0.434	0.083
A1	2	Fresh	0.118	0.131	0.009	15.250	1.060	10.549	2.017	1.611	0.210
A4	2	Clarified	0.093	0.145	0.019	13.360	1.775	10.454	1.901	1.279	0.273
A2	2	Fresh	0.079	0.170	0.006	9.999	0.367	7.163	0.836	0.726	0.077
A3	2	Fresh	0.078	0.158	0.005	12.307	0.394	7.595	1.287	0.945	0.183

Table 7.2: Mean values and Standard Deviations obtained in the different experiments for Dry Weight (DW ( $\text{g L}^{-1}$ ), Biomass Productivity (BP) ( $\text{g m}^{-2} \text{d}^{-1}$ ), Lipid Content (LC) (%) and Lipid Productivity (LP) ( $\text{g m}^{-2} \text{d}^{-1}$ ). Data are ordered by decreasing dilution rates. Types of water and dilution rates are also shown.

<sup>1</sup> Characteristics of PBRs1 during assays 1 and 2 were identical, so that mean values of the two assays are shown.

adjusted between  $D$  values and DW in fresh water PBRs1 ( $R^2 = 0.619$ ). Using this regression model the estimated DW value for  $0.185 \text{ d}^{-1}$  in fresh water was highly significantly lower than the experimental data obtained in the clarified water experiment. Similar results have been obtained previously for reused waters (Castrillo et al. 2013). A highly significant regression line can be also adjusted between  $D$  and DW obtained in PBRs2 in fresh water experiments ( $R^2 = 0.735$ ;  $a = 0.064$ ;  $b = 0.008$ ). The estimated value with this model for  $0.093 \text{ d}^{-1}$  in fresh water was statistically identical to experimental data achieved in clarified water. As for cell number, light attenuation due to turbidity can have a negative effect on microalgae growth at the highest optical densities. This result is coherent with that reported by (Quinn et al. 2012), who saw no apparent effect on the productivity of the system in an experiment testing the water reuse. The fitting of a linear regression line between DW in fresh water PBRs2 and Stress Time (ST, i.e. the time that microalgae remain in PBRs2 with lack of nutrients) resulted on a better adjustment ( $R^2 = 0.807$ ;  $a = 0.095$ ;  $b = 0.009$ ). Stress time values are summarized in Table 7.1 Predicted values for 5.4 days of stress in fresh water ( $D = 0.093 \text{ d}^{-1}$ ) showed no differences to experimental data obtained in clarified water.

With regard to the biomass productivity, shown in Figure 7.8, the highest values for nutrient rich PBRs were achieved in clarified water at  $0.185 \text{ d}^{-1}$ . Among fresh water assays there were no significant differences, which only appeared between  $0.185 \text{ d}^{-1}$  in clarified water and  $0.236 \text{ d}^{-1}$  in fresh water. In PBRs2 highly significant differences appeared among all  $D_s$ , except between  $0.078 \text{ d}^{-1}$  and  $0.093 \text{ d}^{-1}$  in fresh and clarified water respectively. It is remarkable that the BP for  $0.079 \text{ d}^{-1}$ , which corresponds to the highest ST, was significantly lower than in the other  $D_s$ , in spite of

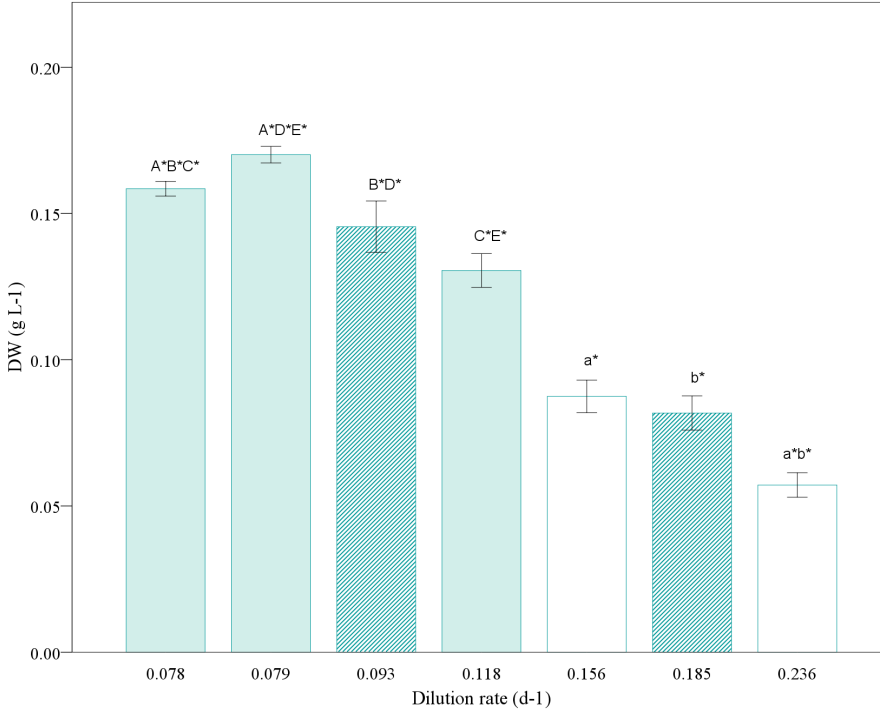


Figure 7.7: Dry weight ( $\text{g L}^{-1}$ ) for each dilution rate ( $\text{d}^{-1}$ ). White bars correspond to PBRs1, whereas colored bars correspond to PBRs2. Stripped bars represent clarified water assays. Significant differences are indicated by means of pairs of letters, with an asterisk in the case of highly significant differences. Lower case letters refer to PBRs1, and capital letters to PBRs2. Error bars show 95 % confidence intervals of the mean.

having the highest DW. In PBRs2 higher BP values were obtained at higher  $D_s$ , on the contrary to the DW tendency. The highest BP value was achieved at  $D = 0.118 \text{ d}^{-1}$ , as can be clearly seen in Figure 7.8.

A highly significant regression line can be used to statistically describe the BP decrease with the increase in the ST. Productivity decrease following N-deprivation has been observed in other works (Rodolfi et al. 2009; Ho, Chen, and Chang 2010). The estimators for this line, not considering the BP values obtained in clarified water experiments are  $a = 20.44$ ;  $b = -1.25$  ( $R^2 = 0.921$ ). Predicted value for 5.4 stress days using this model is statistically equal to real values obtained in clarified water.

According to the Verhulst logistic kinetic model applied to a mass balance of

a fully mixed reactor (Ruiz et al. 2013), the maximum productivity in continuous operation is reached at a hydraulic retention time equal to 2 divided by the maximum specific growth rate in batch experiment. In the batch experiment described above (Section 7.3.1) this value corresponded to a HRT of 7.4 d, near to the 8.4 d of this experimentation. Having into account that at the HRT of 8.4 d, 4.2 d belongs to N-stress conditions ( $A1, D = 0.118 \text{ d}^{-1}$ ), a reduction in the productivity should be expected, but on the contrary, slightly higher productivity values than those predicted from Verhulst logistic kinetic model were reached, revealing that the two-stage operation mode has no negative effects over the biomass productivity.

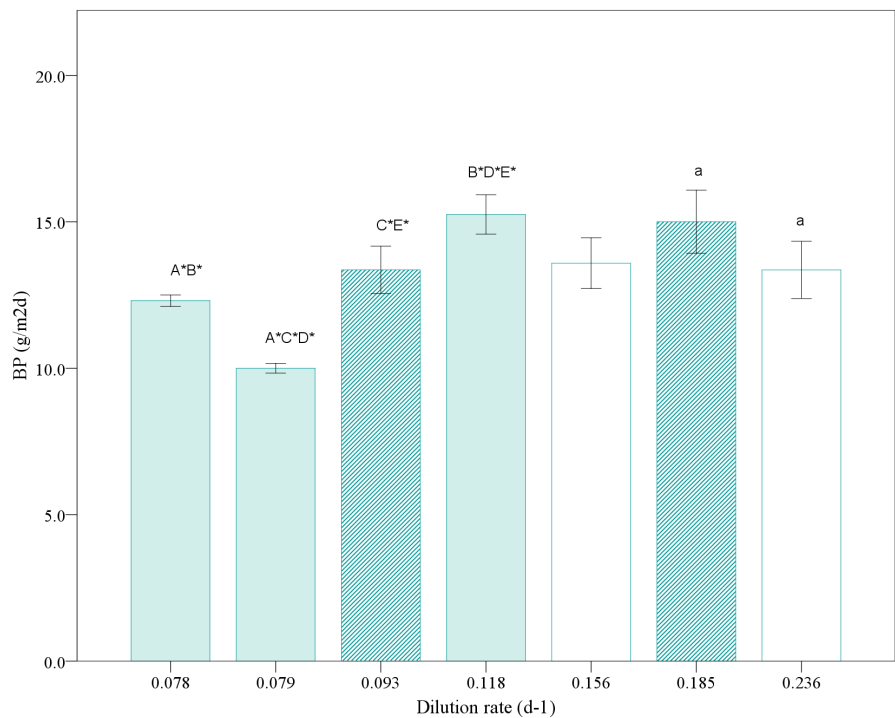


Figure 7.8: Biomass Productivity ( $\text{g m}^{-2} \text{d}^{-1}$ ) for each dilution rate ( $\text{d}^{-1}$ ). White bars correspond to PBRs1, whereas colored bars correspond to PBRs2. Stripped bars represent clarified water assays. Significant differences are indicated by means of pairs of letters, with an asterisk in the case of highly significant differences. Lower case letters refer to PBRs1, and capital letters to PBRs2. Error bars show 95 % confidence intervals of the mean.

Although higher productivity values than those expected were obtained, the fitting is quite satisfactory, since the shape of the dot chart is similar to the line than resulted

from the prediction, except for HRTs 6.4 days and 4.2 days, as shown in Figure 7.9. It was noted that at the lowest HRT the predicted productivity was considerably lower than that obtained experimentally, something very similar to the results presented by (Ruiz et al. 2013), suggesting that this kinetics is not very useful to predict continuous productivity for HRT lower than approximately half of the HRT that provides the highest productivity.

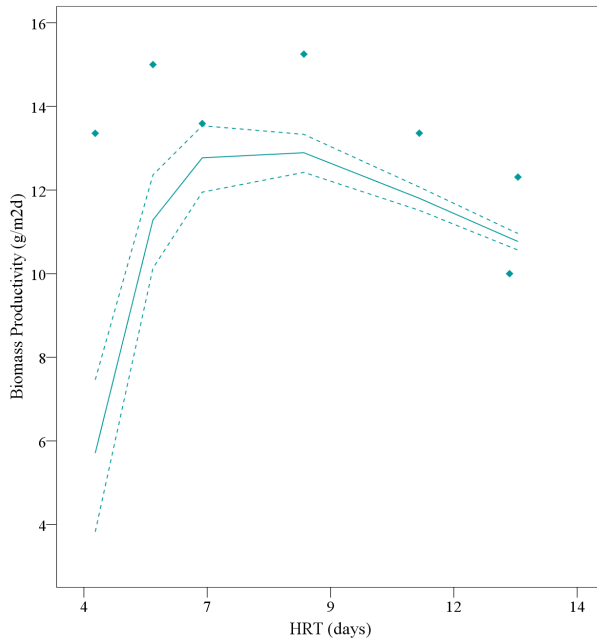


Figure 7.9: Estimated (lines) and experimental (symbols) biomass productivity ( $\text{g m}^{-2} \text{d}^{-1}$ ) as a function of the HRT (days). Dotted lines correspond to maximum and minimum values according to the standard deviation of the mean.

### 7.3.2.3. Nutrients and pH monitoring

The results obtained in the nutrient and pH monitoring of the different PBRs are summarized in Table 7.3. No differences in nitrogen concentration in PBRs1 were noted for the three  $D_s$ . Among PBRs1, lower phosphorus concentration and higher pH values were achieved in clarified water than in fresh water. Clarified water experiments showed also higher biomass productivity. As can be seen in Table 7.3, both daily nitrogen and phosphorous consumption rates decreased with the decrease

---

in *D*. Variations in nutrient consumption with *D* have been previously reported (Ruiz et al. 2013).

Nitrogen and phosphorous concentrations in PBRs2 were near the detection limits of the methods used for the analysis, being considered negligible. PBRs2 pH values showed variations among *D*s except between  $0.079\text{ d}^{-1}$  to  $0.078\text{ d}^{-1}$ .

#### **7.3.2.4. Effect of dilution rate and water reuse on lipid content and lipid productivity**

Figure 7.10 and Figure 7.11 show lipid content and lipid productivity respectively obtained for each *D* analyzed. These data are summarized in Table 7.2. As expected, both parameters were higher in PBRs2 than in PBRs1, because the lipid content increases considerably when the cells are subjected to unfavorable culture conditions, like nutrient starvation (Klok et al. 2013; Hu et al. 2008). Nevertheless, if data for each photobioreactor are considered individually, lipid productivity values for  $0.079\text{ d}^{-1}$ , which corresponds to Assay 2 PBR2, are lower than that obtained at  $0.236\text{ d}^{-1}$  and  $0.185\text{ d}^{-1}$  in PBRs1 during experiments A1, A2 and A4. This finding may be due to a low *D* in PBR2 in the course of Assay 2 ( $0.118\text{ d}^{-1}$ ), which resulted in a high DW, and in consequence a high light attenuation, appearing a large dark volume, where lipid production is not favored (Su et al. 2011).

In PBRs1 cellular lipid content and lipid productivity were equal at  $0.236\text{ d}^{-1}$  and  $0.185\text{ d}^{-1}$ , and lower at  $0.156\text{ d}^{-1}$ . In PBRs2, both the highest lipid content and productivity were achieved at  $0.118\text{ d}^{-1}$  and  $0.093\text{ d}^{-1}$ , as can be seen in Figure 7.10 and Figure 7.11. In these PBRs the two parameters tended to increase with the increase of the *D*. The lowest lipid content and productivity were related with the longest stress time (8.4 d for  $0.079\text{ d}^{-1}$ ), indicating that a stress time is required to reach high lipid productivity, but an excessive stress time could result in a detriment to this purpose (Rodolfi et al. 2009).

Since maximum lipid productivity is reached when the balance between biomass productivity and lipid content takes its maximum value, the coincidence in *D* of these two factors is a considerably advantage for lipid production yield. As can be seen in Figure 7.8 and Figure 7.10, the maximum BP and LC occur at the same *D*, while it has been reported that a fewer *D* is needed to reach the maximum LC (Ruiz et al. 2013). This difference may be due to the two-stage operation system that guarantees nitrogen starvation in the second PBR, thus accelerating the lipid production, while does not compromise the biomass productivity in the first PBR. On the other hand, if only one reactor is used in continuous operating mode, it has been observed that, as it was hypothesized, TAG productivity increased with increasing nitrogen limitation,



		Dilution rates (d <sup>-1</sup> )							
		PBR1				PBR2			
		0.236	0.185	0.156	0.118	0.093	0.079	0.078	
mg N-NO <sub>3</sub> L <sup>-1</sup>	Mean	5.778	4.647	5.331	0.055	0.042	0.081	0.072	
	SD	1.540	0.872	0.438	0.047	0.059	0.131	0.085	
mg P-PO <sub>4</sub> L <sup>-1</sup>	Mean	0.772	a*	0.376 a*b*	0.005	0.009	0.003	0.019	
	SD	0.211	0.134	0.048	0.007	0.010	0.004	0.031	
pH	Mean	6.84	a*	7.69 a*b*	b*	7.04 A*B*C	7.68 A*D*E*	6.88 B*D*	CE*
	SD	0.16	0.11	0.07	0.05	0.14	0.13	0.08	
mg N g DW <sup>-1</sup> d <sup>-1</sup>	Mean	2.095	a*b*	1.506 a*	1.433 b*				
	SD	0.361	0.155	0.156					
mg P g DW <sup>-1</sup> d <sup>-1</sup>	Mean	0.317	a*	0.298 b*	0.192 a*b*				
	SD	0.061	0.036	0.020					

Table 7.3: Mean values and Standard Deviations obtained for nutrient and pH monitoring. Significant differences are indicated by means of pairs of letters, with an asterisk in the case of highly significant differences. Lower case letters refer to PBRs1, and capital letters to PBRs2.

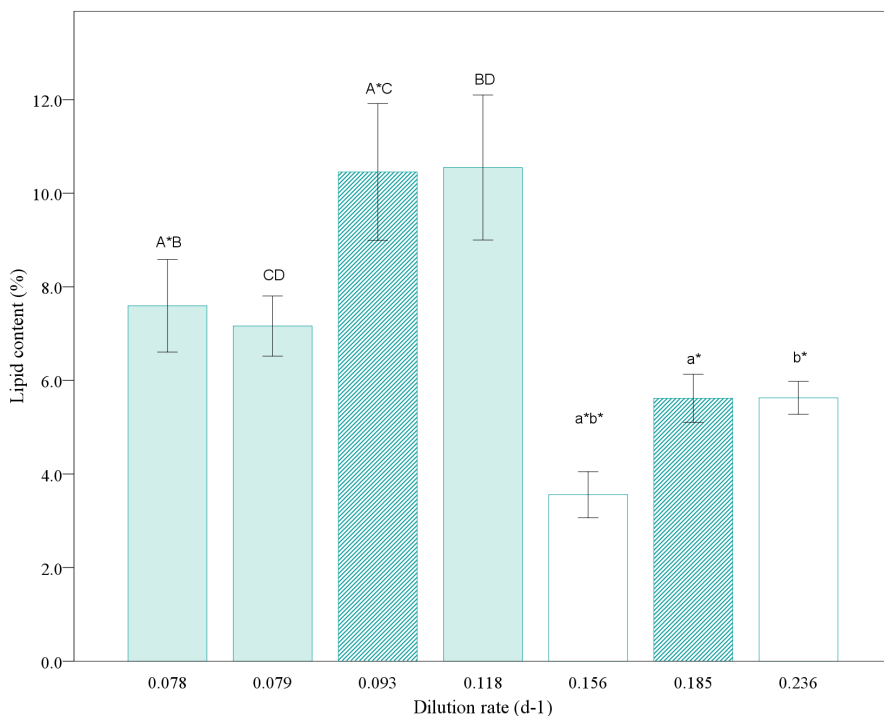


Figure 7.10: Lipid content (%) for each dilution rate ( $d^{-1}$ ). White bars correspond to PBRs1, whereas colored bars correspond to PBRs2. Stripped bars represent clarified water assays. Significant differences are indicated by means of pairs of letters, with an asterisk in the case of highly significant differences. Lower case letters refer to PBRs1, and capital letters to PBRs2. Error bars show 95 % confidence intervals of the mean.

but a large part of the energy absorbed by the system is not ending up in biomass when working at permanent low nitrogen concentrations (Klok et al. 2013), thus causing light energy wastage and limiting the biomass growth yield in relation with the absorbed light. In the present work, separating the two-subprocesses, growth and lipid production, in two compartments is proved to be able to overcome this problem.

#### 7.3.2.5. Effect of dilution rate and water reuse on fatty acid productivity

The fatty acids shown in Table 7.4 were found in the microalgae biomass.

Fatty acid productivities for each  $D$  can be seen in Table 7.5 and these data can be clearly compared in Figure 7.12. In PBRs1, rich in  $NO_3-N$ , almost all fatty acids

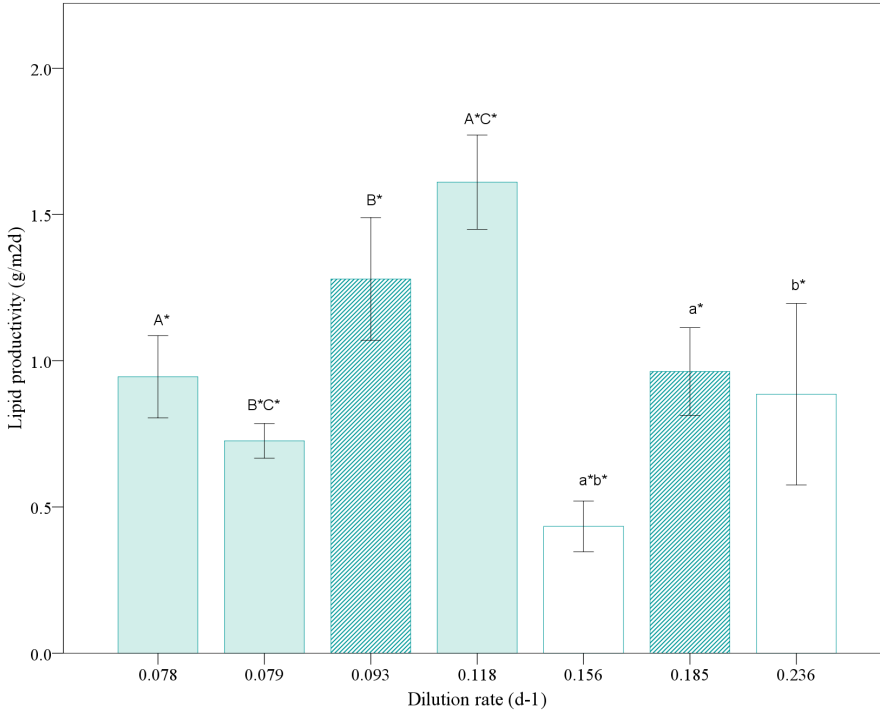


Figure 7.11: Lipid productivity ( $\text{g m}^{-2} \text{d}^{-1}$ ) for each dilution rate ( $\text{d}^{-1}$ ). White bars correspond to PBRs1, whereas colored bars correspond to PBRs2. Stripped bars represent clarified water assays. Significant differences are indicated by means of pairs of letters, with an asterisk in the case of highly significant differences. Lower case letters refer to PBRs1, and capital letters to PBRs2. Error bars show 95 % confidence intervals of the mean.

presented highly significant differences among the different  $D_s$  analyzed. As represented in Figure 7.13, saturated fatty acids productivity increased with the increase of the  $D$ , whereas unsaturated fatty acids productivity decreased. The same tendency was observed for percentage values. The highest unsaturated fatty acid productivity was achieved at  $0.185 \text{ d}^{-1}$ , while at  $0.156 \text{ d}^{-1}$  the highest diversity was obtained (Figure 7.12) as opposed to observations by (Abomohra et al. 2012), and findings in PBRs2. Nevertheless, generally the increase in the relative proportion of saturated and monounsaturated fatty acids and the decrease in the proportion of polyunsaturated fatty acids (PUFAs) are associated with the transition from logarithmic to stationary growth phase (Hu et al. 2008). With the processing in two-stages this transition occurs in PBRs2, being the microalgae cells in PBRs1 in exponential growth regardless the

Common name	Molecular formula	C:D
Palmitic acid	$C_{16}H_{32}O_2$	16:0
Stearic acid	$C_{18}H_{36}O_2$	18:0
Octadecenoic acid (Oleic)	$C_{18}H_{34}O_2$	18:1
Linoleic acid	$C_{18}H_{32}O_2$	18:2
Linolenic acid (EPA)	$C_{18}H_{30}O_2$	18:3
Eicosapentaenoic acid	$C_{20}H_{30}O_2$	20:5

Table 7.4: Common name, molecular formula and C:D number of the fatty acids found in the microalgae biomass.

D. Higher DW values obtained at  $0.185\text{ d}^{-1}$  and  $0.156\text{ d}^{-1}$  (Figure 7.7) imply lower light availability to microalgae, and according to (Hu et al. 2008), it seems that low light favors the formation of PUFAs.

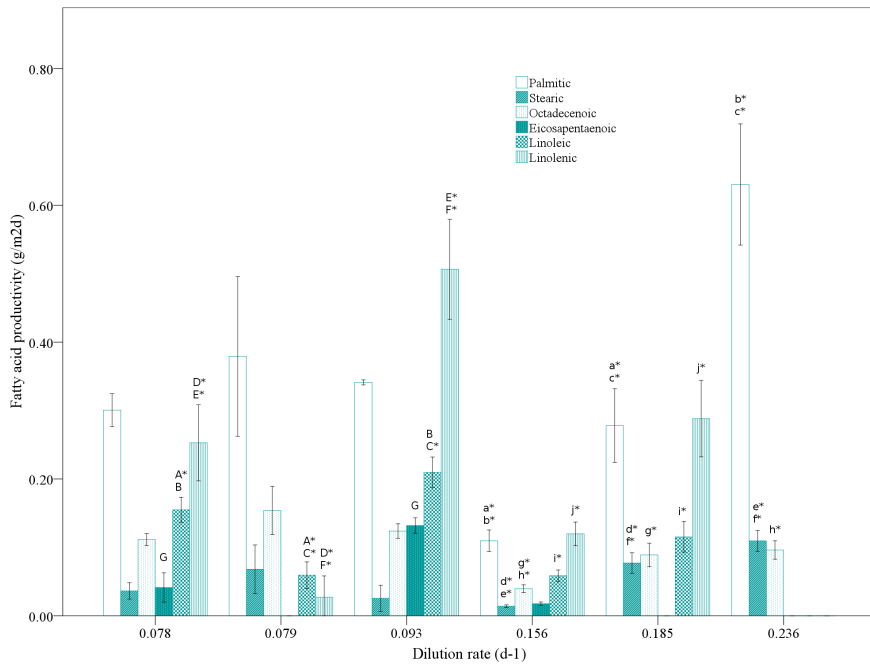


Figure 7.12: Fatty acid productivity ( $\text{g m}^{-2} \text{ d}^{-1}$ ) for each dilution rate ( $\text{d}^{-1}$ ). Significant differences are indicated by means of pairs of letters for each fatty acid, with an asterisk in the case of highly significant differences. Lower case letters refer to PBR1, and capital letters to PBR2. Error bars show 95 % confidence intervals of the mean.

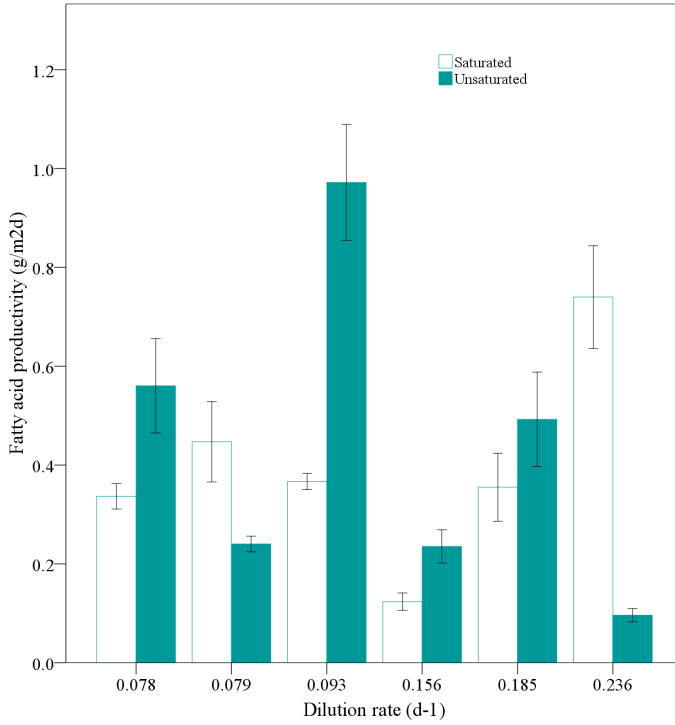


Figure 7.13: Saturated and unsaturated fatty acids productivity ( $\text{g m}^{-2} \text{d}^{-1}$ ) as a function of dilution rate ( $\text{d}^{-1}$ ). Error bars show 95 % confidence intervals of the mean.

In PRRs2 saturated fatty acid productivity was similar between the different  $D_s$ . Polyunsaturated eicosapentaenoic, linoleic and linolenic acid decreased as the stress time increased. In terms of percentage, an increase in saturated fatty acids was observed, as the unsaturated fatty acids decreased with the reduction of  $D$ .

Assay	PBR	Type of water	$D$ (d <sup>-1</sup> )	16:0	18:0	18:1	18:2	18:3	20:5
A1/2	1	Fresh	0.236	M 0.630 SD 0.036	a*b* 0.110 0.006	d*e* 0.096 0.005	g*		
A4	1	Clarified	0.185	M 0.278 SD 0.022	a*c* 0.077 0.006	d*f* 0.089 0.007	h* 0.115 0.009	i* 0.288 0.023	j* 0.018
A3	1	Fresh	0.156	M 0.110 SD 0.006	b*c* 0.014 0.001	e*f* 0.040 0.002	g*h* 0.059 0.003	i* 0.120 0.007	j* 0.001
A4	2	Clarified	0.093	M 0.341 SD 0.002	0.026 0.008	0.124 0.004	0.210 0.009	A*B 0.507 0.029	D*E* 0.132 0.005
A2	2	Fresh	0.079	M 0.379 SD 0.111	0.068 0.034	0.154 0.033	0.059 0.019	A*C* 0.027 0.030	D*F* 0.046
A3	2	Fresh	0.078	M 0.310 SD 0.037	0.040 0.021	0.114 0.013	0.164 0.028	BC* 0.271 0.093	E*F* 0.038

Table 7.5: Mean values and Standard Deviations obtained for the different fatty acids (g m<sup>-2</sup> d<sup>-1</sup>). Significant differences are indicated by means of letters for each fatty acid, with an asterisk in the case of highly significant differences. Lower case letters refer to PBRs1, and capital letters to PBRs2.

Linolenic acid exceeded the 12% fixed by the standard for Fatty Acid Methyl Esters (FAMES) based biodiesel EN14214 (14214 2008) in all the assays except at  $0.079 \text{ d}^{-1}$ , which correspond to the longest stress time. For  $D_s$  of 0.156, 0.093 and  $0.078 \text{ d}^{-1}$ , eicosapentaenoic acid appeared over the 1% established by the standard for PUFA concentration. These results are consistent with other works, (Hu et al. 2008; Tang et al. 2011) which concluded that the light intensity has an effect over the fatty acids profile. According to them, the lower is the light intensity; the higher is the content in unsaturated fatty acids. Then, the outdoor operation of the PBR is expected to reduce the content in PUFA. The high concentration of linolenic acid can be explained by the spectrum of the light source used, poor in red and having two peaks in the wavelengths corresponding to green and yellow. (Tang et al. 2011) found that linolenic acid composition of *Chlorella minutissima* was significantly decreased with red LEDs as light source.

A stress time of 8.4 days ( $A2$ ,  $D = 0.079 \text{ d}^{-1}$ ) resulted in a fatty acid profile that fits the European Standard EN ISO 14214, containing  $4.3 \pm 3.71 \%$  of linolenic acid and no polyunsaturated fatty acid with four or more double bounds.

### 7.3.3. Effect of the harvesting method over the fatty acids composition

Table 7.6 summarizes the obtained data for each fatty acid using the two tested harvesting methods, i.e. centrifugation and high pH flocculation-sedimentation.

Lipid	Harvesting method	Fatty acid percentage (%)		Fatty acid productivity ( $\text{g m}^{-2} \text{ d}^{-1}$ )	
		M	SD	M	SD
16:0	C	33.633	6.303	0.310	0.037
	FS	36.150	3.750	0.273	0.032
18:0	C	4.167	1.521	0.040	0.021
	FS	3.250	0.150	0.025	0.001
18:1	C	12.400	2.127	0.114	0.013
	FS	13.600	1.700	0.103	0.014
18:2	C	17.367	0.436	0.164	0.028
	FS	17.100	0.100	0.129	0.001
18:3	C	28.033	4.709	0.271	0.093
	FS	26.350	5.750	0.198	0.041
20:5	C	4.400	3.435	0.046	0.038
	FS	3.500	0.300	0.026	0.003

Table 7.6: Mean values and Standard Deviations obtained for Fatty acid percentage and Fatty acid productivity using two different harvesting methods: Centrifugation (C); High pH Flocculation-Sedimentation (FS).

No significant differences were obtained in the fatty acid percentage and produc-

tivity between the lipids extracted from centrifuged and flocculated microalgae as can be seen in Figure 7.14. This indicates that the harvesting method had no effects over the fatty acids composition in continuous cultures. These results are in accordance to those of (Castrillo et al. 2013), who did not observe differences in the lipid profile between harvesting methods when the microalgae were cultured in medium recovered by flocculation.

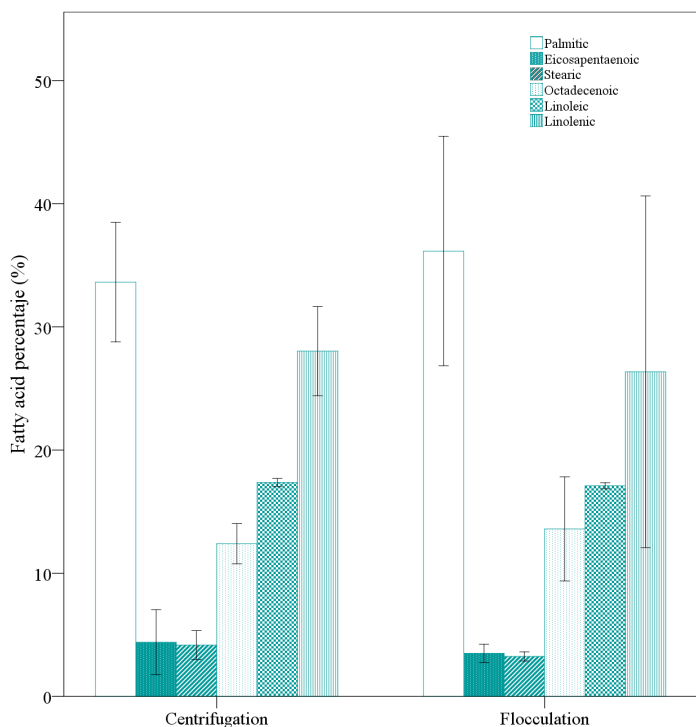


Figure 7.14: Fatty acid percentage when the biomass harvesting was carried out by means of centrifugation and high pH flocculation-sedimentation.

## 7.4. Conclusion

The two-stage operation mode results in a coincidence of the maximum biomass productivity and lipid content at the same dilution rate, maximizing the lipid



productivity. Light intensity, light spectrum and stress time are factors that must be considered, due to their effect over lipid content and fatty acids type and quality. The modulation of these parameters can be used to stimulate the production of desirable compounds in accordance with the objective of the culture.

Data obtained indicate that water reuse via microalgae flocculation and media neutralization with CO<sub>2</sub> is a suitable method to achieve a reduction in water consumption and an increase in CO<sub>2</sub> caption, while biomass and lipid productivities are not negatively affected. It was also confirmed that the biomass harvesting method has no effects over the fatty acids composition.

---

## References

- 12966, E. S. E. I. (2009). *Animal and vegetable fats and oils - Gas chromatography of fatty acid methyl esters - Part 3: Preparation of methyl esters using trimethylsulfonium hydroxide (TMSH)*.
- 14214, E. S. E. I. (2008). *Automotive fuels - Fatty acid methyl esters (FAME) for diesel engines - Requirements and test methods*.
- Abomohra, A. E. F et al. (2012). "Lipid and total fatty acid productivity in photoautotrophic fresh water microalgae: screening studies towards biodiesel production". In: *Journal of Applied Phycology*, pp. 1–6.
- Baky, H. H. A. E. et al. (2012). "Enhancement of lipid accumulation in *Scenedesmus obliquus* by Optimizing CO<sub>2</sub> and Fe<sup>3+</sup> levels for biodiesel production". In: *Bioresource technology* 119, pp. 429–432.
- Borowitzka, M. A. (1992). "Algal biotechnology products and processes - matching science and economics". In: *Journal of Applied Phycology* 4.3, pp. 267–279.
- Castrillo, M. et al. (2013). "High pH-induced flocculation-sedimentation and effect of supernatant reuse on growth rate and lipid productivity of *Scenedesmus obliquus* and *Chlorella vulgaris*". In: *Bioresource technology* 128, pp. 324–329.
- Chisti, Y. (2007). "Biodiesel from microalgae". English. In: *Biotechnology Advances* 25.3, pp. 294–306.
- Evers, E. (1991). "A Model for Light-Limited Continuous Cultures: Growth, Shading, and Maintenance". In: *Biotechnology and bioengineering* 38, pp. 254–259.
- Ho, S. H, W. M Chen, and J. S Chang (2010). "*Scenedesmus obliquus* CNW-N as a potential candidate for CO<sub>2</sub> mitigation and biodiesel production". In: *Bioresource technology* 101.22, pp. 8725–8730.
- Hu, Q. et al. (2008). "Microalgal triacylglycerols as feedstocks for biofuel production: Perspectives and advances". In: *Plant Journal* 54.4, pp. 621–639.
- Klok, A. J. et al. (2013). "Simultaneous growth and neutral lipid accumulation in microalgae". In: *Bioresource technology* 134, pp. 233–243.
- Mata, T. M., A. A. Martins, and N. S. Caetano (2010). "Microalgae for biodiesel production and other applications: A review". In: *Renewable and Sustainable Energy Reviews* 14.1, pp. 217–232.

- Mujtaba, G. et al. (2012). "Lipid production by *Chlorella vulgaris* after a shift from nutrient-rich to nitrogen starvation conditions". In: *Bioresource technology* 123, pp. 279–283.
- Ogbonna, J. C. et al. (1996). "A novel internally illuminated stirred tank photobioreactor for large-scale cultivation of photosynthetic cells". In: *Journal of Fermentation and Bioengineering* 82.1, pp. 61–67.
- Pruvost, J. et al. (2009). "Investigation of biomass and lipids production with *Neochloris oleoabundans* in photobioreactor". In: *Bioresource technology* 100.23, pp. 5988–5995.
- Pruvost, J. et al. (2011). "Systematic investigation of biomass and lipid productivity by microalgae in photobioreactors for biodiesel application". In: *Bioresource technology* 102.1, pp. 150–158.
- Quinn, J. C. et al. (2012). "Nannochloropsis production metrics in a scalable outdoor photobioreactor for commercial applications". In: *Bioresource technology* 117, pp. 164–171.
- Rawat, I. (2012). "Biodiesel from microalgae: A critical evaluation from laboratory to large scale production". In: *Applied Energy*.
- Rodolfi, L. et al. (2009). "Microalgae for oil: Strain selection, induction of lipid synthesis and outdoor mass cultivation in a low-cost photobioreactor". In: *Biotechnology and bioengineering* 102.1, pp. 100–112.
- Ruiz, J. et al. (2013). "Performance of a flat panel reactor in the continuous culture of microalgae in urban wastewater: Prediction from a batch experiment". In: *Bioresource technology* 127, pp. 456–463.
- Salama, E. S et al. (2013). "Biomass, lipid content, and fatty acid composition of freshwater *Chlamydomonas mexicana* and *Scenedesmus obliquus* grown under salt stress". In: *Bioprocess and Biosystems Engineering*, pp. 1–7.
- Su, C. H et al. (2011). "Factors affecting lipid accumulation by *Nannochloropsis oculata* in a two-stage cultivation process". In: *Journal of Applied Phycology* 23.5, pp. 903–908.
- Tang, H. et al. (2011). "Culture of microalgae *Chlorella minutissima* for biodiesel feedstock production". In: *Biotechnology and bioengineering* 108.10, pp. 2280–2287.
- Tang, H. et al. (2012). "Continuous microalgae cultivation in a photobioreactor". In: *Biotechnology and bioengineering* 109.10, pp. 2468–2474.

- 
- Tejero, J. et al. (2011). *Fotobiorreactor para el cultivo de organismos fotótrofos*.
- Wijffels, R. H. and M. J. Barbosa (2010). "An outlook on microalgal biofuels". In: *Science* 329.5993, pp. 796–799.
- Zhou, W. et al. (2012). "A hetero-photoautotrophic two-stage cultivation process to improve wastewater nutrient removal and enhance algal lipid accumulation". In: *Bioresource technology* 110.0, pp. 448–455.

# 8

## **Conclusions and Recommendations**



The results obtained from the theoretical and experimental work carried out within this thesis contribute to the development of technological and operational improvements that could be put into practice in the field of biomass culturing. With the objective of making this process more affordable from the economical and the environmental point of view, some technical advantages have been demonstrated. As a consequence, some suggestions of future work emerged from these findings. Those, together with the conclusions of this thesis are shown below in relation with the initial objectives.

### **Design and feasibility evaluation of a novel area efficient photobioreactor, via modelization**

A key factor in the design of areal efficient cultivation devices is the distribution of light over its surface, avoiding loss of light through reflection as much as possible and minimizing oversaturating conditions in the upper layers of the culture. While conventional photobioreactors exposed to solar light usually receive an excessive amount of energy in the most external layers of the culture, getting away from the maximum theoretical efficiency of photosynthesis, the photobioreactor of the present invention takes advantage of the energy in excess to distribute it over a higher surface. This characteristic leads to minimize the photosaturation phenomenon and increase the culture illuminated volume per occupied surface.

A mathematical model was developed to modelize the areal productivity in the novel photobioreactor and was also applied to a well-known technology, an open pond type. It could be seen that irradiance values under the saturation point could be maintained even in the upper layers of the culture by adjusting the aperture angle of the cone. The architecture of the photobioreactor provided short light paths, with a maximum of 0.15 m for the selected parameters ( $D = 0.30$  m,  $\varphi = 5^\circ$ ) in a photobioreactor unit. While in the case of the pond, the illuminated surface is equal to the ground occupied surface, in the novel photobioreactor, the illuminated surface to occupied surface ratio is 11, complying with the current recommendations for photobioreactor design. Furthermore, in the present design the occupied surface per culture volume is 4.3 times lower than in the open pond. Average daily areal productivity, photosynthetic efficiency and biomass yield were about 2.7 times higher in the novel photobioreactor than in the open pond.

The results provided by the model evidence that, in a mid-latitude location, the longer is the duration of the day and the higher is the irradiance, the more advantage can be taken from this design. In order to validate the model, an outdoor experimentation should be conducted. Since constructing a mobile unit of volume in order to

---

track the Sun may represent some difficulties, a first approach would be solved by maintaining the unit static and directing the Sun beams by means of a mobile mirror.

Afterwards, a tool for helping in the decision of the distributions of the cones when scaling-up this technology was developed and applied with irradiance data of Santander. Several decision variables are involved, being the situation of the pivot joint of the cones, the maximum inclination angle and the relative position of the cones, playing an important role in the yearly performance of the photobioreactor. The illuminated volume through the year per unit surface is increased when the solar altitude along the day is high, thus suggesting that low latitudes are the most appropriate for this design.

Productivity, photosynthetic efficiency and biomass yield values are comparable or higher than those referred to enclosed photobioreactors, however the present photobioreactor is intended for a higher simplicity in constructional and operating terms. For example, the penetration of the cones in the culture medium drives the light deep into the tank, which could make the construction of photobioreactors in semi-buried tanks possible. This is expected to make it more economical and easier to build than conventional closed photobioreactors. Furthermore, the scale-up of this photobioreactor would be carried out by repeating multiple reactor units, thus avoiding shading and empty ground surfaces; on the contrary the culture volume would occupy the entire ground surface available for the facility. Other advantages would be related with some operational drawbacks, as overheating which is expected to be avoided due to the dilution effect of the irradiance over the culture surface. However, in order to clarify these aspects further research should be conducted, accompanied by a cost analysis.

The invention complied with the characteristics of novelty and inventive, therefore it was registered as a patent.

### **Evaluation of the viability of a low cost harvesting method in comparison with a conventional one**

Regarding the harvesting method, in order to test a less energy consuming method than the conventional ones, assays of auto-flocculation by adding two different bases were carried out. It was seen that high microalgal biomass recovery efficiencies can be achieved by high pH-induced flocculation-sedimentation, however further research should be conducted to clarify the flocculation mechanisms. The experiments conducted in this work demonstrated that magnesium is not the sole factor influencing high pH induced flocculation with Na(OH), since it was present during the assays with *C. vulgaris* and the performance of flocculation was not effective.



According to the presented results, the recovery of *C. vulgaris* using high pH-induced flocculation-sedimentation is not as efficient as the recovery of *S. obliquus*, specially when using Na(OH). In the case of *S. obliquus* recovery efficiencies over 80 % can be achieved when using Ca(OH)<sub>2</sub> and around 80 % when using Na(OH). It seems obvious that the mechanisms of Na(OH) are completely different than those of Ca(OH)<sub>2</sub>, which works better even in the situations where Na(OH) is very inefficient. In spite of this, it is worth taking into account that CaCO<sub>3</sub> precipitates when using Ca(OH)<sub>2</sub> may interfere during subsequent steps of downstream processing, thus the final quality of the products must be a criterion when selecting the harvesting method. It was also confirmed that the biomass harvesting method, when comparing centrifugation and auto-flocculation with Na(OH) has no effects over the fatty acids composition. An exception was the case of using tap water, in which the auto-flocculation with Na(OH) had a negative effect on the biomass content, especially on the content of PUFAs. It was associated to the high requirement of Na(OH) to achieve a high pH when using this kind of water, which could had interfered during the hydrolysis step of the lipids extraction.

### **Reduction of inputs to the production system through the recycling of the culture medium and study of its influence on biomass growth, lipid production and fatty acid composition**

As a consequence of the reasons exposed above, Na(OH) was selected as the pH increasing agent in the subsequent assays in which the growth, the biomass productivity, the lipid content and the lipid productivity were studied as a function of the type of water used to prepare the culture medium. The culture medium is an important item in microalgae production costs because huge amounts of water are used; therefore the effect of medium reuse was studied.

In comparison with media prepared with the supernatant of centrifugation, with analytical-grade water and with tap water, when microalgae grew in medium recovered by auto-flocculation with Na(OH), the number of cells was not negatively affected in batch assays, neither in continuous assays except when the culture was exposed to stress conditions. Furthermore, regarding the dry weight, obtained values were higher in reused media than in fresh media in both batch and continuous assays.

Regarding the lipid content, in batch assays was lower when reused water was employed to prepare the media. Nevertheless since the biomass productivity had been higher, the lipid productivity was also higher. In continuous assays obtained lipid content and lipid productivity in reused medium were comparable to those obtained in fresh medium at similar dilution rates.

---

The current results reveal that if the reused medium is supplemented with nutrients, even higher growth and lipid productivity yields can be achieved than with fresh medium. Under the assayed conditions, it can be concluded that the medium reuse do not affect negatively to the biomass and lipids productivity.

The fatty acids from microalgae grown in reused media were richer in PUFAs. Since the accumulation of PUFAs has been recognized as a response to unfavorable conditions, this could mean that the medium reuse produces a kind of stress that leads to the production of PUFA.

Data obtained indicate that water reuse via microalgae flocculation and media neutralization with CO<sub>2</sub> is a suitable method to achieve a reduction in water consumption. These findings are of special importance to microalgae culture in areas with a scarcity of fresh water that usually are those with better solar irradiance. The effect of further successive cycles should be studied in order to determine whether negative effects could occur due to conductivity increasing, bacteria growing, etc.

### **Optimization of a continuous biomass culture operation to enhance lipid productivity**

The two-stage operation mode guaranteed light limited conditions in the first stage and N-stress conditions in the second stage. Lipid content and lipid productivity, both were higher in the second stage than in the first one in all the assays, except when the dilution rate had been too low ( $0.079\text{ d}^{-1}$ ). With a dilution rate in the first stage short enough to guarantee high biomass productivity, and also short enough not to inhibit the lipid production in the second one, the overall lipid productivity can be enhanced. In the developed work, this mode of operation resulted in a coincidence of the maximum biomass productivity and lipid content at the same dilution rate, maximizing the lipid productivity ( $0.236\text{ d}^{-1}$  in the first stage and  $0.236\text{ d}^{-1}$  in the second one). The biomass productivity was slightly higher than that expected according to the batch experiment.

The dilution rates of the two stages must be accurately adjusted. In the first stage, at low dilution rate a high biomass concentration was achieved, leading to low biomass productivity and consequently low lipid productivity. In the second stage, low dilution rates were associated with low PUFA productivity. Therefore, if the target of the culture is the lipid productivity for biofuel production, low dilution rates must be applied in order to comply with the standards for the FAMES for biofuels. On the contrary, applying high dilution rates seems to be interesting when the target is the production of lipids with nutritional interest.



**Experimental parameters  
obtention**



## A.1. Light extinction coefficient determination

The degree of light attenuation as a function of biomass concentration and light path length was evaluated by measuring Photosynthetic Active Radiation (PAR) with a LI-COR Li-192 underwater quantum sensor at several depths under five different cell concentrations and a blank with analytical-grade distilled water.

Cell concentrations were determined by dry weight following the procedure described in the Materials and Methods Chapter. The cell concentrations were:  $0.347 \text{ g L}^{-1}$ ,  $0.259 \text{ g L}^{-1}$ ,  $0.197 \text{ g L}^{-1}$ ,  $0.166 \text{ g L}^{-1}$  and  $0.129 \text{ g L}^{-1}$ .

The experimentally obtained data at nine different depths and six concentrations are showed in Figure A.1. They were correlated with Lambert-Beer Law (4.3) by simple linear regression with an  $R^2$  correlation coefficient of 0.980. The calculated extinction coefficient was  $182 \text{ m}^2 \text{ kg}^{-1}$ .

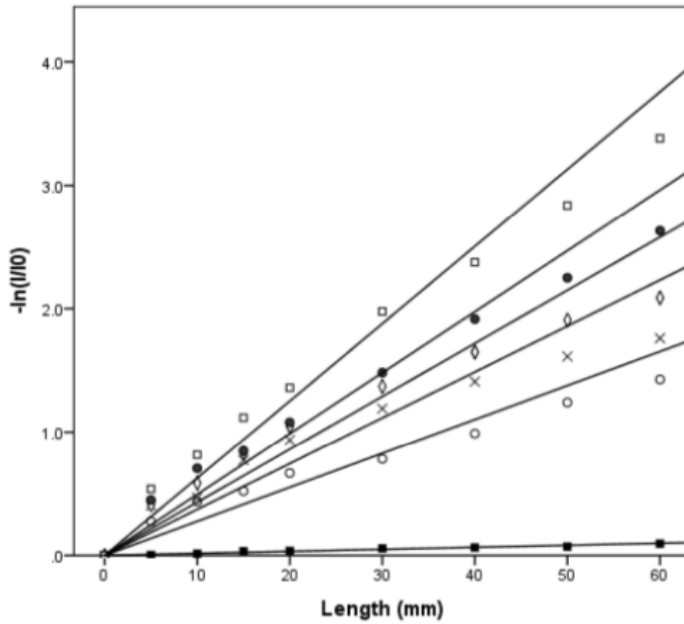


Figure A.1: Relationship between light attenuation and light path length. ( $\square$ )  $0.347 \text{ g L}^{-1}$ , ( $\bullet$ )  $0.259 \text{ g L}^{-1}$ , ( $\diamond$ )  $0.197 \text{ g L}^{-1}$ , ( $\times$ )  $0.166 \text{ g L}^{-1}$ , ( $\circ$ )  $0.129 \text{ g L}^{-1}$ , ( $\blacksquare$ )  $0 \text{ g L}^{-1}$ .

---

## A.2. Kinetic parameters obtaining

Monod kinetic parameters were experimentally obtained in laboratory scale microcosms. *Scenedesmus obliquus* was chosen as model strain. *S. obliquus* CCAP 276/3A was supplied by the Culture Collection of Algae and Protozoa in Scotland, UK.

Relation between light intensity and growth rate was studied at laboratory scale. This strain was cultivated under three different light intensity levels in a modified BG11 medium which contained  $0.4125 \text{ g L}^{-1} \text{ NaNO}_3$ ,  $0.038 \text{ g L}^{-1} \text{ K}_2\text{HPO}_4$ ,  $0.075 \text{ g L}^{-1} \text{ MgSO}_4 \cdot 7 \text{ H}_2\text{O}$ ,  $0.036 \text{ g L}^{-1} \text{ CaCl}_2 \cdot 2 \text{ H}_2\text{O}$ ,  $0.006 \text{ g L}^{-1}$  citric acid,  $0.006 \text{ g L}^{-1}$  green ammonium  $\text{Fe}^{3+}$  citrate,  $0.10 \text{ g L}^{-1} \text{ EDTANa}_2$ ,  $0.02 \text{ g L}^{-1} \text{ Na}_2\text{CO}_3$ ,  $0.0029 \text{ g L}^{-1} \text{ H}_3\text{BO}_3$ ,  $0.0018 \text{ g L}^{-1} \text{ MnCl}_2 \cdot 4 \text{ H}_2\text{O}$ ,  $0.00022 \text{ g L}^{-1} \text{ ZnSO}_4 \cdot 7 \text{ H}_2\text{O}$ ,  $0.00039 \text{ g L}^{-1} \text{ Na}_2\text{MoO}_4 \cdot 2 \text{ H}_2\text{O}$ ,  $0.00008 \text{ g L}^{-1} \text{ CuSO}_4 \cdot 5 \text{ H}_2\text{O}$ ,  $0.00005 \text{ g L}^{-1} \text{ Co}(\text{NO}_3)_2 \cdot 6 \text{ H}_2\text{O}$ . This composition resulted in initial  $\text{NO}_3\text{--N}$  concentration of  $242.97 \text{ mg L}^{-1}$  and  $\text{PO}_4\text{--P}$  initial concentration of  $5.905 \text{ mg L}^{-1}$ , assuring that nutrients were not limiting the microalgae growth.

The cultures were grown in 2 L flasks, inside a growth chamber at temperature  $24.0 \pm 0.2 \%$ . Each light intensity level was studied per triplicate. Incident frontal lights were  $140 \mu\text{E m}^{-2} \text{ s}^{-1}$ ,  $92.5 \mu\text{E m}^{-2} \text{ s}^{-1}$  and  $56 \mu\text{E m}^{-2} \text{ s}^{-1}$ , and average incident irradiance taking into account that the back of the flask received reflected irradiance were  $120 \mu\text{E m}^{-2} \text{ s}^{-1}$ ,  $46 \mu\text{E m}^{-2} \text{ s}^{-1}$  and  $68 \mu\text{E m}^{-2} \text{ s}^{-1}$ . The first level was provided directly by the chamber light sources while the others were reached by placing textile meshes for shading. The inoculum used was at exponential growth phase and previously acclimated to these culture conditions. The cultures were aerated with 2 %  $\text{CO}_2$  enriched air at a flow of 0.027 vvm and shacked by means of magnetic stirrers at 350 rpm.

For the dry weigh analysis the samples were filtered through a previously dried Whatman paper filter GF/C 47 mm and dried at  $103^\circ\text{C}$  for 6 h.

In order to get the most realistic possible irradiance-growth rate relation only growth rates at low optical densities have been taken into account, trying to avoid self-shading phenomena. Growth rates are given in Table A.1.

The Monod equation has been linearized and representing  $\frac{1}{\mu}$  as a function of  $\frac{1}{I}$ , the equation of the line with  $\frac{K_I}{\mu_{max}}$  as the slope and  $\frac{1}{\mu_{max}}$  as the y-intercept.

## A. Experimental parameters obtention

Light intensity $\text{E m}^{-2} \text{s}^{-1}$	Growth rate $\text{d}^{-1}$
120	0.742
120	0.742
120	0.843
68	0.590
68	0.590
68	0.650
46	0.549
46	0.570
46	0.505

Table A.1: Obtained growth rates for each replicate and each light intensity level.

Name	Abbreviation	Unit	Value
Maximum growth rate	$\mu_{\max}$	$\text{d}^{-1}$	1.02
Half-saturation constant	$K_i$	$\mu \text{E m}^{-2} \text{m}^{-1}$	42.5

Table A.2: Monod kinetic parameters

$$\mu = \frac{\mu_{\max} I}{K_I + I}$$

$$\frac{1}{\mu} = \frac{1}{\mu_{\max}} + \frac{K_I}{\mu_{\max} I}$$

The obtained equation is the following:

$$y = 41.427x + 0.997$$

with  $R^2 = 0.8633$ .

The calculated Monod parameters are given in Table A.2.





A large, stylized teal letter 'B' serves as a background element, positioned centrally on the page. It is a solid color with a slightly rounded, modern font style.

**Detailed model calculations**



### B.1. $Q$ optimization as a function of $a$

When a cone with its pivot joint in its base is inclined from  $90^\circ$  to an angle  $\alpha$ , firstly the submerged volume increase, which makes the water level to rise. From a certain angle the submerged volume decreases and then the water level lowers. This variation in the water level has been called  $a$ .

The optimization of  $Q$  has been solved by iteration to make the value of  $Q + a$  higher or equals to the height over the water level needed to tilt to  $\alpha$  ( $R \cos \alpha$ ). These parameters are identified in Figure B.1.

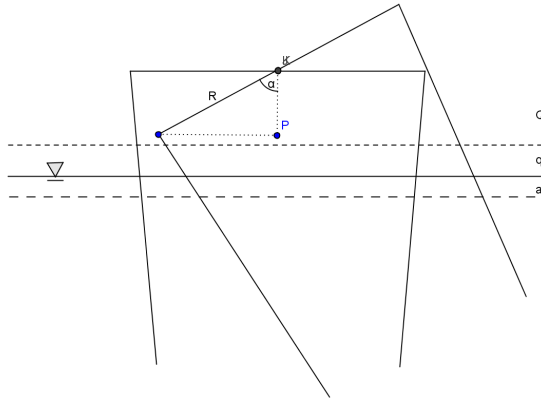


Figure B.1: A cone inclined to an angle  $\alpha$  with its pivot joint in the base.

### B.2. Submerged volume calculation

When a cone is partially or totally submerged, the figure that remains above the water level is a frusto-cone with one of its bases being an ellipse, as represented in Figure B.2.

The volume of this figure can be calculated as follows:

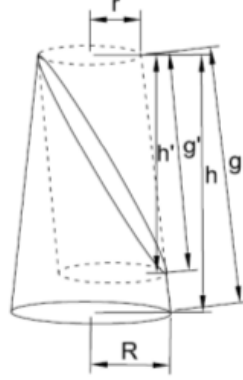


Figure B.2: Geometrical figure that remains above the water level when the cone is tilted to an angle  $\alpha$ .

$$V_{\text{obliquefrusto-cone}} = V_{\text{frusto-cone}} - \frac{V_{\text{cylinder}}}{2}$$

$$V_{\text{frusto-cone}} = \pi \left( R^2 + r^2 + Rr \right) \frac{h}{3}$$

$$V_{\text{cylinder}} = \pi r^2 g'$$

The volume that remains above the water level is:

$$V_0 = \left[ \pi \left( R^2 + r^2 + Rr \right) \frac{h}{3} \right] - \frac{\pi r^2 g'}{2}$$

$$g' = \frac{h'}{\cos \varphi}$$

$$h' = \frac{d}{\tan \alpha} = \frac{2r}{\tan \alpha}$$

$$g' = \frac{\frac{2r}{\tan \alpha}}{\cos \varphi} = \frac{2r}{\cos \varphi \tan \alpha}$$

$$V_0 = \left[ \pi \left( R^2 + r^2 + Rr \right) \frac{h}{3} \right] - \left( \frac{\pi r^3}{\cos \varphi \tan \alpha} \right)$$

$r$  and  $h$  are calculated as follows:

$$h = Q' + q' + \frac{r}{\tan \alpha} = \frac{Q + q}{\sin \alpha} + \frac{r}{\tan \alpha}$$

$$r = R - h \tan \varphi$$

By substituting the equation for  $h$  and the equation for  $r$ :

$$r = R - \left( \frac{Q + q}{\sin \alpha} + \frac{r}{\tan \alpha} \right) \tan \alpha$$

$$r = \frac{R - \frac{Q + q}{\sin \alpha} \tan \varphi}{1 + \frac{\tan \varphi}{\tan \alpha}}$$

### B.3. Distance between two contiguous cones when they are inclined in their alignment direction

The minimum distance between two cones to tilt to an angle  $\alpha$  is determined by its diameter and the angle  $\varphi$ .

The distance  $F$  has been discomposed in  $f + F'$ .



for any other Azimuth angle the distance that limits the inclination of the cones is the distance ( $L$ ) between the two cones in the Azimuth angle.

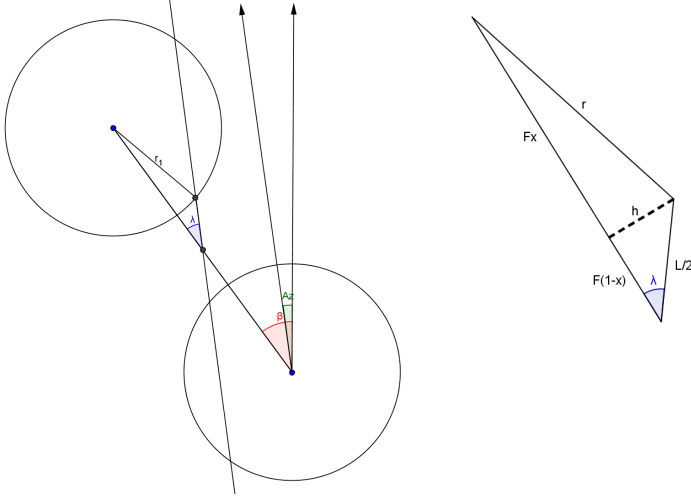


Figure B.4: Floor view of two cones aligned in a direction that makes an angle  $\beta$  with the South direction and that are going to tilt in a plane in the Azimuth direction.

For the calculation of  $L$  a triangle has been extracted from the floor view of the cones (Figure B.4). According to this view:

$$\frac{L}{2} = \frac{F(1-x)}{\cos \lambda}$$

where  $\lambda = \beta - Az$

The value of  $x$  is determined according to the following system of two equations:

$$r^2 = (Fx)^2 + h^2$$

$$h = F(1-x) \tan \lambda$$

Resulting in the following quadratic equation:

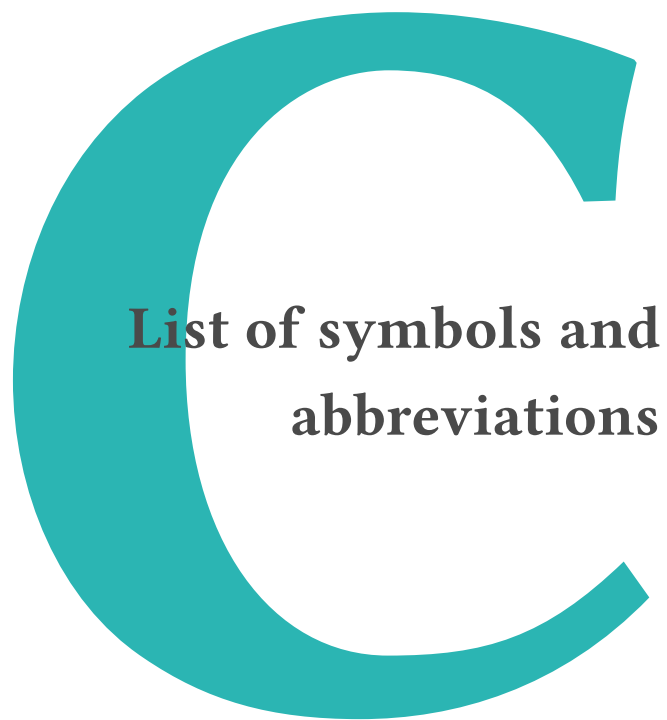
Analogously to the separation of the cones that tilt in the direction that they are aligned, the separation when they tilt in any other plane can be calculated but instead of introducing the diameter of the cone, the chord in the plane of the shortest distance in the direction that the cones tilt ( $C$ ) is introduced.  $C$  and  $L$  are identified in Figure B.5.

Finally, the value of the maximum inclination angle for each Azimuth has been determined by iteration of its value in order to satisfy the following identity:



$$g + G' = L + C$$





**List of symbols and  
abbreviations**



Symbol or abbreviation	Name	Magnitude
$a$	variation in the water level	length
a.s.l.	above sea level	length
Az	Azimuth angle (with reference to the South)	angular
$b$	Pivot joint distance to the apex of the cone	length
BP	Biomass productivity	mass length <sup>-1</sup> time <sup>-1</sup>
$c$	speed of light	length time <sup>-1</sup>
$C$	biomass concentration	mass volume <sup>-1</sup>
$C$	chord of the base that gets in touch to the chord of the base of the contiguous cone in the Azimuth direction	
$C_b$	biomass concentration	mass volume <sup>-1</sup>
CCAP	Culture Collection of Algae and Protozoa	
$C_p$	compensation point	power surface <sup>-2</sup>
$D$	diameter of the cone	length
$D$	dilution rate	time <sup>-1</sup>
DHA	docosahexaenoic acid	
DW	dry weight	mass volume <sup>-1</sup>
EPA	eicosapentaenoic acid	
EPA	Environmental Protection Agency	
EVA	Ethylene Vinyl Acetate	
$F$	distance between two contiguous cones that tilt in the plane that they are aligned	length
$F$	flow rate	volume time <sup>-1</sup>
FAME	fatty acid methyl esters	

Symbol or abbreviation	Name	Magnitude
$g$	gravitational force	length time <sup>-2</sup>
$G$	distance between two contiguous cones that tilt in a different plane that they are aligned	length
GC-MS	Gas chromatography-mass spectrometry	
H	hour angle	angular
h	Plack constant	energy time
HRT	hydraulic retention time	time
I	irradiance	power surface <sup>-2</sup>
$I_h$	inhibition irradiance	power surface <sup>-2</sup>
$I_k$	saturation irradiance	power surface <sup>-2</sup>
$I_s$	light intensity at which Pmax is achieved	power surface <sup>-2</sup>
ISO	International Organization for Standardization	
$K$	light extinction coefficient	length <sup>2</sup> mass <sup>-1</sup>
$K_a$	extinction coefficient	length <sup>2</sup> mass <sup>-1</sup>
$K_i$	half saturation constant when the light is the limiting substrate	
$K_s$	half-saturation constant	
LC	Lipid content	percentaje
L-D	light-dark	
LDPE	Low Density Polyethylene	
LP	Lipid productivity	mass time <sup>-1</sup> length <sup>-1</sup>
$L_R$	the depth of the cone where reflected radiation hits	length
$n^1$	air refractive index	
$n^2$	PMMA refractive index	

Symbol or abbreviation	Name	Magnitude	
$n^3$	culture suspension refractive index		
$\text{NH}_4\text{—N}$	nitrate as amonium		
$\text{NO}_2\text{—N}$	nitrogen as nitrite		
$\text{NO}_3\text{—N}$	nitrogen as nitrate		
P/I	photosynthesis/irradiance		
PAR	photosynthetic active radiation		
PBR	photobioreactor		
$P_{\text{max}}$	maximum productivity	mass time <sup>-1</sup>	length <sup>-1</sup>
$\text{PO}_4\text{—P}$	phosphorus ans ortophosphate		
PUFA	polyunsaturated fatty acid		
PVGIS	Photovoltaic Geographical Information System		
$q$	height above the water level to avoid splashing over the cone's base	length	
$Q$	height above q to avoid splashing over the cone's base when the cones are inclined	length	
$R$	reflected fraction of lighth		
RP	reflectance of an incident light ray that is polarized with its electric field parallel to the plane containing the incident, reflected, and refracted rays		
rpm	revolutions per minute		
RS	reflectance of an incident light ray that is polarized with its electric field perpendicular to the plane containing the incident, reflected, and refracted rays		
$S$	surface		

---

Symbol or abbreviation	Name	Magnitude
$S$	specular factor	
ST	stress time	time
T	transmitted fraction of light	
TAG	triacylglycerol	
td	doubling time	time
TMSH	trimethylsulfonium	
Tr	transmittance	
UV	ultraviolet	
$V$	volume	volume
$V_S$	submerged volume	volume
$V_T$	total volume	volume
vvm	volume per volume per time	volume time <sup>-1</sup> volume <sup>-1</sup>
X	biomass concentration	mass volume <sup>-1</sup>
$z$	normal distance between a point and the irradiated surface	length
$z_{\text{direct}}$	path that an ideal refracted beam would take in the culture	length
$\alpha$	inclination angle of the cones with respect to the horizontal	angular
$\alpha_{\text{max}}$	maximum inclination angle of the cones	angular
$\alpha_S$	maximum inclination angle of the cones towards the South	angular
$\beta$	angle between the South direction and the alignment direction of two cones	angular
$\theta_i$	angle that the incident beam makes to the normal	angular
$\theta_t$	angle that the refracted beam makes to the normal	angular



Symbol or abbreviation	Name	Magnitude
$\lambda$	wavelength	length
$\varphi$	half of the aperture angle of the cone	angular
$\mu$	growth rate	time <sup>-1</sup>
$\mu_{\max}$	maximum growth rate	time <sup>-1</sup>
16:0	palmitic acid	
16:1	palmitoleic acid	
16:2	hexadecadienoic acid	
16:3	hexadecatrienoic acid	
18:0	stearic acid	
18:1	oleic acid	
18:2	linoleic acid	
18:3	linolenic acid	
20:5	eicosapentaenoic acid	
22:6	docosahexaenoic acid	

